Institute of Physical Chemistry
Polish Academy of Sciences
Kasprzaka 44/52
01-224 Warsaw, Poland

PHD THESIS

ELECTROCHEMICAL PROCESSES AT LIQUID|LIQUID INTERFACES IN MICROFLUIDIC SYSTEMS

Dawid Kałuża

Supervisor: dr hab. Martin Jönsson-Niedziółka, prof. IChF PAN

This dissertation was prepared within the International PhD Studies at the Institute of Physical Chemistry of the Polish Academy of Sciences in Warsaw

Warsaw, July 2016

ACKNOWLEDGEMENTS

Firstly, I would like to express my special appreciation to my promotor, dr hab. Martin Jönsson-Niedziółka, for supporting me during these five years. Thank you for encouraging my research and for allowing me to grow as a research scientist.

I would also like to thank prof. dr hab. Marcin Opałło for help me to start my PhD studies.

I am grateful to dr inż Wojciech Adamiak who has introduced me in electrochemistry at the liquid|liquid interfaces and also for being valuable source of support.

I am grateful to dr inż. Ewa Roźniecka who has helped me to make a first step in microfluidic research.

I am also grateful to prof. Frank Marken for fruitful collaboration and opportunity to work in his research group together with PhD Sunyhik Ahn.

Many thanks to all my colleagues from Department of Electrode Processes IPC PAS for everyday nice atmosphere at the work.

Finally, I would like to thank my wife and my family for the understanding and constant support.

THE WORK WAS SUPPORTED BY:

- the project DEC-2011/01/D/ST4/04182 financed by the Polish National Science Centre

- the project NOBLESSE FP7-REGPOT-CT-2011-285949-NOBLESSE financed within the Seventh Framework Programme of the European Union

STRESZCZENIE

Celem naukowym niniejszej rozprawy doktorskiej jest zbadanie i zrozumienie podstawowych procesów elektrochemicznych zachodzących na granicy faz ciecz|ciecz w układach mikroprzepływowych. Całość badań pokazuje możliwości i sposób użycia elektrochemicznych układów mikroprzepływowych.

Całość eksperymentów elektrochemicznych była przeprowadzona w elektrochemicznym układzie mikroprzepływowym (EMD). Układ ten składał się z mikrokanału wykonanego z materiału o nazwie polidimetylosiloksan (PDMS) oraz ze szklanej płytki, na której napylone zostały warstwy złota tworzące system elektrod: pracującej, odniesienia i pomocniczej. W części eksperymentów zastosowano standardową elektrodę chlorosrebrową jako odniesienia. Cechą charakterystyczną badań była obecność granicy trzech faz, która umożliwiała na zajście równoległego procesu przeniesienia ładunku na elektrodę pracującą oraz przejścia anionów przez granicę ciecz|ciecz.

W pierwszej części pracy dokonano sprawdzenia kompatybilności mikrokanału wykonanego z PDMS na wpływ różnych rozpuszczalników organicznych i stwierdzono, że użyty do badań rozpuszczalnik *N*-oktylo-2-pirrolidon (NOP) nie deformuje ani nie niszczy struktury PDMS w trakcie przepływu, któremu towarzyszy elektrochemiczne utlenienie ferrocenu (Fc). Zbadano również nietypowe zachowanie się prądu granicznego towarzyszącemu tranferowi anionu do fazy organicznej podczas reakcji elektrochemicznego utlenienia Fc i zmonitorowano obecność granicy trzech faz w zależności od zadanych warunków przepływu.

W kolejnej części badań dokonano reakcji transferu różnych anionów i scharakteryzowano je pod kątem ich zdolności do przejścia przez granicę ciecz|ciecz. Otrzymane wyniki w warunkach mikroprzepływowych były zgodne z termodynamiką transferu anionów obowiązującą dla warunków stacjonarnych z zastosowaniem elektrody trójfazowej (TPE) i mogłby być analizowane w oparciu o równanie Nernsta. Stwierdzono, że obecność hydrofobowych anionów w fazie wodnej podczas utleniania dekametyloferrocenu (DMFc) w fazie organicznej, powodowała przejście anionów do fazy organicznej i odwrotnie w przypadku anionów hydrofliowych następowało przejście kationu dekametyloferroceniowego ($DMFc^+$) do fazy wodnej. Ostatnia część pracy zawiera eksperymenty związane z chemicznym utlenieniem substancji nielektroaktywnej difenynokarbonolu (DPC) do benzofenonu (BP), która to reakcja zachodzi w obecności elektroaktywnego mediatora w postaci rodnika

2,2,6,6-tetrametylo-1-piperydyno-oksylu (TEMPO). Wykazano, że różne pochodne TEMPO działają z różną szybkością na przekształcenie DPC do BP. Otrzymane wyniki są dobrym wstępem do przeniesienia badań do układów mikroprzepływowych, które pozwalają w wyniku obecności konwekcyjnego transportu mediatora na zwiększenie szybkości reakcji utlenienia DPC do BP.

Wyniki przeprowadzonych badań w ramach pracy doktorskiej wnoszą nowe wiadomości na temat elektrochemicznych procesów na granicy dwóch niemieszających się cieczy w warunkach mikroprzepływowych i mogą być początkiem do wykorzystania elektrochemicznych układów mikroprzepływowych jako kompaktowych urządzeń do analizy składu jakościowego wodnych roztworów soli. Wstępne wyniki z TEMPO jako elektrochemicznym mediatorem są przykładem możliwości przeniesienia eksperymentów do elektrochemicznych układów mikroprzepływowych i wykorzystania ich zalet.

ABSTRACT

The scientific goal of this doctoral dissertation is to examine and understand the basic electrochemical processes that occur at liquid|liquid interfaces in microfluidics. The performed research shows the possibilities of using an electrochemical microfluidic device (EMD). The microfluidic system consisted of a microchannel made with polydimethylsiloxane (PDMS) material and a glass slide contained a sputtered gold electrode system: working, reference and counter, respectively. In the some parts of measurements a silver-silver chloride reference electrode was used. The characteristic feature of these experiments was presence of three-phase boundary located between the working electrode and two immiscible flowing liquid phases.

In the first part of work, the verification of PDMS material compatibility on different organic solvents, it was determined that *N*-octyl-2-pyrrolidone organic solvent (NOP) used in this thesis does not destroy and deform the PDMS microchannel structure and in fact it does not have an impact on electrochemically oxidation of ferrocene (Fc). Also examined was the unusual behavior of the transfer limited current accompanied with the oxidation of Fc and the three-phase boundary was monitored in the function of different flow conditions.

In the next part of thesis, the ion transfer reactions across liquid|liquid interfaces under microfluidic conditions were studied in presence of wide range of anions dissolved in the aqueous phase. The obtained results were in good agreement with the thermodynamic theory of ion transfer processes valid under static three-phase electrode (TPE) and they could be analyzed using a Nernst-like equation. It has been noticed that in presence of more hydrophobic anions in the aqueous phase, during oxidation of decamethylferrocene (DMFc) in the organic phase under the microfluidic control, the transfer of anions to the organic phase occurs according to Nernst-like equation.

The last part of the work is related to electromediated oxidation of diphenylcarbinol (DPC) to benzophenone (BP). It has been shown that various type of (2,2,6,6-Tetramethylpiperidin-1-yl)oxyl (TEMPO) mediator operates at different speeds in conversion of DPC to BP. The obtained results with different TEMPO mediators are good starting point to transfer these experiments to electrochemical microfluidic device which allows to increase the delivering of mediator via convective way of transport.

All results of this dissertation bring a valuable knowledge in electrochemistry at the liquid|liquid interfaces with microfluidics. Electrochemical microfluidic device can be used as

a useful platform which can be employ towards more oriented practical applications e.g. construction of microdevice for analysis of aqueous solutions of anions.

MAJOR ABBREVIATIONS

Abbreviation:	Description
PDMS	Polydimethylsiloxane
ITIES	Interface between two immiscible liquid electrolyte solutions
ET-IT	Electron-ion transfer process
C^+	Aqueous electrolyte cation
An^-	Aqueous electrolyte anion
EMD	Electrochemical microfluidic device
W	Aqueous phase
Ox	The oxidize form of the compound
Red	The reduced form of the compound
Fc	Ferrocene
DMFc	Decamethylferrocene
NB	Nitrobenzene
DCE	1,2-Dichloroethane
DCB	1,2-Dichlorobenzene
TPE	Three-phase electrode
DP	Dinitrophenol
NaOH	Sodium hydroxide
TFE	Thin film electrode
$IrCl_6^{2-}$	Iridium chloride
FIA	Flow injection analysis
PVDF	Polyvinylidene fluoride
PMMA	Polymethylmethacrylate
PS	Polystyrene
PC	Polycarbonate
UV	Ultra violet
ABTS	2,2'-azino-bis(3-ethylbenzothiazoline-6-sulphonic acid)
TEMPO	(2,2,6,6-Tetramethylpiperidin-1-yl)oxyl

$THepA^+$	Tetraheptylammonium cation
$THxA^+$	Tetrahexylammonium cation
TOA^+	Tetraoctylammonium cation
$TPAs^+$	Tetraphenylarsonium cation
TPB^-	Tetraphenylborate anion
$TPBCl^-$	Tetrakis(4-chlorophenyl) borate anion
CV	Cyclic voltammetry
SWV	Square wave voltammetry
CA	Chronoamperometry
GC	Glassy carbon electrode
WE	Working electrode
RE	Reference electrode
CE	Counter electrode
SCE	Saturate calomel electrode
TMPD	*N,N,N′,N′*-tetramethyl-*p*-phenylenediamine
LSCM	Laser scanning confocal microscopy
ACN	Acetonitrile
TFT	Trifluorotoluene
NOP	*N*-octyl-2-pyrrolidone
PPP	4-(3-Phenylpropylpyridine)
TBAP	tetrabutylammonium perchlorate
nBuFc	*N*-Butyloferrocene
DPC	Diphenyl carbinol
BP	Benzophenone
EC’	Catalytic reaction of regeneration of electroactive species in a homogenous reaction

LIST OF CONTENTS

PUBLICATIONS

The work presented in this dissertation is based on the following publications:

- D. Kaluza, W. Adamiak, T. Kalwarczyk, Sozanski K., M. Opallo, M. Jonsson-Niedziolka, *Langmuir* **2013**, *29*, 16034.
- D. Kaluza, W. Adamiak, M. Opallo, M. Jonsson-Niedziolka, *Electrochim. Acta* **2014**, *132*, 158.
- D. Kaluza, M. Jonsson-Niedziolka, S. D. Ahn, R. E. Owen, M. D. Jones, F. Marken, *J. Solid State Electrochem.* **2015**, *19*, 1277.
- W. Adamiak, D. Kałuża, and M. Jönsson-Niedziolka, submitted to *Microfluidics and Nanofluidics*, **2016**.

Other work published during PhD studies:

- S. D. Ahn, D. Kaluza, M. Jonsson-Niedziolka, J. M. Mitchels, F. Marken, *Electroanal.* **2015**, *27*, 1043.

INTRODUCTION

Over the recent years the interest with miniaturizing analytical equipment to one compact miniplatform is still in development. From a theoretical point of view microfluidics is the science and technology of systems, manufacturing and formulating devices that process or manipulate small volumes of liquids. The channel dimensions range from tens to hundreds of micrometers. Over the last years the yield of microfluidic devices was highly develop by application of soft photolithography methods which provide precise performance of microfluidic chip and control the process in each step of its microfabrication. These features make microfluidics devices very popular in diverse analytical methods and for the use as microreactors.

Microfluidic devices have also become dedicated towards electrochemical applications. People started to use electrochemical microfluidic devices for many purposes e.g. as electrochemical sensors or electrochemical fuel cells. The flow stream present in the microfluidic device can be applied as one single flow or as multiphase flows. The biggest advantages of application the electrochemical microfluidic devices over classical electrochemical cell is possibility precisely control mass transfer of electroactive compound using microband electrodes array and finally to obtain the convenient signal to noise ratio.

The main goal of this dissertation is fundamental studies of electrochemical processes at the liquid|liquid|electrode three-phase-boundary in biphasic microfluidic systems. We used microband electrodes located perpendicularly to the flow direction. In order of presented investigations this dissertation contains work connected with transfer of ions driven by electrochemical reaction of electroactive compound dissolved in organic phase with simultaneous electron transfer. The preliminary experiments were concerned o with ion and electron transfer processes between two immiscible liquids. The second chapter presents characteristics of electrochemistry under microfluidic conditions with typical features of experiments.

Chapter 1

ELECTROCHEMICAL PROCESSES AT THE LIQUID|LIQUID INTERFACE

1.1 INTRODUCTION

Liquid|liquid interfaces of two immiscible electrolytes are very common and occur in many forms in the nature. This kind of interface exists in many biological, technological and physico-chemical processes [1].

Investigations of electrochemical processes at the liquid|liquid interface were very intensive in the second half of the 20th century. It established a strong theoretical background of electrochemical processes at the liquid|liquid interface and finally allowed to establish the electrochemistry of liquid|liquid interfaces.

Nowadays this field of science is still useful source of knowledge. The liquid|liquid interfaces are divided into two main systems. The first one is water|polar electrolyte and the second one is where water|non-polar system occurs. In the first case organic electrolytes have high electrical permeativity and allows to dissociate the dissolved electrolyte to ions. In the second case non-polar organic solvent creates surface potential at the liquid|liquid interface [2].

1.2 LIQUID|LIQUID INTERFACE CHARACTERISTIC

Two adjacent immiscible electrolyte solutions form the interface between two immiscible liquid electrolyte solutions (ITIES). In recent years many studies of characteristic the nature of the liquid|liquid interface have been appeared [3,4]. The first studies of the ITIES structure was carried out in tetraalkylammonium bromide salt portioned between water and nitrobenzene [5]. Obtained results gave valuable information about specific adsorption of big tetraalkylammonium ions at the liquid|liquid interface. The shape of the interfacial structure between two immiscible liquids has its own dynamic and the structure of the boundary between them is determined by timescale dependence [6]

The macroscopic structure of the liquid|liquid interface was described in many ways using e.g. scanning electrochemical microscopy [7], neutron reflection measurements [8], measurement of interfacial tension [9] or measurement of the interfacial electric capacity [10]. Another used techniques based on combination of X-ray diffraction [11] and neuron scattering [12].

Three models describe the structure of the liquid|liquid interface. The first one called Gouy, Chapman and Stern describes the liquid|liquid interface similarly to classical interface between the solid electrode and electrolyte. The distinguished feature of this model is presence of two interacting double diffusion layers and possibility of ion penetration or transfer through the interface. Another significant difference between that two approaches is infinite relative permittivity of the solid electrode.

The modification of Gouy, Chapman and Stern model is Verwey and Niessen model and that model assumes that liquid|liquid interface consists with two back-to-back Gouy-Chapman diffuse layers.The adjacent diffuse layers contain two separately positive and negative charges, respectively.

The second model well known as modified Verwey-Niessen (Fig. 1.2.1) contains aspect of interface diffuse layer (inner layer) where oriented dipoles molecules separate two diffuse layers [13].

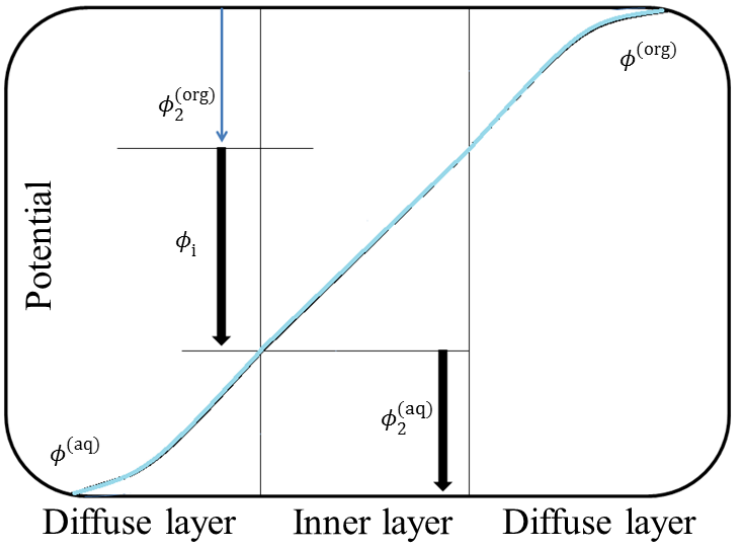

Fig. 1.2.1 Schematic sketch of the modified Verwey-Niessen model of the liquid|liquid interface. $\phi^{w}$and ϕ^{o} symbolize the Galvani potentials of the aqueous and organic phase, respectively. $\phi_2^{w}$and ϕ_2^{o} represent potentials across the space charge regions in the aqueous and organic phase, respectively. ϕ_i is the potential difference across the inner layer.

The liquid|liquid interface is electrified since there is a distribution of dipoles at the boundary. Inside this structure two potentials can be distinguished. The first one concerns potential of the dipoles at the interface vicinity and the second one is related to presence of free charges separated by the interface. The inner potential ϕ (Eq. 1.2.1) of the interfacial diffuse layer is given as the sum of the surface potentials at the vicinity of the interface, χ, and the outer potential of the phase, ψ.

$$\phi = \chi + \psi \qquad \text{(Eq. 1.2.1)}$$

The inner potential magnitude is established via chemical equilibrium conditions which are distributed between organic and aqueous phases [14].

1.2.1 Liquid junction potential of two immiscible liquid electrolytes

At the liquid|liquid interface there is a region where two liquids can interact each other and mass transport processes of components between them take place. Two adjacent immiscible phases potential is established at the liquid|liquid boundary. The liquid junction potential between two immiscible phases is described as the Galvani potential difference (Eq. 1.2.2)

$$\Delta_{(aq)}^{(org)}\phi = \phi_{(org)} - \phi_{(aq)} \qquad \text{(Eq. 1.2.2)}$$

where $\phi_{(org)}$ and $\phi_{(aq)}$ are Galvani potential of the organic and aqueous phase, respectively [14].

From practical point of view three liquid junction types exist (Fig. 1.2.2) [15]:

- The liquid junction between two phases contains the same electrolytes (Fig. 1.2.2a).
- The liquid junction between two phases contains different electrolytes with an ion in common (Fig. 1.2.2b).
- Where the liquid junction is not in agreement with the cases above (Fig. 1.2.2c).

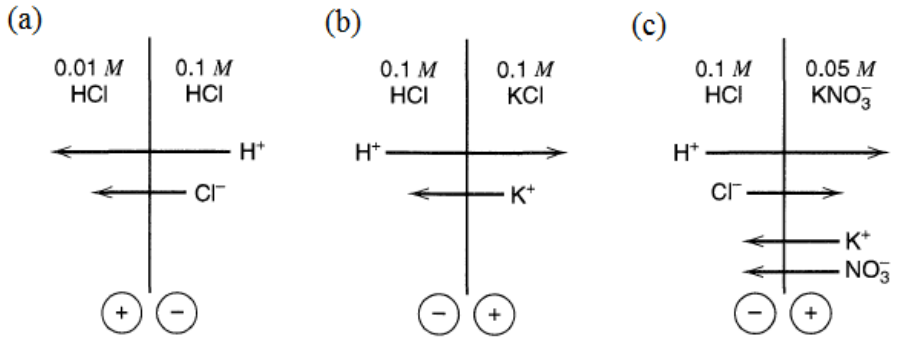

Fig. 1.2.2 Types of the liquid junction [15].

1.2.2 Ideally polarizable and ideally non-polarizable liquid|liquid interface

a) Ideally polarizable liquid|liquid interface.

In case of polarizable liquid|liquid interface the ions are accumulated at the liquid|liquid boundary. In the consequence when the desired potential is applied the ion or electron transfer is not observed. In this situation the liquid|liquid interface behaves like a capacitor. From thermodynamic point of view the value of the Gibbs free energies ΔG for transfer of ions are big so the accumulation of ions at the interface is observed. The ideally polarizable liquid|liquid interface requires the presence of strong hydrophilic ions in aqueous phase and strong hydrophobic in the organic one. It has to be noted that the liquid|liquid interface has a similar structure to standard boundary between electrode and electrolyte solution. In case of classical electrochemical cell the diffusion double layer is located from the one side of the electrode and at given potential the charge is accumulated on the electrode surface q^{E} and in the solution q^{S}. The charges at the electrode and in the solution are equal $q^{\mathrm{E}} = -q^{\mathrm{S}}$. In the opposite situation the liquid|liquid interface has the diffusion double layer which is located in

the both sides of the boundary and the drop of the potential is occurred on the both sides of the boundary [16]. The difference between diffusion layer in electrode-electrolyte solution and at the liquid|liquid interface is depicted in Fig. 1.2.3.

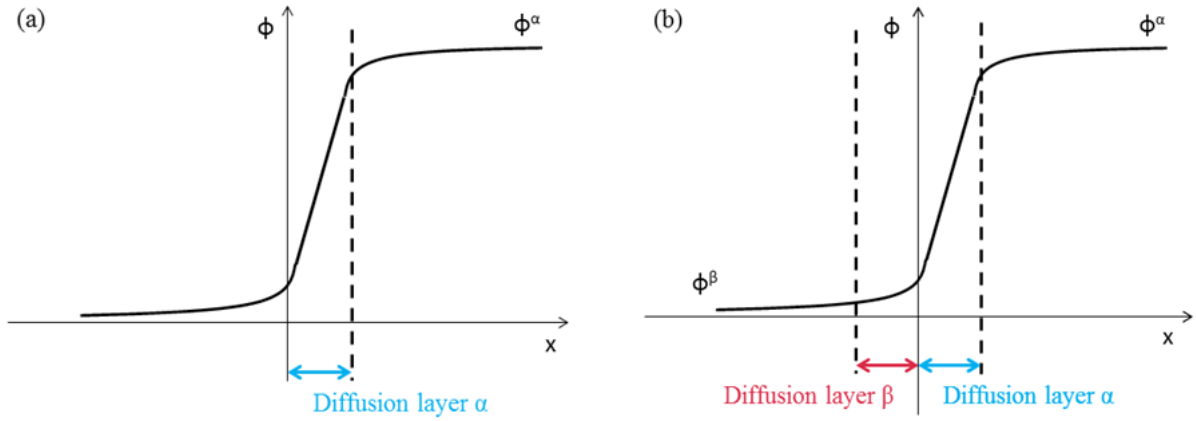

Fig. 1.2.3 (a) Diffusion layer for the electrode|electrolyte solution. **(b)** Diffusion layer for the liquid|liquid interface.

a) Ideally non-polarizable liquid-liquid interface

The characteristic feature of non-polarizable liquid|liquid interface is constant value of $\Delta\phi^{(aq)\rightarrow(org)}$. Since the two adjacent phases contain common ions the applied potential does not affect on $\Delta\phi^{(aq)\rightarrow(org)}$ value. At the liquid|liquid interaface the electrochemical process is carried out by applied potential. In this case two typical situations can be distinguished [17]. The Galvani potential value here $\Delta\phi^{(aq)\rightarrow(org)}$ is determined only by ability the ion to transfer from aqueous phase to the organic one. In the basic example both organic and aqueous phase contain the same electrolyte:

$$C^{+}_{(org)}, An^{-}_{(org)} \mid C^{+}_{(aq)}, An^{-}_{(aq)} \qquad \text{(Eq. 1.2.3)}$$

The potential distribution between two phases in Eq. 1.2.3 has a form:

$$\Delta^{(org)}_{(aq)}\phi = \frac{\Delta\phi^{o,\ (aq)\rightarrow(org)}_{C^+} + \Delta\phi^{o,\ (aq)\rightarrow(org)}_{An^-}}{2} \qquad \text{(Eq. 1.2.4)}$$

In equation above $\Delta\phi^{o,\ (aq)\rightarrow(org)}_{C^+}$ and $\Delta\phi^{o,\ (aq)\rightarrow(org)}_{An^-}$ indicates the standard transfer potentials for the cations and anions, respectively. Since the concentrations of both ions are fixed, the value of $\Delta\phi^{(aq)\rightarrow(org)}$ depends on values of standard values of the Galvani potentials of ions.

$\Delta\phi_{C^+}^{o,\ (aq)\rightarrow(org)}$ and $\Delta\phi_{An^-}^{o,\ (aq)\rightarrow(org)}$. The next situation relates to the case where two liquid phases have the same ion e.g. cation (Eq. 1.2.5).

$$C^+, An_1^-|C^+, An_2^- \qquad \text{(Eq. 1.2.5)}$$

In this particular case the distribution potential is described as:

$$\Delta_{(aq)}^{(org)}\phi = \Delta\phi_{C^+}^{o,\ (aq)\rightarrow(org)} + \frac{RT}{F}\ln\frac{c_{C^+}(aq)}{c_{C^+}(org)} \qquad \text{(Eq. 1.2.6)}$$

The liquid junction potential of this system depends on C^+concentration and value of $\Delta\phi_{C^+}^{o,\ (aq)\rightarrow(org)}$ [16].

Non-polarizable liquid|liquid interfaces have a many application including e.g. design of reference electrodes. Important aspect of these electrodes is fact that their potential does not vary with current and finally it gives a possibility to control potential between the working (indicator) electrode. Non-polarizable electrodes give opportunity also to study processes with ion and charge transfer [18].

1.3 THERMODYNAMIC ASPECT OF ION TRANSFER PROCESSES ACROSS THE LIQUID|LIQUID INTERFACE

In the situation when the aqueous electrolyte contains component *i* and when it has a contact with the adjacent organic one, the transfer of component *i* to the second liquid can occur due to difference in their chemical potentials. In the situation when the concentration of component *i* is the same in both phases, the chemical potentials of both phases are equal (Eq. 1.3.1):

$$\mu_i^{(aq)} = \mu_i^{(org)} \qquad \text{(Eq. 1.3.1)}$$

The chemical potential of component *i* in aqueous or in organic phase is defined as:

$$\mu_i^{(aq)\ or\ (org)} = \mu_i^{o,\ (aq)\ or\ (org)} + RT\ln a_i^{(aq)\ or\ (org)} \qquad \text{(Eq. 1.3.2)}$$

where $\mu_i^{o,\ (aq)\ or\ (org)}$ is the standard chemical potential of component i in the aqueous or in the organic phase. R depicts the gas constant and T is temperature. The activity coefficient a of the component i in both phases in the Eq. 1.3.2 can be rewritten as:

$$\frac{a_i^{(org)}}{a_i^{(aq)}} = \exp\left(\frac{\mu_i^{o,\ (org)} - \mu_i^{o,\ (aq)}}{RT}\right) \qquad \text{(Eq. 1.3.3)}$$

If the conditions of pressure and temperature are assumed as constant, the expression for the standard chemical potential can be define as the Gibbs free energy $\mu_i^{o,\ (aq)\ or\ (org)} = G_i^o$ and Eq. 1.3.3 can be rewritten as:

$$\frac{a_i^{(org)}}{a_i^{(aq)}} = \exp\left(\frac{G_i^{o,\ (org)} - G_i^{o,\ (aq)}}{RT}\right) \qquad \text{(Eq. 1.3.4)}$$

where $G_i^{o,\ (aq)}$ and $G_i^{o,\ (org)}$ are the Gibbs free energy of solvation of component i in the aqueous and organic phases, respectively. The difference between the values of the Gibbs free energy of solvation gives finally the value of the Gibbs free energy of transfer of component i from the aqueous to organic phase $\Delta G_i^{o,\ (aq)\rightarrow(org)}$. To summarize the meaning of Eq. 1.3.4, the activity of component i in both phases is characterized by the values of the Gibbs free energies of the transfer of that compound [2].

1.4 CHARGE TRANSFER PROCESSES ACROSS TWO IMMISCIBLE PHASES

Charge transfer processes across two immiscible electrolyte solutions can be divided into ion and electron transfer.

The ion transfer mechanism concerns the movement of ions from the aqueous phase to the organic and vice versa. In the simplest case aqueous phase contains a redox couple $Ox^1_{(aq)}/Red^1_{(aq)}$ and organic phase contains a redox couple $Ox^2_{(org)}/Red^2_{(org)}$. In the case when none of the redox components is transferred across the liquid|liquid interface only electron transfer can be observed. The parameter characteristic for ion transfer processes is Gibbs free energy which is required to move the ion from one phase to another. It can be distinguished four types of processes across the ITIES that can be driven electrochemically.

a) Simple Ion Transfer

The simple ion transfer between two immiscible phases is achieved when the ion is moved directly from one phase to another. The driving force of whole processes is the Galvani potential difference between the phases and providing the enough value of the Gibbs transfer energy of the ions. The pathway of ion transfer process includes three main stages:

- mass transport in one phase (in the aqueous or in organic) to the interface,
- direct ion transfer reaction,
- mass transfer in the second phase from interface to the bulk.

From practical point of view it can be distinguished two kinds of ion transfer process according to which type of liquid|liquid interface is taking account. In case of ideally polarizable liquid|liquid interface (Fig. 1.4.1 a) the electrostatic equilibrium between two phases occurs due to the presence of strong hydrophilic ions in aqueous phase and strong hydrophobic ions present in the organic one [19].

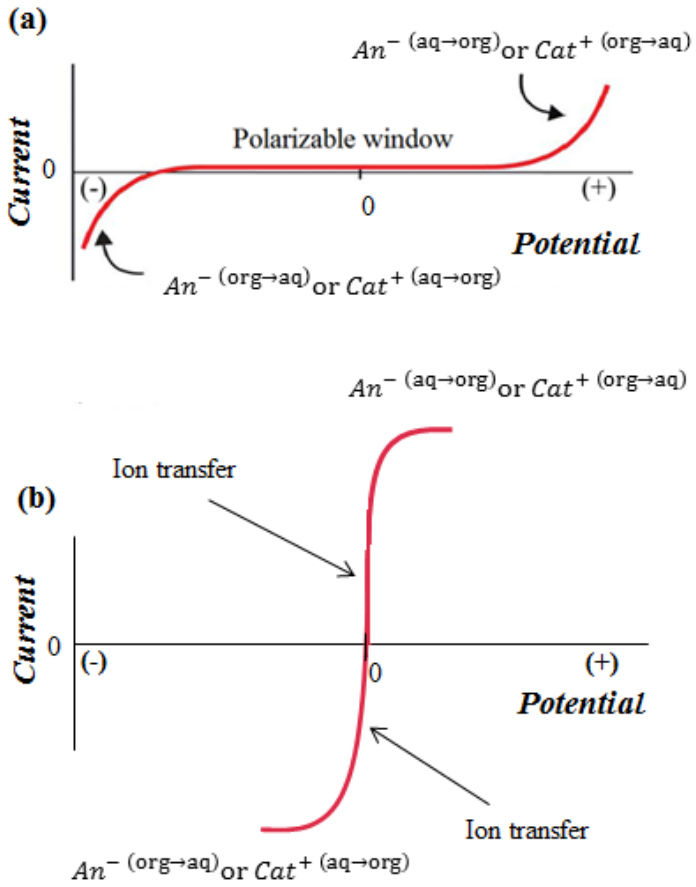

Fig. 1.4.1 Ideally **(a)** polarizable and **(b)** non-polarizable liquid|liquid interface voltammograms.

The range of the polarization window depends on the difference in lipophilicity of ions in both phases. When the potential is applied in is not too far from the equilibrium value, due to

the high values of ΔG in both adjacent phases, there is no current flow. When the value of applied potential reaches the extremes, an ionic current indicating the transfer of ions can be registered.

In the situation concerning a non-polarizable liquid|liquid interfaces, the equilibrium state is present when no potential is applied and distribution of common ion in both phases determines the liquid junction potential $\Delta\phi^{(\mathrm{aq})\rightarrow(\mathrm{org})}$. In case of polarization in region of negative values cations present in the organic phase begin to move towards the aqueous phase according to the Eq. 1.2.6 where the ratio of C^+ concentration in aqueous and in organic phase should increase due to that a more negative $\Delta\phi^{(\mathrm{aq})\rightarrow(\mathrm{org})}$ is applied. In opposite situation when more positive potential is applied the transfer of cations from organic to aqueous phase can be seen. The characteristic current for these two cases are visible in Fig. 1.4.1b. The same reasoning can be applied for the anions, but with opposite sign.

b) Assisted ion transfer

The whole idea of the assisted ion transfer based on adding the agent which facilitates the transport of studied ion. The reaction is also involving the neutral species like a ligands which can be distributed on the both side of the liquid|liquid interface. The different types of assisted ion transfer can be distinguished (Fig. 1.4.2) [20]:

- the ion transfer by interfacial complexation (Fig. 1.4.2a),
- transfer by interfacial decomplexation (Fig. 1.4.2b),
- complexation in the aqueous phase followed by transfer (Fig. 1.4.2c),
- assisted ion transfer followed by organic phase complexation; where the ion is bonded with ligand in the organic phase (Fig. 1.4.2d).

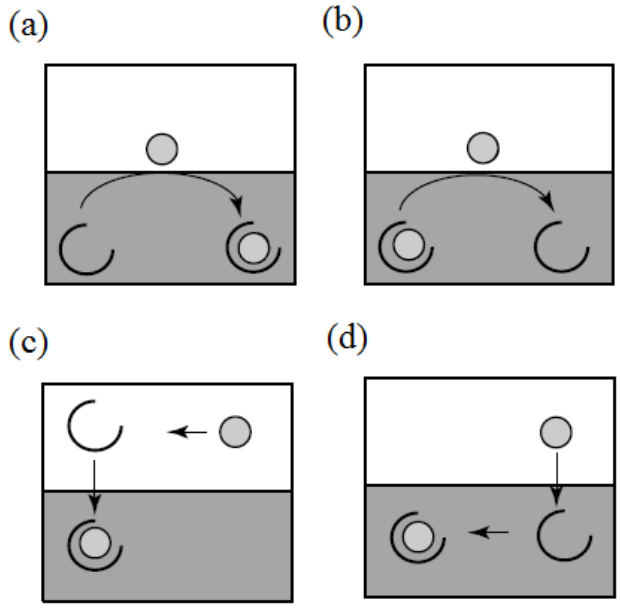

Fig. 1.4.2 Schematic diagrams of assisted ion transfer reactions [19].

The assisted ion transfer plays an important role in electroanalytical studies. In 1979 Koryta et al. studied first time the transfer of potassium from water to nitrobenzene assisted by the crown ether ionophore dibenzeno-18-crown-6 and it was first electrochemical observation of the assisted ion transfer process [21].

This type of process has been applied to study the transfer of molecule: *N*, *N*,-Dicyclohexyl-*N*', *N*'-diisobutyl-*cis*-cyclohexane-1,2-dicarboxyamide across the water|l,2-dichloroethane interface [22], interfacial complexation reaction of Sr^{2+} with octyl(phenyl)-*N*, *N*-diisobutylcarbamoylmethylphosphine oxide [23], facilitated ion transfer reactions of different ligands across oil|water interfaces [24]. In field of pharmacokinetics Senda et al. performed the investigations of drug in example of 2,4-dinitrophenol as the facilitated agent of the ion transfer [25]. The ionophores application in assisted ion transfer has been shown by Simon and coworkers who have developed 2-dioxaazelaamides as ionophores [26].

c) Electron transfer

The third type of the processes which can takes place at the liquid|liquid interface is heterogeneous electron transfer. This particular kind of process can happen when two adjacent immiscible phases contain separated redox species. The key point of whole process is transfer of electron from donor in the one phase to the acceptor of electron in second one. For the simple processes the electron transfer equation has a form of:

$$Ox_1^{(aq)} + Red_2^{(org)} \rightleftharpoons Red_1^{(aq)} + Ox_2^{(org)} \qquad \text{(Eq. 1.4.1)}$$

The Nernst equation in that case has a form:

$$\Delta\phi^{(\mathrm{aq})\rightarrow(\mathrm{org})} = \Delta\phi_{e^-}^{o,\ (\mathrm{aq})\rightarrow(\mathrm{org})} + \frac{RT}{nF}\ln\left(\frac{a_{\mathrm{Ox}_1}^{(\mathrm{aq})} a_{\mathrm{Red}_2}^{(\mathrm{org})}}{a_{\mathrm{Ox}_2}^{(\mathrm{org})} a_{\mathrm{Red}_1}^{(\mathrm{aq})}}\right) \qquad \text{(Eq. 1.4.2)}$$

where $\Delta\phi_{e^-}^{o,\ (\mathrm{aq})\rightarrow(\mathrm{org})}$ is the standard potential of electron transfer at the interface between organic and aqueous phase. The characteristic feature of the electron transfer processes at the liquid|liquid interface is coexistence of two species in the adjacent phases (easy oxidizable in one phase and easily reducible in the second one) if the Galvani potential difference between two phases has a value that the Gibbs transfer energy for equilibrium is positive.

The complicated aspect of electron transfer reaction is precision in resolving of the reaction mechanism. The important thing is proper selection of system where the Gibbs energy of transfer of the reactants and products are known and finally the registered current comes directly from electron transfer and the reaction products do not cross the liquid|liquid interface. It is also necessary to notice that the supporting electrolyte should be appropriate to avoid mistake in measuring the current from ion transfer process instead to measure the electron transfer current [13].

Samec and coworkers conducted one of the first experiment where electron transfer were associated with the registered current at the liquid|liquid interface. In these studies the simple system where electron transfer reaction of hexacyanoferrate redox associated with electrooxidation of ferrocene (Fc) in organic nitrobenzene (NB) solvent was showed. In past decades many studies with electron transfer process were carried out [27]. The popular experimental systems consisted with electroactive species dissolved in organic phase like: Fc [28,29], decamethylferrocene (DMFc) [29], porphyrin derivatives [30] were good examples of electron transfer reactions. Organic solvents used in biphasic systems with water were e.g.: nitrobenzene (NB) [31,32], 1, 2-dichloroethane (1,2-DCE) [33] or 1, 2-dichlorobenzene (1,2-DCB) [29,34]. The main aspects of these work was related with the electron transfer systems to find out the rate constant of the process or to estimate a kinetic of the electron transfer due to used redox species.

d) Ion transfer process driven by electrochemical reactions

The ion transfer processes across liquid|liquid interface can be also driven by electrochemical reaction of the redox species dissolved e.g. in the droplet of the organic solvent and submerged in the aqueous electrolyte (Fig. 1.4.3a). According to applied potential to the

working electrode, two main processes can occur. Fig. 1.4.3b shows the system where electrooxidation reaction inside the organic droplet occurs. When the potential is scanned towards more positive potentials the anions have been forced into the organic phase. As a result of electrooxidation reaction inside the droplet, anions cross the liquid|liquid interface between aqueous and organic phase. In reverse process when the negative potential is applied the anions expulsion from the droplet towards aqueous phase can be observed (Fig. 1.4.3c) [35].

The development of ion transfer driven electrochemical reaction is extensively studied topic [35]. The ion transfer process plays a crucial role in many systems such as biological membranes or in physiology [36,37]. In a field of biological applications the amino acids [38], oligo-peptides [39] or redox liquids [40] were investigated. The two major ways of performing the ion transfer processes can be distinguished: the three-phase electrode or thin-film electrode system [41].

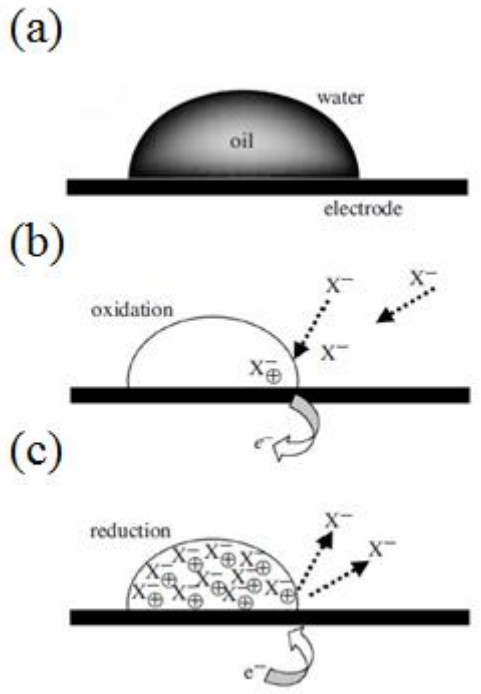

Fig. 1.4.3 The scheme of **(a)** an immiscible organic droplet sessiles onto electrode surface and submerged into aqueous electrolyte solution; **(b)** an electrochemical oxidation within the droplet and transfer of anions from aqueous towards organic phase; **(c)** the reverse electrochemical reduction process within the droplet connected with expulsion of anions from organic to aqueous phase [35].

1.5 THREE-PHASE ELECTRODE (TPE) CONSISTING OF A DROPLET WITH ELECTROACTIVE COMPOUND

The characteristic feature of the three-phase electrode system is close contact between each phase. The surface of the working electrode is not covered completely by organic solvent and the interface boundary exists between three phases.

The three-phase boundary is defined by the line where three phases meet (Fig. 1.5.1) [42]. The most common three-phase electrode system comprises a droplet of organic solvent with electroactive compound on an electrode immersed into an aqueous electrolyte. Other examples of the three-phase electrode setup are microdroplets arrays which cover the electrode surface or emulsions at which oil droplets are dispersed in water phase and some of droplets can be in contact with surface of the working electrode [43]. Or simply a wire or flat electrode immersed through a liquid|liquid interface [44,45].

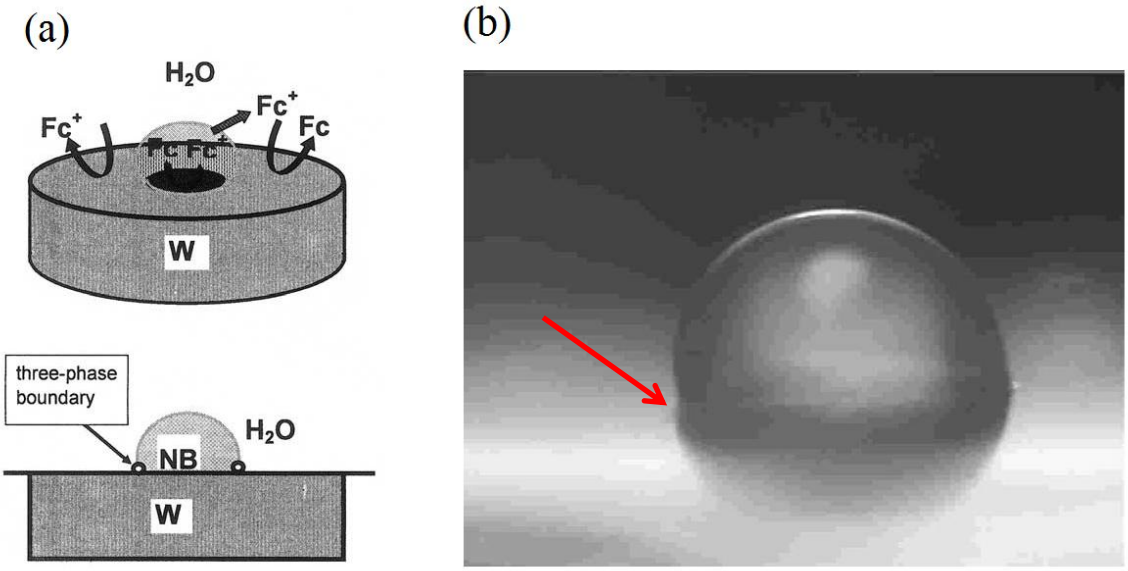

Fig. 1.5.1 (a) Organic solvent droplet onto working electrode (here: W) surface. Three-phase boundary is located in the form of a ring at the NB|water|electrode. **(b)** The photograph of the droplet of nitrobenzene on the working electrode surface in an aqueous solution. The red arrow indicates three-phase boundary [42].

A very useful feature of the TPE is the fact that the organic droplet does not need to contain a supporting electrolyte to provide sufficiently high conductivity of the solution. Good example of the experiments with TPE both droplet of the organic solvent and electroactive species were immiscible in water. Spectroelectrochemical experiments using a Pt microelectrode submerged in an organic droplet of nitrobenzene containing decamethylferrocene as the electroactive compound and other measurements with Pt microelectrodes immersed in a droplet have shown the pathway of the electrode reaction in

TPE system. Due to appropriate polarization of the working electrode, the electrochemical reaction in TPE starts at the three-phase boundary and expands towards the center of the droplet [46]. This useful feature of the TPE makes it possible to extends the range of organic solvents that can be used to non-polar solvents like toluene [47], hexane [48], decane [49], hexadecane and other alkanes [50,51].

1.5.1 Thermodynamic of TPE

Thermodynamic aspect of the TPE describes a three-phase electrode as redox center and shows electrochemical correlation between each phase.

The picture below shows a sketch of three-phase electrode system with an organic droplet immobilized onto the working electrode surface (I. phase) (Fig. 1.5.2a).

In electrochemical processes which take place at the three-phase boundary the electron transfer between the organic droplet (II. phase) and I. phase is connected with the ion transfer across the II. phase and the electrolyte solution (III. phase) to provide charge neutrality inside the droplet (Fig. 1.5.2b) [52].

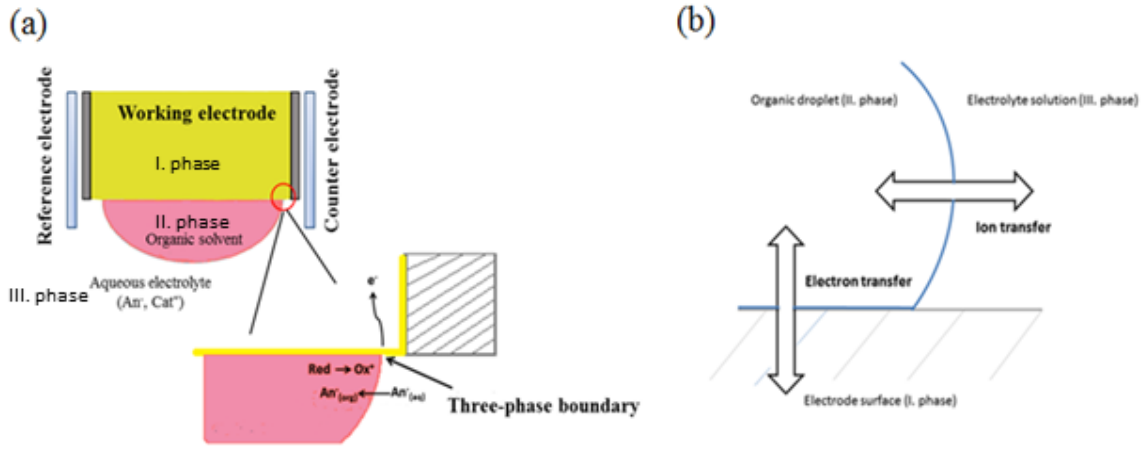

Fig. 1.5.2 (a) Schematic sketch of the three-phase electrode with the organic droplet which is attached onto working electrode surface. The organic droplet contains electroactive species. The zoom inset in this sketch shows details of electrochemically driven ion transfer processes. The reference and counter electrode are drawn, respectively. **(b)** Illustration of parallel ion and electron transfer process at the three-phase electrode system.

The TPE experimental approach is often used to perform measurements to determine the standard Gibbs energy of ion transfer from one liquid phase to the another. The general formula for the reaction takes place in the droplet modified electrode (Fig. 1.5.2a) can be given by formula:

$$\mathrm{Red}_{(\mathrm{org})} + \mathrm{An}^{-}_{(\mathrm{aq})} - \mathrm{e}^{-} \rightleftharpoons \mathrm{Ox}^{+}_{(\mathrm{org})} + \mathrm{An}^{-}_{(\mathrm{org})} \qquad \text{(Eq. 1.5.1)}$$

In case above the electrooxidation process in droplet occurs and transfer of anions takes place to maintain electroneutrality which requires the same amount of the charge inside the droplet. The electroneutrality condition require equal concentrations of oxidized forms and anions:

$$c_{\mathrm{Ox}^+_{(\mathrm{org})}} = c_{\mathrm{An}^-_{(\mathrm{org})}} \qquad \text{(Eq. 1.5.2)}$$

In the opposite case when the electroactive compound undergoes electroreduction (Eq. 1.5.3), transfer of cations can be expected:

$$\mathrm{Ox}_{(\mathrm{org})} + \mathrm{Cat}^+_{(\mathrm{aq})} + \mathrm{e}^- \rightleftharpoons \mathrm{Red}^-_{(\mathrm{o})} + \mathrm{Cat}^+_{(\mathrm{o})} \qquad \text{(Eq. 1.5.3)}$$

The electroneutrality in the electroreduction reaction requires:

$$c_{\mathrm{Red}^-_{(\mathrm{org})}} = c_{\mathrm{Cat}^+_{(\mathrm{org})}} \qquad \text{(Eq. 1.5.4)}$$

The formal potentials of the electroactive compound in Eq. 1.5.1 and Eq. 1.5.3 can be derived from the Nernst-like equation [52]. Concerning the reaction (Eq. 1.5.1) where the electroactive compound undergoes electrooxidation the formal potential is given by:

$$E^{\mathrm{o}\prime}_{\mathrm{Ox/Red}} = E^{\mathrm{o}}_{\mathrm{Ox}^+_{(\mathrm{org})}/\mathrm{Red}_{(\mathrm{org})}} + \Delta\phi^{\mathrm{o},\ (\mathrm{aq})\rightarrow(\mathrm{org})}_{\mathrm{An}^-} - \frac{RT}{F}\ln c_{\mathrm{An}^-_{(\mathrm{aq})}} + \frac{RT}{F}\ln\frac{c^*_{\mathrm{Red}_{(\mathrm{org})}}}{2} \qquad \text{(Eq. 1.5.5)}$$

where $E^{\mathrm{o}\prime}_{\mathrm{Ox/Red}}$ indicates formal potential of the redox couple $\mathrm{Ox}^+/\mathrm{Red}$ in the organic droplet and $E^{\mathrm{o}}_{\mathrm{Ox}^+_{(\mathrm{org})}/\mathrm{Red}_{(\mathrm{org})}}$ describes the standard potential for the $\mathrm{Ox}^+_{(\mathrm{org})}/\mathrm{Red}_{(\mathrm{org})}$ species. $\Delta\phi^{\mathrm{o},\ (\mathrm{aq})\rightarrow(\mathrm{org})}_{\mathrm{An}^-}$ is the standard potential of transfer of anions from the aqueous to the organic phase; $c^*_{\mathrm{Red}_{(\mathrm{org})}}$ is initial concentration of the electroactive species in the organic phase. For the reaction (Eq. 1.5.3) the Nernst equation characterizes the process where the cations are moved to the organic phase:

$$E^{\mathrm{o}\prime}_{\mathrm{Ox/Red}} = E^{\mathrm{o}}_{\mathrm{Ox}^+_{(\mathrm{org})}/\mathrm{Red}_{(\mathrm{org})}} + \Delta\phi^{\mathrm{o},\ (\mathrm{aq})\rightarrow(\mathrm{org})}_{\mathrm{Cat}^+} + \frac{RT}{F}\ln c_{\mathrm{Cat}^+_{(\mathrm{aq})}} + \frac{RT}{F}\ln\frac{2}{c^*_{\mathrm{Ox}_{(\mathrm{org})}}} \qquad \text{(Eq. 1.5.6)}$$

The characters which are included in above formula have the analog meaning to the previous Eq. 1.5.5. The formal potential strongly depends on the facility of the ions present in the aqueous phase to transfer to the organic phase. The nature of the ion in the aqueous phase is related with the value the standard potential of transfer ions (anions or cations) $\Delta\phi^{o,\ (aq)\rightarrow(org)}_{An^-\text{or }Cat^+}$ from the aqueous phase to the organic phase. Analyzing the ion transfer in the situation of transfer of anions to the organic phase the more negative is the value of $\Delta\phi^{o,\ (aq)\rightarrow(org)}_{An^-}$ indicates the presence the more lipophilic anions in the aqueous phase. Due to this rule the electrooxidation of component in organic droplet will occur at more negative potentials. In the opposite situation when the electroactive compound is going through an electroreduction reaction, more lipophilic cations are present in the aqueous phase the more positive will be $\Delta\phi^{o,\ (aq)\rightarrow(org)}_{An^-}$ [52].

The three-phase electrode setup offers a lot of advantages in field of study ion and electron transfer processes. The first one is eliminating the problem of low conductivity of the organic solvent according to the presence of the three-phase boundary. TPE also offers electrochemical measurements without using the supporting electrolyte in the organic phase. The presence of the three-phase boundary gives opportunity also to perform the measurements without applying a reference electrode into the organic phase. It is also not necessary to employ a four electrode setup.

The study of the ion and electron transfer processes with using the three-phase electrodes is popular among different techniques. A very interesting parameter to analyze is the partition coefficient $P = \frac{a_i^{(org)}}{a_i^{(aq)}}$ where a is the activity coefficient of the electroactive species in the biphasic systems such as both organic and aqueous phase [6]. The partition coefficient is very important parameter in pharmaceutical sciences where the drugs metabolism and realize is investigated [53]. Girault introduced ionic partition diagrams which are drawn the equiconcentrated boundaries between two phases as a function of the Galvani potential difference.

1.5.2 Determination of transfer potentials and standard Gibbs energies of transfer of anions across the liquid|liquid interface

In this subchapter the methodology of determination of thermodynamic parameters of the ion transfer process like transfer potential or standard Gibbs energies will be explained. This methodology is performed with utilizing the three-phase electrode system.

The idea of whole process is based on the electrochemical oxidation reaction of the hydrophobic electroactive species dissolved in the organic droplet. The redox species uses for the ion transfer investigations should be [54]:

- immiscible in aqueous phase,
- reversible electrooxidizable and electroreducible,
- chemically neutral for the transferred ions.

The typical electroactive species using in electrochemical studies of ion transfer processes are e.g. Fc or DMFc (Fig. 1.5.3). They are commonly used as the calibrating redox couple for a nonaqueous solvents and both oxidized and reduced form (Fc/Fc^+ or $DMFc/DMFc^+$) are stable in many organic solvents and behave according to the Nernst characteristic.

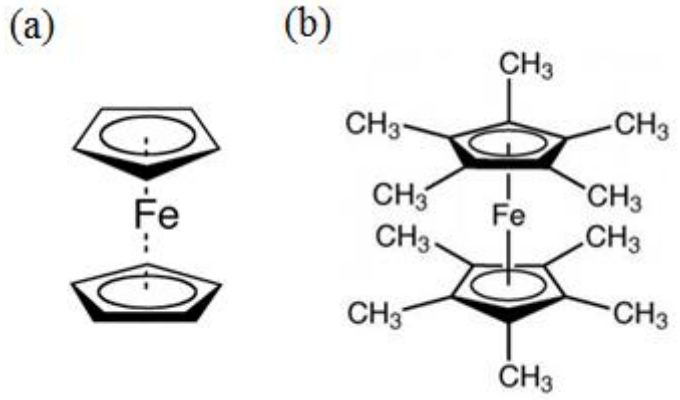

Fig. 1.5.3 (a) Chemical structure of ferrocene (Fc) and **(b)** decamethylferrocene (DMFc).

The electroanalytical methods like voltammetry or square-wave voltammetry can be utilized to monitor progress of the transfer of the anions across liquid|liquid interface driven by electrochemical reaction inside the droplet of the organic solvent. The overall electrochemical reaction at the three-phase boundary in the presence of a reference standard with the transfer of anions are described in previous subchapter (Eq. 1.5.1).

Fig. 1.5.4 shows the square wave voltammograms of DMFc in a droplet of nitrobenzene immobilized on a graphite electrode and submerged in aqueous solutions

of amino-acids. The transfer of anions of aminoacids is accompanied with redox reaction inside the droplet due to their values of standard Gibbs transfer energies [55].

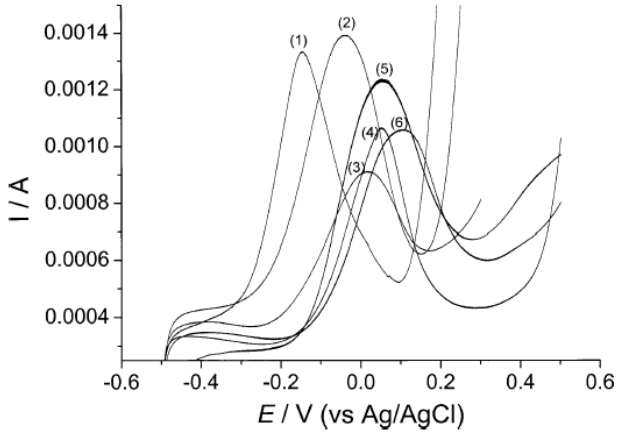

Fig. 1.5.4 Square-wave voltammograms of nitrobenzene droplet immobilized onto graphite working electrode surface containing 0.1 mol dm^{-3} DMFc. The electrode with the droplet is submerged in aqueous solutions containing 1 mol dm^{-3} NaOH and 1 mol dm^{-3} sodium salts of the following amino-acids: tryptophane (1), tyrosine (2), methionine (3), histidine (4), lysine (5), and proline (6) [55].

The ion transfer reaction can be analyzed by showing the dependence of redox reaction peak $E_{\mathrm{Ox}^{+}_{(\mathrm{org})}/\mathrm{Red}_{(\mathrm{org})}}$ versus the standard potential of transfer of anions (Fig. 1.5.5) [29].

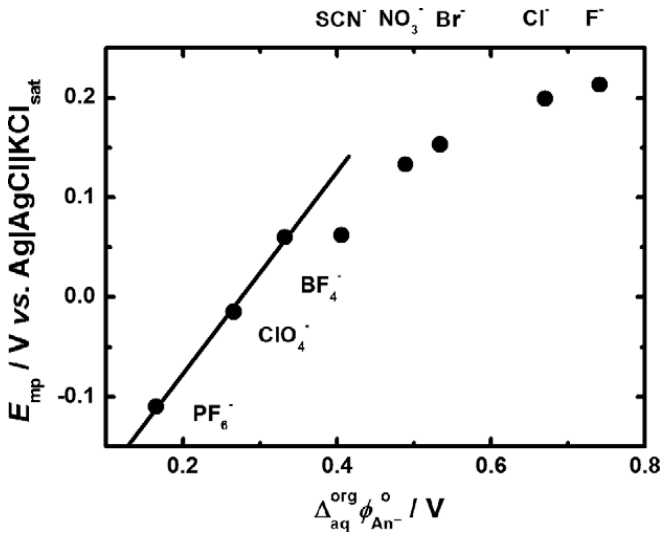

Fig. 1.5.5 Dependence of the mid-peak potential in case of DMFc/$DMFc^{+}$ couple, E_{mp} on the standard transfer potential of anions $\Delta\phi^{\mathrm{o},\ (\mathrm{aq})\rightarrow(\mathrm{org})}_{\mathrm{An}^{-}}$ [29].

To determine the Gibbs transfer energy of ions towards organic phase the key point is to analyze the ion solvation in aqueous and organic phase which is the important aspect to understand the behavior of electrolyte solution. Solvation is the process of where the molecules of solvent surround the solute and this process has the most crucial impact on

the distribution of the solute in the solution. On the way to calculate the standard Gibbs free energy of the ion solvation ΔG_s^o the Max Born equation can be used. Born assumed that thesolvation of ion can be compared to electric work necessary to move the ion from the vacuum to the solvent:

$$\Delta G_s^o = -\frac{z_i^2 e^2 N_A}{8\pi\varepsilon_o r_i}\left(1-\frac{1}{\varepsilon_r}\right) \quad \text{(Eq. 1.5.7)}$$

where z_i is the charge number of the ion charge, e is the elementary charge, N_A is the Avogadro constant, r_i is the ionic radius, ε_o is the diaelectric permittivity of vacuum and ε_r is relative permittivity of the solvent [56]. The difference between the standard Gibbs free energy of solvation in aqueous phase and the organic droplet:

$$\Delta G_{An^-}^{o,\ (aq)\rightarrow(org)} = G_{An^-}^{o,\ (org)} - G_{An^-}^{o,\ (aq)} \quad \text{(Eq. 1.5.8)}$$

gives the Gibbs transfer energy of ions $\Delta G_{An^-}^{o,\ (aq)\rightarrow(org)}$. The values of the standard potential of transfer of anions are given by:

$$\Delta\phi_{An^-}^{o,\ (aq)\rightarrow(org)} = -\frac{\Delta G_{An^-}^{o,\ (aq)\rightarrow(org)}}{zF} \quad \text{(Eq. 1.5.9)}$$

where z is the charge number of the process and F is the Faraday constant. To identify the proposed mechanism of the ion transfer process (Eq. 1.5.1) the dependence of the formal potentials on the logarithm of concentration of anions in the aqueous phase can be performed [57].

In the Fig. 1.5.6 example values of $\Delta\phi_{An^-}^{o,\ (org)\rightarrow(aq)}$ and $\Delta G_{An^-}^{o,\ (org)\rightarrow(aq)}$ as well for different polyanions, obtained for nitrobenzene|water interface are shown. The measurements show that the values of transfer potential and the Gibbs free energy depend on the ionic size and charge [2].

Tab. 1.5.1 Values of $\Delta\phi^{o,\ (org)\rightarrow(aq)}_{An^-}$ and $\Delta G^{o,\ (org)\rightarrow(aq)}_{An^-}$ of polyanions for the nitrobenzene|aqueous system. r is the polyanion radius and E^o is the surface electric field strength. Data has been taken from ref. [2].

Polyanion	r (nm)	E^a (10^{10} V m^{-1})	$\Delta\phi^{o,\ (org)\rightarrow(aq)}_{An^-}$ (V)	$\Delta G^{o,\ (org)\rightarrow(aq)}_{An^-}$ (kJ mol^{-1})
α, β-$[XM_{12}O_{40}]^{4-}$ (X = Si, Ge; M = Mo, W)	0.56[b]	-1.84	0.067 ± 0.003	25.9
α, β-$[XM_{12}O_{40}]^{3-}$ (X = P, As; M = Mo, W)	0.56[b]	-1.38	0.248 ± 0.004	71.8
α, β-$[X_2Mo_{18}O_{62}]^{3-}$ (X = P, As)	0.648[c]	-2.06	0.005 ± 0.000	2.9
α-$[S_2Mo_{18}O_{62}]^{4-}$	0.648[c]	-1.37	0.269	103.8
$[S_2VMo_{17}O_{62}]^{5-}$	0.648[c]	-1.72	0.085	41.0
$[P_2Mo_{17}O_{61}]^{4-}$ (containing $P_2O^{4-}_7$)	0.644[c]	-1.39	0.239	92.2
$[Mo_6O_{19}]^{2-}$	0.437[c]	-1.51	0.164	31.6
$[VMo_5O_{19}]^{3-}$	0.437[c]	-2.26	-0.119	-34.4
α-$[Mo_8O_{26}]^{4-}$	0.435[c]	-2.45	-0.137	-52.9

1.6 THIN FILM ELECTRODES (TFE)

The working electrode surface is covered completely by the organic droplet in case of thin film electrodes (TFE) (Fig. 1.6.1). In that reason due to the absence of three-phase boundary between the electrode and two immiscible liquids is necessary to add supporting electrolyte to the organic phase to ensure sufficient conductivity to perform electrochemical measurements [58]. It is also possible to add electrolyte of the aqueous phase by partition. The potential difference between the organic and the aqueous phase can be controlled by the concentrations of common ions present in two phases. In case of TFE in contrast to TPE the whole electrode surface is involved in electrochemical reaction. In fact the electron transfer between electroactive compound in the organic droplet induces simultaneously the ion transfer process between the aqueous and the organic phase to preserve electroneutrality of the organic phase.

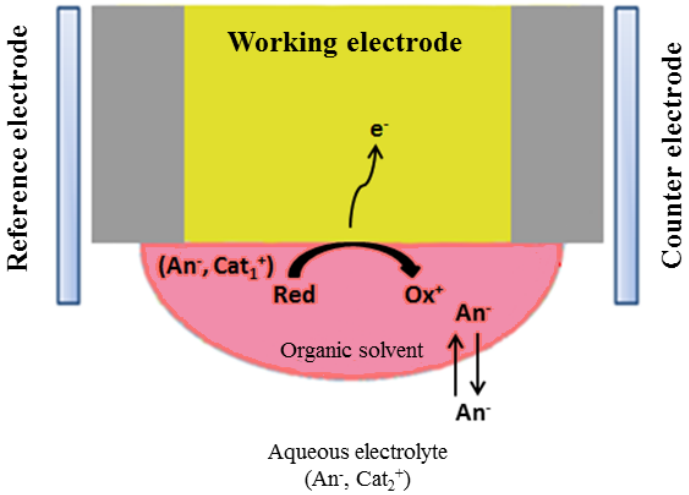

Fig. 1.6.1 The schematic picture of the TFE where the thin film of the organic solvent containing the supporting electrolyte with the common ion (An^-) with the aqueous phase. The electrochemical reaction at the electrode surface is accompanied with the transfer of anions (An^-) to neutralize the positive charge (Ox^+) inside the droplet. On the right and left side of the working electrode the reference electrode and counter one are located. The whole electrode system is immersed in aqueous electrolyte solution.

The application aspect of TFE in electrochemistry is clearly visible in electroanalysis. L'Her and coworkers applied TFE configuration to determine the Gibbs transfer energy of strongly hydrophilic ions and calculated values that were close to the literature data [59]. Basically, they registered square-wave voltammograms of electrooxidation of DMFc as a redox species. The organic thin film electrodes were submerged in aqueous solutions on ions and the organic thin film and aqueous solution contained electrolytes with the ions in common. Further examples of TFE applications are found in a studies of organic redox liquids [60,61] or measuring the rate of electron transfer across liquid|liquid interface with electroactive compounds like 1,1′,3,3′ tetrakis (2-methyl-2-hexyl) ferrocene in thin layer of NB and $IrCl_6^{2-}$ in aqueous solution [62] or 7,7,8.8 tetracyanoquinodimethane in 1,2-DCE [63].

1.7 BIBLIOGRAPHY

[1] Z. Koczorowski, Z. A. Figaszewski, A. D. Petelska, *Elektrochemia cieczowych granic fazowych*, WUM, **2011**.

[2] A. G. Volkov, *Liquid Interfaces in Chemical, Biological, and Pharmaceutical Applications* **2001**, Marcel Dekker, New York.

[3] B. D'Epenoux, P. Seta, G. Amblard, C. Gavach, *J. Electroanal. Chem.* **1979**, *99*, 77.

[4] H. H. Girault and D. J. Schiffrin, *J. Electroanal. Chem.* **1985**, *195*, 213.

[5] C. Gavach, P. Seta, B. D'Epenoux, *J. Electroanal. Chem.* **1977**, *83*, 225.

[6] C. G. Zoski, *Handbook of Electrochemistry* **2007**, Elsevier.

[7] Y. Shao, M. V. Mirkin, *J. Phys. Chem. B* **1998**, *102*, 9915.

[8] G. Fragneto-Cusani, *J. Phys.: Condens. Matter* **2001**, 13, 4973.

[9] S. Rana, X. Yu, D. Patra, D. F. Moyano, O. R. Miranda ,I. Hussain, V. M. Rotello, *Langmuir* **2012**, *28*, 2023.

[10] G. I. Guerrero-Garcia, M. O. de la Cruz, *J. Chem. Theory Comput.* **2013**, *9*, 1.

[11] D. Vaknin, *X-Ray Diffraction and Spectroscopic Techniques for Liquid Surfaces and Interfaces* **2012**, John Wiley & Sons, Inc.

[12] J. Penfold, R. K. Thomas, *J. Phys. A. Condens .Matter* **1990**, 2, 1369.

[13] H. H. Girault, *Modern Aspects of Electrochemistry* **1993**, Plenum Press, New York.

[14] A. G. Volkov, *Liquid-Liquid Interface Theory and Methods*, **1996**, CRC Press, Inc.

[15] A. J. Bard, L. R. Faulkner, *Electrochemical Methods: Fundamentals and Applications* **2001**, John Wiley & Sons, New York.

[16] A. G. Volkov, V. S. Markin, *Encyclopedia of Electrochemistry* **2007**, Wiley-VCH Verlag GmbH & Co.

[17] G. Lee Warren, S. Patel, *J. Phys. Chem. C* **2008**, *112*, 7455.

[18] P. Hunenberger, M. Reif, *Single-Ion Solvation Experimental and Theoretical Approaches Elusive Thermodynamic Quantities*, **2011**, RSC Theoretical and Computational Chemistry Series No. 3.

[19] H. H. Girault, P. Peljo, *Encyclopedia of Analitical Chemistry*, 2012, John Wiley & Sons, Ltd.

[20] Y. Shao, M. D. Osborne, H. H. Girault, *J. Electroanal. Chem.* **1991**, *318*, 101.

[21] J. Koryta, *Electrochim. Acta* **1979**, *24*, 293.

[22] Y. Shao, S. N. Tan, H. H. Girault, *J. Chem. Soc. Faraday Trans.*, **1993**, *24*, 4307.

[23] T. J. Stockmann, Y. Lu, J. Zhang, H. H Girault, Z. Ding, *Chemistry*, **2011**, *47*, 13206.

[24] J. I. Garcia, R. A. Iglesias, S. A. Dassie *J. Electroanal. Chem.*, **2005**, *580*, 255.

[25] S. Ozaki, K. Kano, O. Shirai *Phys. Chem. Chem. Phys.* **2008**, *30*, 4449.

[26] E. Metzger, R. Aeschimann, M. Egli, G. Suter, R. Dohner, D. Ammann, M. Dobler, W. Simon, *Hel. Chim. Acta*, **1986**, *69*, 1821.

[27] Z. Samec, V. Marecek, and J. Weber, *J. Electroanal. Chern.* **1977**, *96*, 245.

[28] P. Peljo, T. Rauhala, L. Murtomaki, T. Kallio, K. Kontturi, *Int. J. Hydr. Energ.* **2011**, *36*, 10043.

[29] W. Adamiak, M. Opallo, *J. Electroanal. Chem.* **2010**, *643*, 82.

[30] W. Adamiak, G. Shul, E. Rozniecka, M. Satoh, J. Chen, M. Opallo, *Electroanal.* **2011**, *23*, 1921.

[31] S. Bu, S. Zhang, Y. Yuan, J. Guo, L. Gan, Y. Shao, *Anal. Chem.* **2002**, *2*, 373.

[32] Z. Hu, W. Zhang, P. Zhao, D. Qi, *Electroanal.* **1995**, *7*, 681.

[33] U. Nestor, H. Wen, G. Girma, Z. Mei, W. Fei, Y. Yang, C. Zhang, D. Zhang, *Chem. Commun.* **2014**, *50*, 1015.

[34] W. Adamiak, G. Shul, M. Opallo, Electrochem. Commun. **2009**, 11, 149.

[35] F. Marken, *Phil. Trans. R. Soc. Lond. A* **2004**, *362*, 2611.

[36] M. Velicky, K. Y. Tam, R. A. W. Dryfe, *Anal. Chem.* **2014**, *86*, 435.

[37] K. T. Brown; D. G. Flaming, *Advanced micropipette techniques for cell physiology* **1986**, Wiley, New York.

[38] F. Scholz, R. Gulaboski, V. Mirceski, P. Langer, *Electrochem. Commun.* **2002**, *4*, 659.

[39] R. Gulaboski, F. Scholz, *J. Phys. Chem. B* **2003**, *107*, 5650.

[40] U. Schroder, J. Wadhawan, R. G. Evans, R. G. Compton, B. Wood, D. J. Walton, R. R. France, F. Marken, P. C. Bulman Page, C. M. Hayman, *J. Phys. Chem. B* **2002**, *106*, 8697.

[41] V. Mirceski, R. Gulaboski, F. Scholz, *J. Electroanal. Chem.* **2004**, *566*, 351.

[42] P. Tasakorn, J. Chen, K. Aoki, *J. Electroanal. Chem.* **2002**, *533*, 119.

[43] D. Rayner, N. Fietkau, I. Streeter, F. Marken, B. R. Buckley, P. C. B. Page, J. del Campo, R. Mas, F. X. Munoz, R. G. Compton, *J. Phys. Chem. C* **2007**, *111*, 9992.

[44] E. Bak, M. Donten, Z. Stojek, *Electrochem. Commun.* **2005**, *7*, 483.

[45] I. Kaminska, M. Jönsson-Niedziółka, A. Kaminska, M. Pisarek, R. Holyst, M. Opallo, J. Niedziółka- Jönsson, *J. Psych. Chem. C* **2012**, *116*, 22476.

[46] M. Donten, Z. Stojek, F. Scholz, *Electrochem. Commun.* **2002**, *4*, 324.

[47] G. Shul, W. Adamiak, *Electrochem. Commun.* **2008**, *10*, 1201.

[48] F. M. Llave, K. D. Luks, J. P. Kohn, *J. Chem. Eng. Data*, **1986**, *31*, 418.

[49] L. Yan, H. Ma, B. Wang, Y. Wang, Y. Chen, *Desalination* **2011**, *276*, 397.

[50] M. A. Lizardi-Jimenez, G. Saucedo-Castaneda, F. Thalasso, M. Gutierrez-Rojas, *Int. J. Chem. React. Eng.* **2011**, *9*, 1.

[51] T. Kakiuchi, *Anal. Chem.* **1996**, *68*, 3658.

[52] F. Scholz, U. Schroder, R. Gulaboski, *Electrochemistry of Immobilized Particles and Droplets*, **2005**, Springer-Verlag, Berlin.

[53] F. Reymond, D. Fermin, H. J. Lee, H. H. Girault, *Electrochim. Acta* **2000**, *45*, 2647.

[54] A. J. Bard, G. Inzelt, F. Scholz, *Electrochemical Dictionary*, **2008**, Springer-Verlag Berlin Heidelberg.

[55] R. Gulaboski, V. Mirceski, F. Scholz, *A. Acids* **2003**, *24*, 149.

[56] P. W. Atkins, *Chemia Fizyczna 6. Edycja*, **2003**, Wyd. PWN, Warszawa.

[57] F. Scholz, *Electroanalytical Methods*, **2010**, Springer-Verlag Berlin Heidelberg.

[58] S. Komorsky-Lovric, V. Mirceski, C. Kabbe, F. Scholz, *J. Electroanal. Chem.***2004**, *566*, 371.

[59] F. Quentel, V. Mirceski, C. Elleouet, M. L'Her, *J. Phys. Chem. C* **2008**, *112*, 15553.

[60] F. Marken, A. N. Blythe, J. D. Wadhawan, R. G. Compton, S. D. Bull, R. T. Aplin, S. G. Davies, *J. Solid State Electrochem.* **2001**, *5*, 17.

[61] U. Schroder, R. G. Compton, F. Marken, S. D. Bull, S. G. Davies, S. Gilmour, *J. Phys. Chem. B* **2001**, *105*, 1344.

[62] Ch. Shi, F. C. Anson, *J. Phys. Chem. B* **2001**, *105*, 1047.

[63] T. Solomon, A. J. Bard, *Anal. Chem.* **1995**, *67*, 2787.

Chapter 2

ELECTROCHEMISTRY IN MICROFLUIDICS

2.1 INTRODUCTION

The theory and experimental of electrochemical analysis with microfluidic devices is well established topic. It is widely using in many applications including electrochemical screening [1], electrochemical velocimetry [2] or in monitoring of electrochemical reaction pathway [3]. In a popular approach the electrochemical microfluidic device (EMD) consists of a polydimethylsiloxane (PDMS) made microchannel and a glass slide with a microband electrode array. The analyte is pumped through the EMD under laminar flow regime by syringe pump. Established microfluidic conditions like flow rate and possibility to control the mass transport of electroactive compound make EMD very powerful tool in electroanalysis.

2.2 THE PRINCIPLES OF THE MICROFLUIDIC TECHNIQUE

Microfluidics is the technique and science of working with small volumes of liquid in a channel with parameters from tens to hundreds of micrometers. The small dimensions of the microchannel determine the Reynolds number of the flow to be in the range of the laminar regime. In recent years the research with application of microfluidic devices as a useful experimental platform is extensively explored. Ones of the biggest advantages of using microfluidic devices as microreactors are:

- small volumes of reagents consumed since the area of the reaction is determined by the microchannel dimensions,
- possibility to divide one single stream of the liquid into several separate experiments,
- high reproducibility of experiments [4].

The microfluidics devices technology was established in the 1970s at Stanford University where Terry et al. used a miniaturized gas chromatograph where all components were

produced using photolithography and chemical etching techniques [5]. It enabled them to reduce the dimensions of the gas chromatograph by three orders of magnitude.

The microfluidic technology is a good alternative for classical analytical equipment where big size peripherals are required. Another application example of the earliest microfluidic technology was described by Ruzicka, where the microfluidic device consisted of integrated microconduits to allow the miniaturization of flow injection analysis (FIA) (Fig. 2.2.1) [6]. Basically FIA is the introduction of a liquid sample from a sample cup (S) into a moving carrier stream (C) and a stream of reagents (R). A stream of sample and reagents are pumped through the coil where the sample reacts with components of the carrier stream and finally forming a colored species to be sensed by a spectrophotometer.

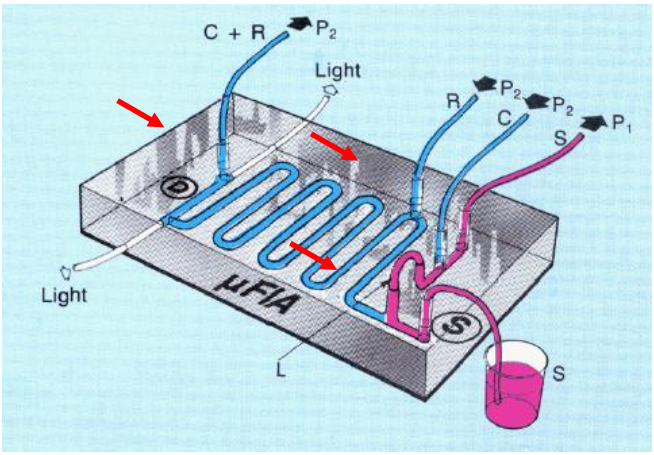

Fig. 2.2.1 The scheme of the flow injection analysis (FIA) with the integrated microconduits (are shown with red arrows). The pump P1 sucks the sample into the sample loop L. Another pump P2 keeps the flow of reagents R and the carrier phase C still in the system. The ratio of incoming streams (P2, C of carrier phase and reagents R) are equal to outgoing one (P2, C+R). The reaction between the reagents takes place into the channel loop and finally the resulting color of the reaction is monitored by measuring the light in a flow cell through the light is transmitted by optical fibers system [6].

There are a number of different microfluidic strategies which integrate microfluidic chips towards the lab-on-a-chip concept [7]. Other well-known integrations of microfluidic chip as a complete microreactor are multiphase aqueous microfluidics which are using as a tool in the separation of DNA, proteins or cells [8], electrowetting-on-dielectric where applying of external voltage allows to control the shape and position of liquid phases into the microchannel regardless of capillary, inertial and viscous forces [9] or centrifugal microfluidics devices on disc-shaped platform where the flow is driven by rotation of the disc [10]. Whitesides presented a low cost microfluidic sensors based on a sheet of paper (μPAD) instead of traditionally fabricated microfluidic chips [11]. The paper acts as a both microchannel and the physical filter. In others studies the microfluidic reactors gave

opportunity to miniature capillary electrophoresis [12] where authors show the possibility to perform postcolumn labeling of analyzing compounds in order to be detected. Microfluidic chip allows to mixing of solutions and finally provide efficient electrophoretical separation. In another example the capillary electrophoresis was miniaturized in a microfluidic device and connected with pulse amperometric detection of the commonly use triazine herbicides [13]. Throckmorton and coworkers proposed a microfluidic chip as electrochromatograph where separation of aminoacids (arginine, serotonin, glycine, phenylalanine and tryptophan) takes place on polymer base which structure can be precisely controlled under photolithography conditions [14].

The dynamic growth of biology and medical research forced the invention of complex analytic devices which give the analytic information from small volumes of biological samples. A novel approach for the Western blot method under PDMS (polydimethylsiloxane) based microfluidic chip was presented by Jijang and coworkers (Fig. 2.2.2) [15].

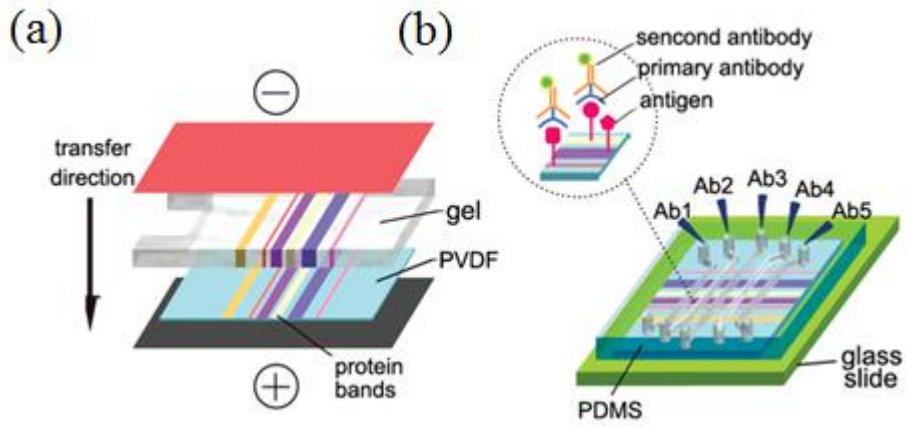

Fig. 2.2.2 The scheme of the microfluidic Western blot chip. (a) The proteins transfer from polyacrylamide gel to polyvinylidene fluoride (PVDF) membrane in traditional Western blot technique. (b) The microfluidic Western blot microchannels network incorporated with the blotted PVDF membrane. Antibodies for specific proteins are located in parallel microfluidic channels [15].

In contrast to classical Western blot method, which allows the detection of only one protein, the microfluidic Western blot chip is able to analyze at least 10 proteins simultaneously from one sample. The microfluidic processing of protein identification with matrix-assisted laser desorption/ionization were presented by Gustafsson et al. [16]. In 1997 Mathies and coworkers made genetic analysis of DNA using microfabricated capillaries [17].

The dynamic in the number of microfluidics publications is shown in Fig. 2.2.3. The growth in the number of papers is substantial during the last decade and the most

occupied topic is engineering studies. The level of amount in biology and medicine journals became similar to interdisciplinary journals (9 % and 6 %) [18].

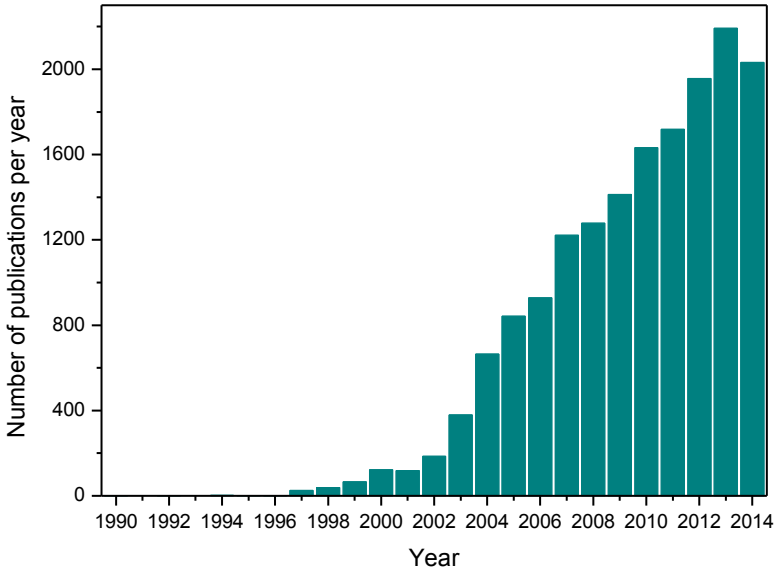

Fig. 2.2.3 The dynamic of the growth of the microfluidic publications in topic from 1990 to 2014 according to data taken from the Web of Science.

Another microfluidic approach which can be applied instead of a continuous flow stream is droplet microfluidics. The most elementary droplet microfluidics system consists of a mixture of two immiscible fluids, comprising a liquid core suspended in a second immiscible liquid, as water-in-oil microdroplets or in oil-in-water microdroplets. Microdroplet microfluidics is an established field of science [19,20]. The microfluidic droplets can be formed and transported through the microchannel and can realize different operations. The application of different shapes and geometries of the microchannel gives the opportunity to merge the droplets to facilitate chemical reactions.

One of the most popular microfluidic droplet setup generates the microdroplets using a T-junction design of inlets in the microchannel (Fig. 2.2.4a). This idea was presented for the first time by Quake and coworkers [21]. The characteristic feature of this system is the presence of two inlets which cross each other at 90°. One of them introduces the carrier phase which carries the droplets and other the dispersed phase. The carrier phase cuts the dispersed phase and thereby generates the microdroplets. Formation of microdroplets by T-junction microfluidic shape has a number of advantages like the tempo of the process [22], stability [23], uniformity [24], controllability of the amount of reagent in each microdroplet [25],

and low cost of chip fabrication [26]. This method has been used to generate a wide range of microdroplets, including aqueous droplets in oil [27], viscous aqueous microdroplets in oil [28], oil microdroplets in water [29], and also aqueous microdroplets in ionic liquid [30].

Garstecki et al. described the physical mechanism of microdroplets formation [31]. The genesis of microdroplets formation says that the dimension of microdroplets depends on volume flow rate of both streams. The dependence of length of the microdroplet to width is given by [31]:

$$\frac{L}{w} = 1 + \alpha \frac{Q_\mathrm{d}}{Q_\mathrm{c}} \qquad \text{(Eq. 2.2.1)}$$

where L is the length of the immiscible slug, w is the width of the microchannel, α is a constant that depends on the geometry of the T-junction, Q_d and Q_c are the rates of the flow of the dispersed and carrier phases, respectively. The dependence depicted in Eq. 2.2.1 is independent of the parameters of the liquid phase and other parameters like viscosity at the interface between two liquids [31].

The second possibility of microdroplet break up is application of a flow-focusing system (Fig. 2.2.4b [32]). In 2003 appeared the work of Anna and coworkers [33] where authors presented first time flow-focusing microfluidic device. The characteristic feature of the flow-focusing system is presence of two channels which introduce continuous liquid phases. Two liquid phase streams cut the third stream which is dispersed to droplets.

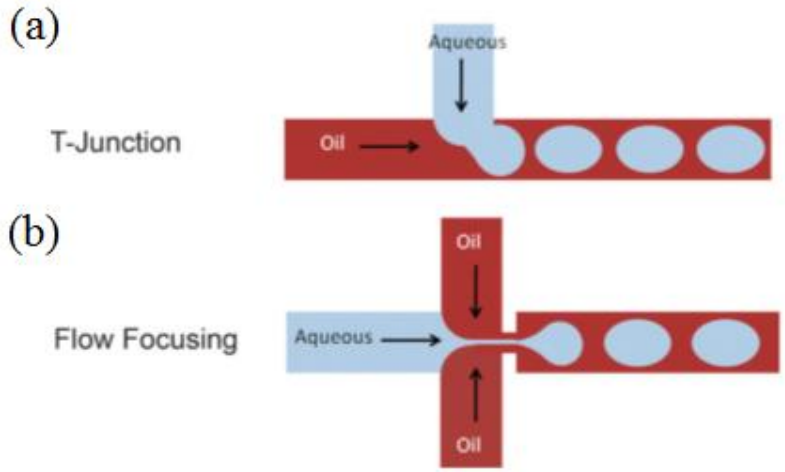

Fig. 2.2.4 The schematic of microdroplet generation strategies: **(a)** T-junction system; **(b)** flow-focusing system [32].

Droplet microfluidic has for example been successfully used to study the kinetics of single enzymes [22]. Application of microdroplet system as a separate experiment is the work of Nossal and Lederberg [19] where single cell stimulated with two antigens can be isolated and detect in microdroplet. The monitoring of kinetic of release of ATP enzyme via microfluidic device was proposed by Stone and coworkers [34].

2.2.1 Fabrication aspect of microfluidic device

In recent years it has become more popular using a larger array of different materials for microfluidic fabrication. The earliest materials used in preparing microfluidic devices were glass and silicon and fabrication of microfluidic devices in these materials were well-developed since the methods for fabrication of microfluidic devices came from the microelectronic and semiconductor technology [35]. First, widely used material in manufacturing of microfluidic devices was silicon [36,37]. The fabrication process of microfluidic device based on silicon material has a number of steps such as: substrate cleaning, photolithography, metal deposition and wet or dry etching. Silicon materials are expensive from fabrication point of view. Instead of silicon, glass and others polymer materials were introduced like polymethylmethacrylate (PMMA), polystyrene (PS), polycarbonate (PC) or polydimethylsiloxane (PDMS). Amongst those polymer materials, PDMS became the most popular because is easy in moulding and stamping, transparent and compatible with many analyzing substances.

a) Photolitography

Photolitography is the most important stage in the microfabrication technique. Basically it is a process of transferring of a desired pattern onto a material like silicon or polymer. The crucial point of whole technique is exposing photoresist e.g. AZ or SU-8 to UV light and developing the desired pattern of the microfluidic channel or electrodes array.

Briefly, photolithography consists of a number of steps such as:

- mask design (glass, quartz plate with a metal pattern etc.)
- wafer cleaning,
- spreading of photoresist by spin coater on the wafer surface,
- UV exposure of photoresist,
- final development of the photoresist.

Photoresist is exposed to UV radiation under appropriate time duration. The time duration is directly determined by the energy of adsorption of photoresist. To obtain high quality pattern, any contaminants should be removed from the wafer surface before application of the

photoresist. TO clean the wafer surface several techniques can be applied like e.g. oxygen plasma exposure, cleaning in a solution of NH_4OH and H_2O_2 and final heating in 80 °C.
The photoresist is developed to remove the undesired region. In case of positive photoresist the surface exposed by UV light becomes easy to remove by developer and the opposite situation is in case of negative photoresist. The photolithography process in case of glass slide as a material is presented in Fig. 2.2.5a. The metal or other semiconductor layer bonds together with glass slide via application of adhesion metal layer e.g. titanium or chromium and finally the metal layer is sputtered on a top [38,39,40].

b) Micromoulding

Micromoulding is the technique based on self-assembly and replica moulding for performance of microfluidic device fabrication. The major advantages of this technique are fast prototyping and non-complicated fabrication. Other well-known techniques are: microcontact printing, microtransfer moulding and micromoulding in capillaries.

From theoretical point of view, micromoulding is technique that replicates the microstructure on polymer material. In the last years PDMS was the major used polymer.
Utilization of PDMS as micromoulding material has several valuable features:

- relatively non-expensive material,
- easily hot-molded and designed,
- etching the microchannel is not needed,
- strongly bonded to glass slide,
- optically clear, nontoxic and also nonflammable.

Fig. 2.2.5b presents details of PDMS replication process on a silicon master.
PDMS is basically poured to silicon master and allowed to cure. The moulding template is fabricated by pattering negative photoresist (SU-8) on an e.g. silicon wafer. Later degassed and mixed PDMS prepolymer and curing agent is applied on silicon master. In the end, the whole structure is kept at 70 °C for appropriate time period to cure PDMS polymer. Ready PDMS microchannel is peeled off from the template. Cured PDMS is ready to use as the microchannel [39,40].

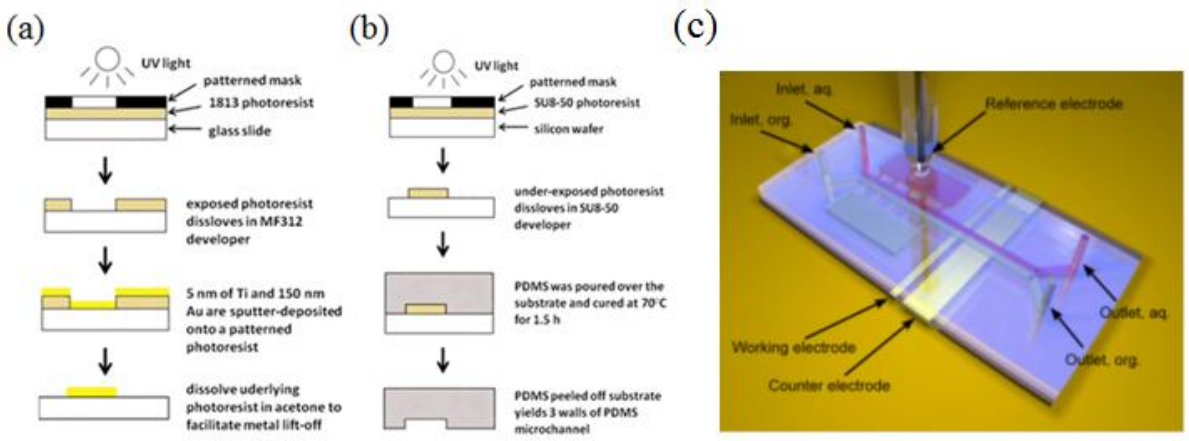

Fig. 2.2.5 The schematic sketch of **(a)** microband electrodes and **(b)** microchannel fabrication. **(c)** Assembled electrochemical microfluidic device with visible gold microband electrodes system and standard reference one. It also visible PDMS microchannel prepared to introduce two phase microflow.

2.3 ELECTROCHEMICAL PROCESSES UNDER MICROFLUIDIC CONTROL

Electrochemical microfluidic devices (EMD) give opportunity to monitor continuous electrochemical process with well define flow-through regime. This kind of electrochemical cell is easy to construct and a wide diversity of electrode materials are available. The characteristic feature of the flow inside the microchannel is easy to define since laminar conditions prevail [41]. The dimensions of the microchannel and microband electrodes are well defined and make it possible to clearly describe the behavior of the electrochemical processes. Electrochemical experiments under microfluidic conditions can be used with other analytical techniques to detect the product of the reaction e.g. spectroelectrochemical methods, microfluidic electrospray ionization, MALDI mass spectrometric methods or fluorescence lifetime-techniques [42].

In microfluidic techniques, the most important effort is the reduction of analytical periphery equipment. The previous subchapter included information that the ultimate goal of the microfluidic technique is the integration all of the necessary analytical components in a lab-on-a-chip system. Electrochemical analysis with EMD is suitable for lab-on-a-chip integration due to the versatility of the size, geometry and nature of electrodes that can be integrated within a microfluidic platform. What is more, electrochemical detection is reliable, selective and highly sensitive [43]. The biggest difference between traditional electrochemical setup and EMD is possibility to manipulate of picolitres or nanolitres

of analyte solution. Another benefit relates with the electrochemistry under microfluidic conditions is implementation of the microband electrodes which allow to monitor the electrochemical reaction in flowing liquid phase. It also can distinguished that in case of EMD the experiments are performed under hydrodynamic conditions and that fact characterizes the type of mass transport of analytes towards working electrode surface. The experimental approach with electrochemistry under microfluidics conditions can be realized in main three ways. All of this types depend on construction of microfluidic device. The first one is EMD with single phase microflow of dissolved electroactive compound, the another way is multiphase microflow and third one consists generation of microdroplets flowing in the carrier solution with or without electroactive species.

a) Electrochemical single phase microfluidics

The electrochemical single phase microfluidics is the simplest and basic experimental approach. In this experimental system the electroactive compound is dissolved in the single flowing phase. Compton and coworkers made fundamental work in the theoretical foundation of hydrodynamic voltammetry at microelectrodes and the response of electrodes in microreactors [44]. In the opposite to traditional electrochemical setup, under the single flow microfluidics a large number of single measurements can be evaluated under the same conditions. Another characteristic feature of the electrochemical experiment with flow of electroactive species is minimizing the uncontrolled oxidation and contamination of electroactive reagent since the reaction is isolated from external conditions. The single phase microfluidics has successfully been used in e.g. biosensing aims like counting of flowing living cells (bacteria or blood cells) [45] or in determination of electrokinetic data and transport mechanistic in the drug delivery microfluidic device [46]. The flow rate of the liquid phase is varied independently and the effect on the mass transport controlled limiting currents for electrochemical processes can be studied.

The mass transport of electroactive compound towards microband electrode is convective/diffusion process. The equation which describes the convective-diffusion effect on limited transfer current on flow-rate in a rectangular microchannel is the Levich equation (Eq. 2.3.1) [47] and comes originally from rotating disc electrode equation and is adjusted to microchannel application:

$$I_{\mathrm{lim}} = 0.925nFcD^{2/3}(h^2 d)^{-1/3} w x^{2/3} V_{\mathrm{f}}^{1/3} \qquad \text{(Eq. 2.3.1)}$$

where n is the number of electrons transferred per molecule transported to the electrode surface, F is the Faraday constant, c is the concentration of the electroactive compound, D is the diffusion coefficient, h is the half height of the microchannel, d is the microchannel width, w, the microelectrode width, x, the microelectrode length and V_f, is the value of the flow rate. Fig. 2.3.1 presents the schematic sketch of the EMD with microband working electrode in the bottom of microchannel [48]. In most cases the microband electrode spans the width of the microchannel so that $w = d$.

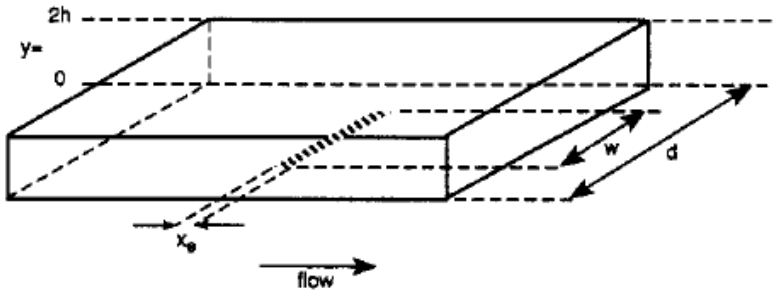

Fig. 2.3.1 The scheme of the EMD with the microband working electrode in the bottom of the channel. Letter: d, w, x_e represents microchannel width, the working electrode width and the electrode length, respectively. h multiplied by 2 is the total height of the microchannel. [48].

In the EMD cell it is the V_{f} that controls the convection of electroactive compound to the microband working electrode surface since the other parameters in Levich equation are constant.

Fig. 2.3.2a shows the typical cyclic voltammogram for simple redox system under microfluidic conditions. The values of transfer limited currents are proportional to applied V_{f} values. The plot in Fig. 2.3.2b presents that the transfer limited currents are indeed consistent with Eq. 2.3.1 and correspond with experimental data.

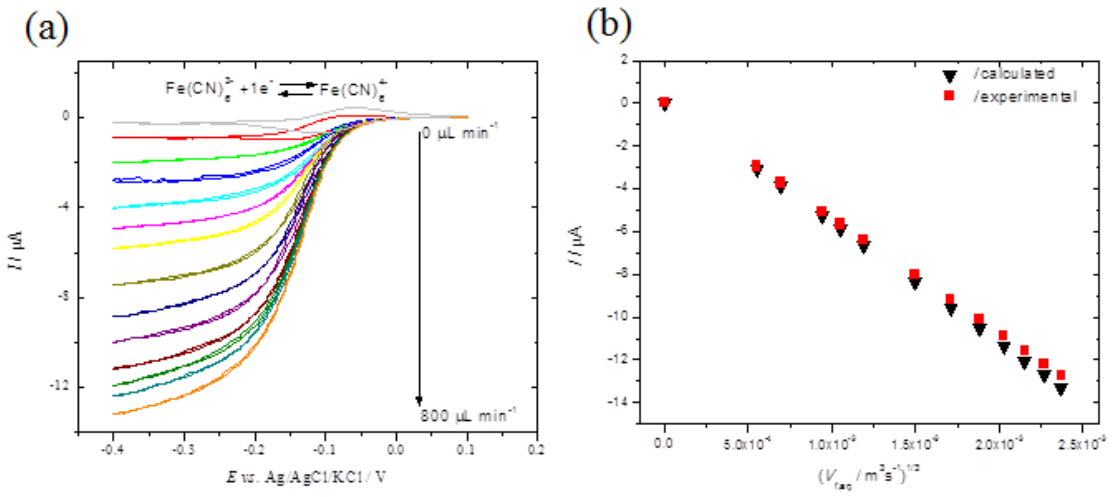

Fig. 2.3.2 (a) Cyclic voltammograms for electrochemical reduction of 1 mM $K_3[Fe(CN)_6]$ in aqueous 0.1 M KCl at gold microband electrodes in EMD (h =0.1 mm, $w = d$=2 mm, V_f (0÷800 µL min^{-1}). Diffusion coefficient for $K_3[Fe(CN)_6]$ is 0.9 x 10^{-5} cm^2 s^{-1} [45]. **(b)** Plot of the cathodic transfer limited currents versus the cube root of flow rate (m^{3}s^{-1}). Black triangles indicate calculated values of transfer limited currents from Levich equation and red squares are experimental values of transfer limited currents.

b) Electrochemical multiphasic microfluidics

The EMD can be also employed to perform electrochemical reactions with multiphase flows. In that case two adjacent flowing immiscible phases in contact with working microband electrode form a three-phase boundary.

In case of electrochemical processes at the two immiscible liquids flows the basic parameter which can be manipulated is as previously single phase microfluidics the flow rate values. The dynamic three-phase boundary allows to perform processes like: sensing the substances at the three-phase boundary [49], electrosynthesis [50] or generally to produce nanomaterials of defined size and anisotropy like: cadmium sulphide, cadmium selenide, copper or ZnS core-shell nanoparticles [51].

The one of the most well-known application of EMD with the three-phase boundary is electrochemical extraction process. The characteristic feature of the above process is that the electrochemical reactions have their origin at the border between three phases: a liquid containing electroactive species, aqueous phase containing an electrolyte, and a working electrode constituting the third phase. Extraction with EMD can be used e.g. the separation of amino acids or proteins [52,53]. The principles of the polarization of the liquid|liquid interface and ion transfer processes were described in the previous chapter.

Marken and coworkers presented experiments with two immiscible phases flowing perpendiculary through the microband electrodes system and this experimental system formed three-phase boundary between these phases (Fig. 2.3.3) [54]. The ion transfer of ClO_4^- from

aqueous phase to the organic (*N*-octyl-2-pyrrolidone) is connected with the electron transfer (electrochemical oxidation of *N*-butyl-ferrocene, nBuFc to $nBuFc^+$).

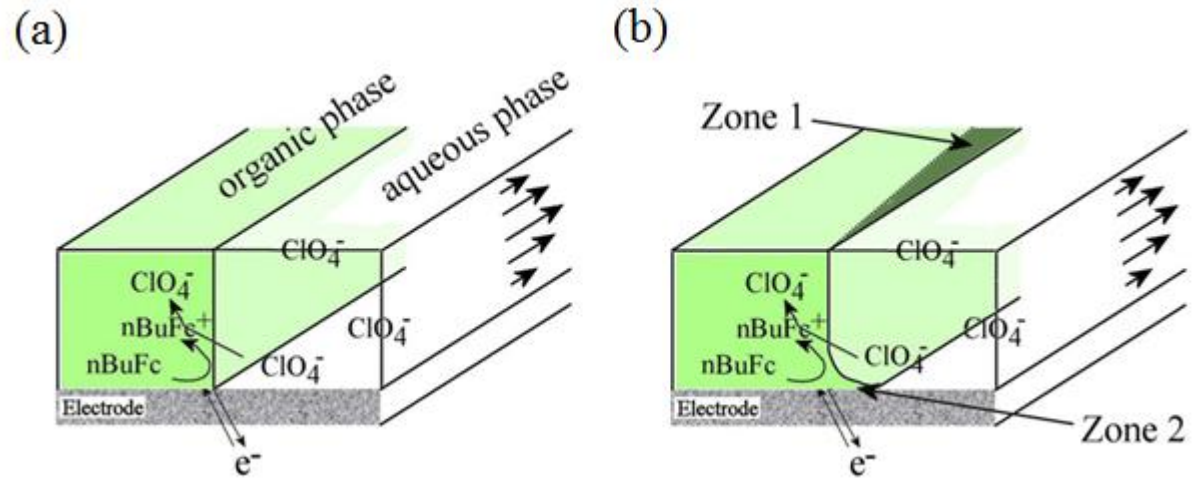

Fig. 2.3.3 (a) Schematic representation of electrochemical processes at the three-phase boundary with simultaneous transfer of ions ClO_4^- from flowing aqueous to the organic phase (*N*-octyl-2-pyrrolidone) and the electron transfer (electrochemical oxidation of nBUFc to $nBUFc^+$) In scheme **(b)** zone 1 indicates the expanding nature of three-phase boundary with the values of the flow rate. Zone 2 shows the real profile of undercutting the aqueous phase by the organic one [54].

It was one of the few examples of using the solution of electroactive compound without the supporting electrolyte [55,56]. The electrochemical processes at the three-phase boundary strongly depend on the nature of both aqueous and organic phase (viscosity, density etc.) and on the microchannel geometry [57].

c) Electrochemical microfluidics with microdroplets generation

The second approach of creating the multiphasic EMD is the generation of microdroplets in a carrier phase. Electrochemical measurements with microdroplets application are less popular than typical approach with single or biphasic EMD. In comparison of EMD with microdroplets application to standard analytical methods with microdroplets like spectroscopy [58], mass spectroscopy [59], electrophoresis [60], EMD with microdroplets offers low cost of analysis and relative simple analytical procedures. Each microdroplet in contact with the microband working electrode can be assumed as a separate experiment and gives information about mass transfer of the substrate, about electron transfer and can be source of kinetic information [61]. Fisher and coworkers used chronoamperometric measurements to detect real time formation of aqueous microdroplets in carrier oil flow contained electroactive species [62]. Crooks and Liu presented amperometric measurements of size, frequency and velocity of formed microdroplets which perturbated electrochemical response comes from the carrier phase [63].

In a very valuable paper, Huck and coworkers showed that is possible to electrochemically detect of flowing aqueous microdroplets in microfluidic device [64]. The carrier organic phase contained ferrocene as a redox species and flowing aqueous microdroplest perturbated the amperometric measurement of ferrocene electrooxidation. In other work Xingyu et al. performed amperometric measurements of aqueous microdroplets with dissolved $K_3[Fe(CN)_6]$ [65]. Here the application of wettability-patterning of the microchannel surface allowed to avoid typical experimental problems like repeatability or detectability of microdroplets (Fig. 2.3.4).

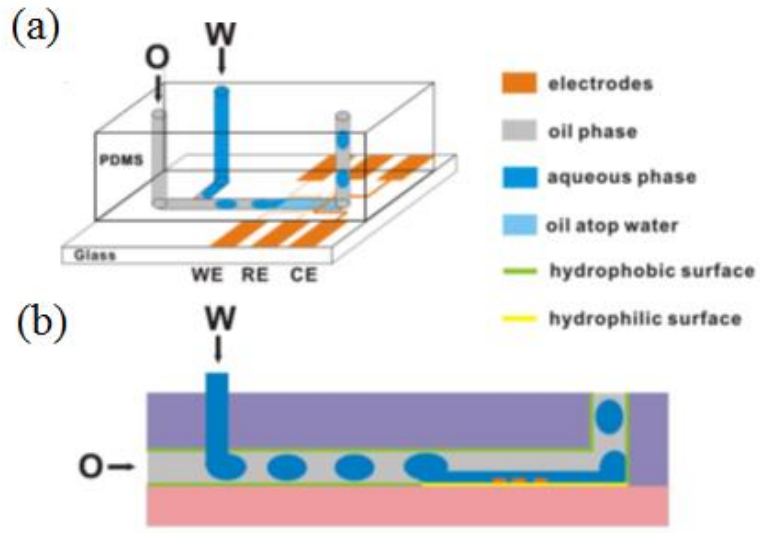

Fig. 2.3.4 (a) The schematic illustration of PDMS-glass microfluidic device with integrated microband electrodes for of aqueous microdroplets generation, counting and detection. **(b)** The cross-section of microchannel with T-junction type inlet. Green line symbolizes hydrophobic surface and yellow line shows hydrophilic region on a glass surface [65].

The special part of electrochemistry in microfluidics is biofuel cell research. In this area enzymes often are used as a biocatalyst of electrode reaction in generation of fuel. Enzymes provide high values of the mass transport rate and have an impact on energy density [66]. In work of Zedba et al. the glucose is going through oxidation by glucose oxidase enzyme [67]. At the cathode oxygen is reduced by the laccase enzyme in presence of 3-ethylbenzohiazoline-6-sulfonate (ABTS) as a reduction mediator. This work shows very gently feasibility of tuning the enzyme activity by colaminar microfluidic flow. Biological materials very often assist in development of low cost and green energy of biofuel cell

2.4 THEORETICAL MODELS FOR ELECTROCHEMISTRY UNDER MICROFLUIDIC CONDITIONS

Nowadays electrochemistry research and research in general shows that obtained experimental results should have reliable designed theoretical models.

The theoretical model of electrochemical reactions in EMD should take in account a specific aspect of the character of experiments under microfluidic conditions. The mentioned previously advantages of analysis with EMD are: small volumes of using analytic liquid and quick time of the analysis, however is difficult to precisely theoretically monitor the analysis pathway with such small volumes of analytical solutions [48]. The necessary aspect is proper fabrication procedures needed to perform EMD with accurate dimensions of microband electrodes and microchannel. Precise designed parameters of the EMD give expected result of electrochemical measurements and this data can be transfer as an input into electroanalytical modeling software. The simple mathematical problems can be solve with well-known software like MS EXCEL or MATLAB. To visualize more specific aspects of electrochemistry like voltammetry measurements the COMSOL software can be use [68].

Fig. 2.4.1 shows application of the COMSOL software in simulation of experiments where microfluidic device was employed as selective and sensitive electrochemical sensor of sub-micromolar of dopamine in presence of electroactive interferents (ascorbic acid, acetaminophen) [69].

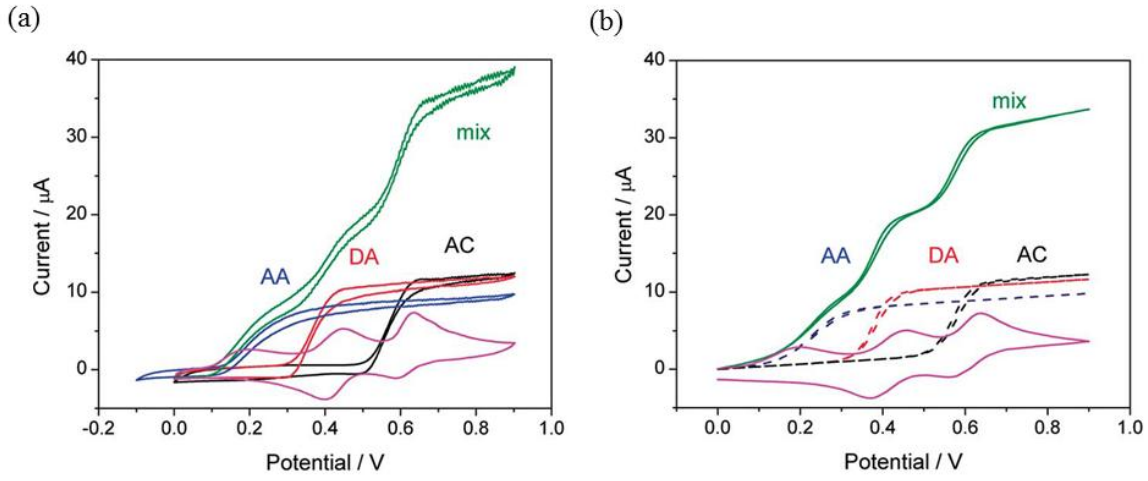

Fig. 2.4.1 (a) Cyclic voltammograms recorded in presence of 1 mM ascorbic acid (AA, green curve), 1 mM dopamine (DA, red curve), 1 mM acetaminophen (AC, black curve) and in a mixture of these substances (mix, green curve) under microfluidic control (V_f = 50 µL min^{-1}, scan rate 20 mV s^{-1}) in phosphate buffer (pH 5). **(b)** Simulated cyclic voltammograms of substances used experimentally in (a) under the same conditions.

The voltammetric response (Fig. 2.4.1a) of all electroactive species recorded experimentally is in good agreement with the model obtained with COMSOL (Fig. 2.4.1b). Whole electrochemical reactions of dopamine and other interferents were simulated by calculating the mass transport (diffusion and convection) of reduced and oxidized form of each.

The important aspect of designing the processes with EMD is selection of appropriate electrode dimensions. The microband electrodes are good for that purpose because they provide the enhancement of mass transfer of electroactive compound towards the electrode surface and more convenient signal to noise ratio. In 1993 Compton et al. used the hopscotch algorithm to calculate the equation describing the mass transfer of electroactive compounds by diffusion-convective transport [70]. Their theoretical model was in good agreement with the experiment. There is a big number of papers by Amatore and coworkers where they studied such tasks of theory of voltammetry under microfluidic conditions like: simplification of flow velocity profile [71], the determination of flow profile connected with steady-state currents [72], optimization of electrode locations [73] or reconstruction of hydrodynamic flow profile using experimental data [74].

2.5 BIBLIOGRAPHY

[1] K. Yamanaka, M. Saito, K. Kondoh, M. M. Hossain, R. Koketsu, T. Sasaki, N. Nagatani, K. Ikuta, E. Tamiya, *Analyst.* **2011**, *136*, 2064.

[2] K. Abi-Samra, T. H. Kim, D. K. Park, N. Kim, J. Kim, H. Kim, Y. K. Cho, M. Madou, *Lab Chip*, **2013**, *16*, 3253.

[3] A. Birzu, Y. Jia, V. Sankuratri, Y. Liu, I. Z. Kiss, *Chemphyschem*, **2015**, *3*, 555.

[4] G. M. Whitesides, *Nature* **2006**, *442*, 368.

[5] S. C. Terry, J. H. Jerman, J. B. Angell, *IEEE Trans. Electron Devices*, **1979**, *26*, 1880.

[6] J. Ruzicka, *Anal. Chem.* **1983**, *55*, 1040.

[7] M. Gao, L. Gui, *Lab Chip* **2014**, *14*, 1866.

[8] Y. Song, A. Sauret, H. C. Shum *Biomicrofluidics* **2013**, *7*, 61301.

[9] F. Saeki, J. Baum, H. Moon, J.-Y. Yoon, C.-J. Kim, R. L. Garrell, *Polym. Mater. Sci. Eng.* **2001**, *85*, 12.

[10] R. Gorkin, J. Park, J. Siegrist, M. Amasia, B. S. Lee, J. M. Park, J. Kim, H. Kim, M. Madou, Y. K. Cho, *Lab Chip* **2010**, *10*, 1758.

[11] A. W. Martinez, S. T. Phillips, B. J. Wiley, M. Gupta, G. M. Whitesides, *Lab Chip* **2008**, *8*, 2146.

[12] K. Fluri, G. Fitzpatrick, N. Chiem, D. J. Harrison, *Anal. Chem.* **1996**, *68*, 4285.

[13] K. Islam, S. K. Jha, R. Chand, D. Han, Y. S. Kim, *Microelect. Eng.* **2012**, *97*, 391.

[14] D. J. Throckmorton, T. J. Shepodd, A. K. Singh, *Anal. Chem.* **2002**, *74*, 784.

[15] W. Pan, W. Chen, X. Jiang, *Anal. Chem.* **2010**, *82*, 3974.

[16] M. Gustafsson, D. Hirschberg, C. Palmberg, H. Jornvall, T. Bergman, *Anal.Chem.* **2004**, *76*, 345.

[17] S. Liu, Y. Shi, W. W. Ja, R. Matthies, *Anal. Chem.***1999**, *71*, 566.

[18] E. K. Sackmann, A. L. Fulton, D. J. Beebe, *Nature* **2014**, *507*, 181.

[19] G. J. V. Nossal, J. Lederberg, *Nature* **1958**, *181*, 1419.

[20] M. L. Y. Sin, J. Gao, J. C. Liao, P. K. Wong, *J. of Biol. Eng.*, **2011**, *5*, 1.

[21] T. Thorsen, R. W. Roberts, F. H. Arnold, S. R. Quake, *Phys. Rev. Lett.* **2001**, *86*, 4163.

[22] D. Hess, A. Rane, A. J. deMello, S. Stavrakis, *Anal. Chem.* **2015**, *87*, 4965.

[23] B. Zheng, J. D. Tice, R. F. Ismagilov, *Anal. Chem.* **2004**, *76*, 4977.

[24] M. Bouquey, C. Serra, N. Berton, L. Prat, G. Hadziioannou, *Chem. Eng. J.* **2008**, *135*, 93.

[25] C. G. Yang, Z. R. Xu, J. H. Wang, *T. Anal. Chem.* **2010**, *29*, 141.

[26] P. Bhandari, T. Narahari, D. Dendukuri, *Lab Chip* **2011**, *11*, 2493.

[27] F. Chen, Y. Zahn, T. Geng, H. Lian, P. Xu, C. Lu, *Anal. Chem.* **2011**, *83*, 8816.

[28] Z. Nie, M. Seo, S. Xu, P. C. Lewis, M. Mok, E. Kumacheva, G. M. Whitesides, P. Garstecki, H. A. Stone, *Micro. Nanofluid.* **2008**, *5*, 585.

[29] Y. Schaerli, F. Hollfelder, *Mol. Biosyst.* **2009**, *5*, 1392.

[30] Z. Barikbin, M. T. Rahman, P. Parthiban, A. S. Rane, V. Jain, S. Duraiswamy, S. H. Lee, S. A. Khan, *Lab Chip*, **2010**, *10*, 2458.

[31] P. Garstecki, M. J. Fuerstman, H. A. Stone, G. M. Whitesides, *Lab Chip* **2006**, *6*, 437.

[32] X. Casadevall i Solvas, A. deMello, *Chem. Commun.* **2011**, *47*, 1936.

[33] S. L. Anna, N. Bontoux, H. A. Stone, *Appl. Phys. Lett.* **2003**, *82*, 364.

[34] W. D. Ristenpart, J. Wan, H. A. Stone, *Anal. Chem.* **2008**, *80*, 3270.

[35] K. E. Petersen, *Proc. IEEE* **1982**, *70*, 420.

[36] Y. Li, T. Pfohl, J. H. Kim, M. Yasa, Z. Wen, M. W. Kim, C. R. Safinya, *Biomed. Microdevices* **2001**, *3*, 239.

[37] N. R. Harris, M. Hill, S. Beeby, Y. Shen, N. M. White, J. J. Hawkes, W. T. Coakley, *Sens. Actuators B* **2003**, *95*, 425.

[38] J. C. Mcdonald, D. C. Duffy, J. R. Anderson, D. T. Chiu, H. Wu, O. J. A. Schueller, G. M. Whitesides, *Electrophoresis* **2000**, *21*, 27.

[39] K. F. Lei, *Microfluidics in Detection Science: Lab-on-a-chip Technologies* **2015**, The Royal Society of Chemistry.

[40] J. Cooper Mcdonald, G. M. Whitesides, *Accounts of Chem. Research* **2002**, *35*, 491.

[41] D. Cheng, J. Greenwood, X. Zeng, C. Lo, S. S. Sridharamurthy, L. Dong, Y. Choe, T. Khang, A. Arteaga, H. Jiang, *Laminar Flow in Microfluidic Channels*, **Expo 2007**.

[42] C. A. Baker, C. T. Duong, A. Grimley, M. G. Roper, *Bioanalysis.* **2009**, *5*, 967.

[43] J. S. Swensen, Y. Xiao, B. S. Ferguson, A. A. Lubin, R. Y. Lai, A. J. Heeger, K. W. Plaxco, H. T. Soh, *J. Am. Chem. Soc.* **2009**, *12*, 4262.

[44] W. J. Aixill, A. C. Fisher, Q. Fulian, *J. Phys. Chem.* **1996**, *100*, 14067.

[45] J. Claudel, M. Nadi, O. Elmazria, D. Kourtiche, *Proceedings of the 8th International Conference on Sensing Technology*, **Sep. 2-4, 2014**, Liverpool, UK.

[46] A. J. Chung, D. Kim, D. Erickson, *Lab Chip* **2008**, *8*, 330.

[47] C. M. A. Brett, A. M. O. Brett, *Electrochemistry: Principles, Methods, and Applications*, Oxford University Press: New York, **1993**.

[48] I. E. Henley, K. Yunus, A. C. Fisher, *J. Phys. Chem.* **1993**, *97*, 10410.

[49] A. P. Vollmer, R. F. Probstein, R. Gilbert, T. Thorsen, *Lab Chip* **2005**, *5*, 1059.

[50] S. M. MacDonald, J. D. Watkins, S. D. Bull, I. R. Davies, Gu Y., K. Yunus, A. C.Fisher, P. C. Bulman Page, Y. Chan, C. Elliott, F. Marken, *J. Phys. Org. Chem.* **2008**, *22*, 52.

[51] A. J. deMello, *Nature* **2006**, *442*, 394.

[52] D. C. Duffy, J.C. MacDonald, O.J.A. Schueller, G.M. Whitesides, *Anal. Chem.* **1998**, *70*, 4974.

[53] C. Wang, R. Oleschuk, F. Ouchen, J. Li, P. Thibault, D.J. Harrison, *Rapid Commun. Mass Spectrom.* **2000**, *14*, 1377.

[54] S. M. MacDonald, J. D. Watkins, Y. Gu, K. Yunus, A. C. Fisher, G. Shul, M. Opallo, F. Marken, *Electrochem. Commun.* **2007**, *9*, 2105.

[55] R. Horcajada, M. Okajima, S. Suga, J. Yoshida, *Chem. Commun.* **2005**, *10*, 1303.

[56] D. Horii, M. Atobe, T. Fuchigami, F. Marken, *Electrochem. Commun.* **2005**, *7*, 35.

[57] M. P.C. Marques, P. Fernandes, *Molecules* **2011**, *16*, 8368.

[58] C. D. Syme, Chiara Martino, Rama Yusvana, Narayana M. S. Sirimuthu, J. M. Cooper, *Anal. Chem.* **2012**, *84*, 1491.

[59] D. Gao, H. Liu, Y. Jiang, J. Lin, *Lab Chip* **2013**, *13*, 3309.

[60] S. Hernandez-Navarro, P. Tierno, J. Ignes-Mullol, F. Sagues, *Soft Matter* **2013**, *9*, 7999.

[61] K. Nakatani, M. Uchino M S. Suzuki, T. Negishi , T. Osakai, *Anal. Sci.* **2009**, *25*, 183.

[62] Y. Gu and A. C. Fisher, *Analyst* **2013**, *138*, 4448.

[63] H. Liu and R. M. Crooks, *Lab Chip* **2013**, *13*, 1364.

[64] S. Liu, Y. Gu, R. B. Le Roux, S. M. Matthews, D. Bratton, K. Yunus, A. C. Fisher, W. T. S. Huck, *Lab Chip* **2008**, *8*, 1937.

[65] L. Xingyu, H. Xianqiao, B. Zeqing, H. Qiaohong, C. Hengwu, Y. Yangzhi, D. Zhihua, Anal. Chim. Acta **2014**, *828*, 70.

[66] J. W. Lee, E. Kjeang, *Biomicrofluidics 4*, **2010**, *4*, 41301.

[67] A. Zebda, J. Renaud, M. Cretin, F. Pichot, C. Innocent, R. Ferrigno, and S. Tingry, *Electrochem. Commun.* 2009, 11, 592.

[68] E. Rozniecka, M. Jonsson-Niedziolka, A. Celebanska, J. Niedziolka-Jonsson, M. Opallo, *Analyst* **2014**, *139*, 2896.

[69] J. Parisi, Y. Liu, L. Su,Y. Lei, *RSC Adv.* **2013**, *3*, 1388.

[70] R. G. Compton, A. C. Fisher, R. G. Wellington, *J. Phys. Chem.* **1993**, *97*, 10410.

[71] C. Amator, O. Klymenko, I. Svir, *Electrochem. Commun.* **2010**, *12*, 1165.

[72] C. Amatore, O. V. Klymenko, A. I. Oleinick, I. Svir, *Anal. Chem.* **2009**, *81*, 7667.

[73] C. Amatore,Oleksiy V. Klymenko, I. Svir, *ChemPhysChem* **2006**, *7*, 482.

[74] O. V. Klymenko, A. I. Oleinick, C. Amatore, I. Svir, *Electrochim. Acta* **2007**, *53*, 1100

SUMMARY AND GOAL OF THE DISSERTATION

The theory of ion transfer processes at polarized liquid|liquid interfaces is a well described topic and has been the topic of many books and publications. The oxidation or reduction of an electroactive compound dissolved in one liquid phase provokes a charge imbalance in that phase. As a result of the generated charge imbalance ions are driven across the liquid|liquid boundary. Another aspect of processes across liquid|liquid interfaces is the possibility of the presence of a three-phase boundary between the two immiscible liquids in contact with a solid electrode surface. The three-phase boundary allows us to consider interaction between compounds dissolved in immiscible phases and electron transfer between the redox species and the solid electrode.

The fundamental goal of this dissertation is to transfer the idea of the electrochemical processes across liquid|liquid interface using three-phase electrode setup (TPE) to electrochemical microfluidic device system (EMD) and finally to understand the electrochemical processes in microfluidics systems where co-laminar flow of two immiscible liquid phases is applied.
The particular investigations presented in this thesis can be divided into several parts:

1. To determine how much a selection of organic solvents, commonly used in electrochemical measurements, affect the physical properties of PDMS and if there is any effect of so-called PDMS non-compatible solvents on recorded electrochemical signals.
2. To determine the effect of flow rate on the electrochemical analysis (cyclic voltammetry) with application of the three-phase boundary over a wide range of flow rate conditions in the EMD.
3. To determine if the theory of thermodynamics of electrochemically driven ion transfer processes at TPEs under static conditions can be transferred to EMD.
4. To determine the mediated electrochemical sensing of an antioxidant compound at the solid|solid interface.

Chapter 3

MATERIALS AND METHODOLOGY

This chapter shows practical aspects of applying microfluidic devices as electrochemical cells. The principle knowledge of ion and electron transfer processes driven by electrochemical reaction included in chapter 1 is extended to our studies with electrochemical microfluidic device (EMD). With an EMD one can introduce two immiscible liquid phases flowing parallel and these two streams together with the working band electrode create the three-phase electrode under microfluidic conditions. As in the previous chapter the ion transfer takes place between the two adjacent immiscible liquids and the electron transfer in the phase where the electrochemical reaction goes on.

3.1 CHEMICALS AND MATERIALS

3.1.1 Chemicals

Redox compounds: decamethylferrocene (DMFc) (97 %, ABCR), ferrocene (Fc) (98 %, Aldrich), TEMPO (97 %), 4-carboxy-TEMPO (98 %), 4-methoxy-TEMPO (97 %), 4-amino-TEMPO (97 %), 4-acetamido-TEMPO (97 %) (Sigma-Aldrich)

Antioxidant: diphenyl carbinol (DPC).

Organic salts: tetraheptylammonium tetraphenylborate ($THepA^+TPB^-$) (Selectophore, Fluka), tetrahexylammonium perchlorate ($THxA^+ClO_4^-$) (ABCR), tetraoctylammonium nitrate ($TOA^+NO_3^-$) (99 %, Sigma-Aldrich), tetraoctylammonium bromide (TOA^+Br^-) (98 %, SigmaAldrich), tetraphenylarsonium chloride ($TPAs^+Cl^-$) (99 %, StremChemicals), sodium tetraphenylborate (Na^+TPB^-) (Selectophore, Fluka), potassium tetrakis(4-chlorophenyl) borate (K^+TPBCl^-) (98 %, Sigma-Aldrich).

Inorganic salts: KPF_6 (98 %, Sigma-Aldrich), $NaClO_4$ (>99 %, Fluka), NaSCN (purum, Fluka), KNO_3 (99 %, POCh), KBr (pure p.a., POCh), NaCl (>99.99 %, Fluka), NaF (pure p.a., POCh).

Organic solvents: *N*-octyl-2-pyrrolidone (NOP), acetonitrile (ACN) (99.8 %, Sigma-Aldrich), 1.2-dichlorobenzene (DCB) (99 %, Aldrich), 4-(3-Phenylpropyl)-pyridin (PPP) (97 %, Aldrich), trifluorotoluene (TFT) (99 %, Acros Organics).

Materials for microfluidic preparation

Polydimethylsiloxane (PDMS) (elastomer and curing agent) Sylgard 184 (Dow Corning Corporation), AZ ECI 3027 photoresist, AZ 400 K Developer (MicroChemicals GmbH), SU-8 negative photoresist, (MicroChem), glass slides (Roth GmbH), silicon wafers were obtained from Topsil. All chemicals were used without further purification. Filtered and demineralized water was taken from an ELIX purification system (Millipore).

3.1.2 Equipment and methodology

Cyclic voltammetry (CV), square wave voltammetry (SWV) and chronoamperometry (CA) were carried out in a three-electrode setup (Fig. 3.2.1a) and registered with Autolab potentiostat (Metrohm Autolab B.V.). Parameters for SWV were: frequency 8 Hz, step potential 0.001 V, amplitude 0.05 V. Both in experiments with TFE and TPE systems under the static conditions, a GC working electrode was used (surface area of 0.031 cm^2) (Fig. 3.1.1). The procedure for preparation of the GC working electrode (WE) includes polishing of the electrode surface with 1, 0.3 and 0.05 μm Al_2O_3 (Buehler) slurry and sonication in demineralized water and in ethanol. Next, a microliter droplet of the organic phase was deposited on the GC surface with a micropipette. The volume of the droplet was 2 μL (for TFEs) or 1 μL (for TPEs).The droplet-modified electrodes were immersed in the aqueous electrolyte solutions. All measurements were performed with a silver-silver chloride reference electrode (Ag|AgCl|3 M KCl) (RE) and Pt wire used as the counter electrode (CE).

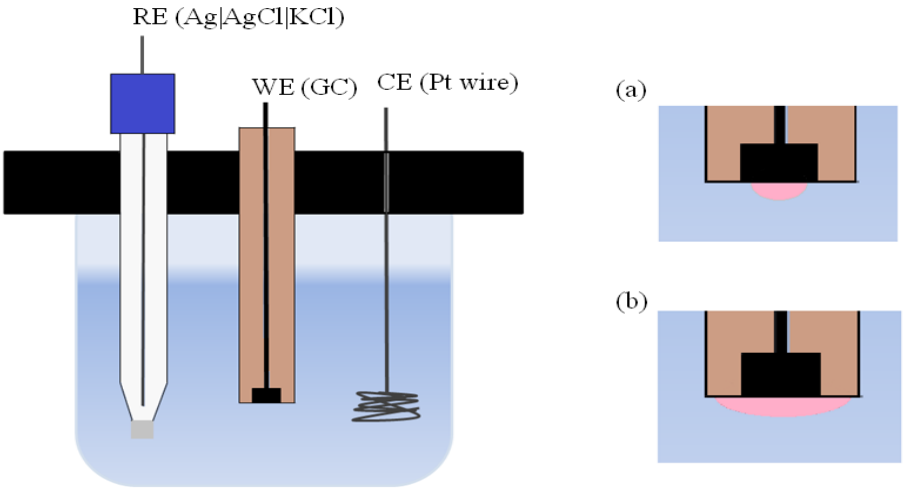

Fig. 3.1.1 Schematic illustration of the experimental setup under the static conditions in **(a)** TPE system and in **(b)** TFE.

Part of the work related with mediated electrocatalytic conversion were carried out using a graphite working electrode (GE) with 4.9 mm diameter mounted in a Teflon holder and with saturated calomel electrode (SCE) and Pt wire used as the reference and counter electrodes, respectively (Fig. 3.1.2). All experiments were carried out at room temperature (22 ± 2 °C).

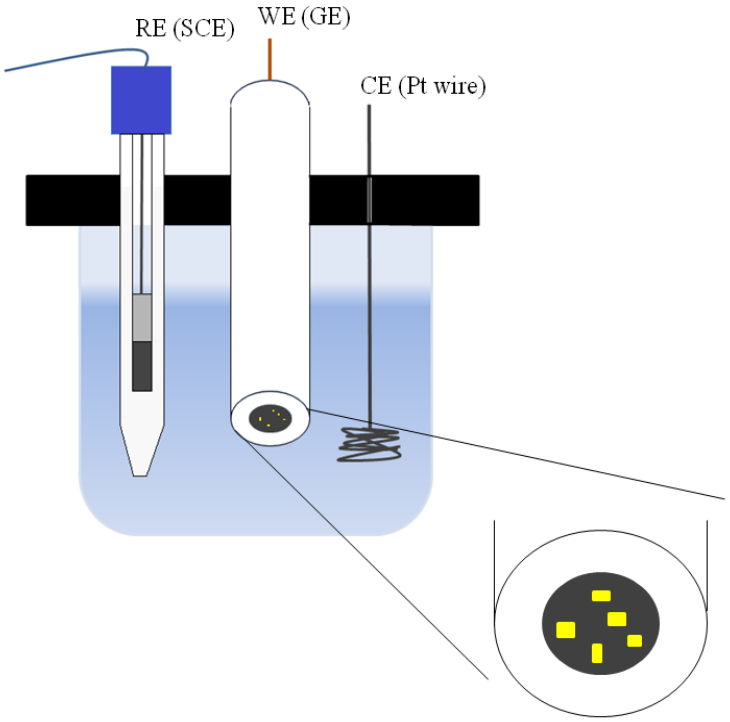

Fig. 3.1.2 Schematic illustration of the experimental setup under the static conditions with mediated electrocatalytic conversion.

a) Electrochemical microfluidic device fabrication

The two phase microfluidic channel was fabricated in PDMS using the replica micromolding method. Photolithographic masters were prepared from SU-8 in base relief on silicon wafers and a PDMS/curing agent mixture (ratio 1:10) was poured onto the master and dried at 80 °C for 1.5 h. The system consists of a straight channel with Y-junctions for inlets and outlets for the aqueous and organic phases separately (Fig. 3.1.3). The main channel has a width of 500 μm and height of 200 μm. Capillary channels (2 mm long and 50 μm wide) connect the two side reservoirs with the main channel. In the reservoir on the aqueous side the reference electrode (RE) was placed. The hole around the RE was sealed with a small amount of PDMS. The reservoir on the organic side is not used in these experiments but could house a second reference electrode for using a four-electrode setup. Gold working (width from 100 μm to 1 mm) and counter electrodes (width from 1 mm to 5 mm) were patterned on a glass microscope slide using standard photolithography. The thickness of the sputtered gold electrodes was 150 nm with a 5 nm titanium adhesion layer. The PDMS channel was mounted to the glass plate with the electrodes perpendicular to the channel. The assembly was held together using a polycarbonate holder. For the confocal microscopy measurements the PDMS was bonded to the glass plate by exposure to an O_2 plasma for 50 s (Harrick, Model PDC-32G-2, 100 W). To control the flow of the aqueous and organic phases, two synchronized syringe pumps (Harvard Apparatus, Pump 11 elite) were used. The syringes were connected to the channel using polyethylene tubing.

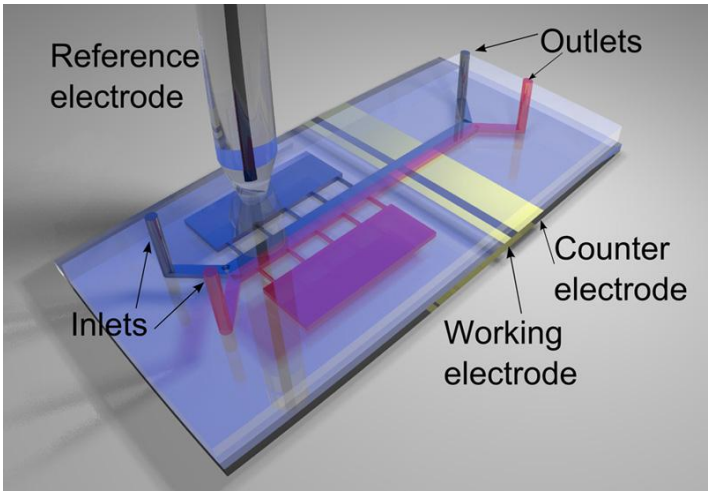

Fig. 3.1.3 Schematic illustration of the assembled EMD.

b) Biphasic electrochemical microfluidic device

Working and counter gold band electrodes were located at the bottom of the main channel perpendicular to the flow direction. The Ag|AgCl|3 M KCl reference electrode was placed in the aqueous-side reservoir. During the electrochemical measurements, the flow rate of the aqueous phase ($V_{f,\ aq}$) was set 8 times higher than the flow rate of the organic phase ($V_{f,\ org}$) to keep the widths of the parallel aqueous and organic phases streams equal. In the result the position of the three-phase boundary can be well defined and stable over a wide range of flow rate conditions. The position of the three-phase boundary is determined by the relative viscosities of immiscible liquids [1-3]:

$$\frac{w_{aq}}{w_{org}} = \frac{\eta_{aq}}{\eta_{org}} = \frac{1}{\alpha} \qquad \text{(Eq. 3.1.1)}$$

where w_{aq} and w_{org} describe widths of the aqueous and organic streams of flowing liquids, respectively. η is the viscosity and the parameter α is the ratio of the viscosity of the organic to the aqueous phase. The effect of the adjustment of the same width of two immiscible flow phases in our EMD can be observed in the optical microscopy photograph presented below.

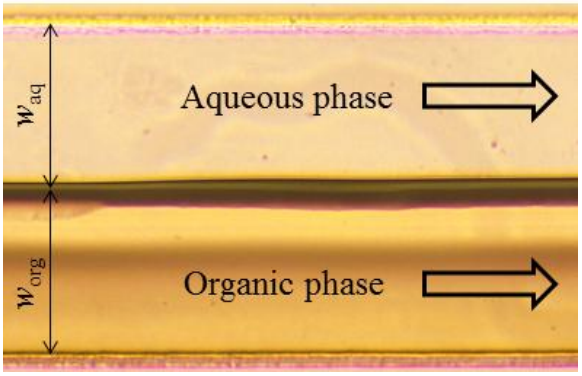

Fig. 3.1.4 Photograph showing our EMD from the top with the parallel flowing aqueous and organic phase (*N*-octyl-2-pyrrolidone), respectively. The widths of the aqueous (w_{aq}) and organic (w_{org}) phase were adjusted at the same level. The flow rate of the aqueous phase was set on 5 μL min^{-1} and flow of the aqueous phase was set on 40 μL min^{-1}.

If not specifically mentioned, the flow rates were kept constant at $V_{f,\ aq}$ = 40 μL min^{-1} and $V_{f,\ org}$ = 5 μL min^{-1}. To control the flow of the aqueous and organic phases, two syringe pumps (Harvard Apparatus, Pump 11 elite) were used. The syringes were connected to the microfluidic system via polyethylene tubing.

3.2 TECHNIQUES

3.2.1 Voltammetry

Voltammetry is the electroanalytical technique to analyze the dependence of the current which flows through the working electrode as a function of the applied electrode potential. The voltammetry measurements are carried out by application of an electrode potential that is varied over time. The obtained voltammetry curves give both qualitative and quantitative information about the electrochemical reactions taking place at the working electrode. The main advantage of voltammetry techniques is the high sensitivity in detection of the analytical signal and that the direction of the potential sweep can be reversed when a given value of the potential is reached. The obtained slope of potential, E vs time, t is called the potential scan rate (in V s^{-1}) and the response of the electrochemical system is usually represented by a curve $I = f(E)$. The electrochemical oxidation/reduction in case of voltammetry is determined by the kinetics of the electrode reaction as well as by the rate of transport of analyte towards the surface of the working electrode. In the classic voltammetric system three electrodes are used.

Controlling of the electrochemical system can be provided by a potentiostat (Fig. 3.2.1).

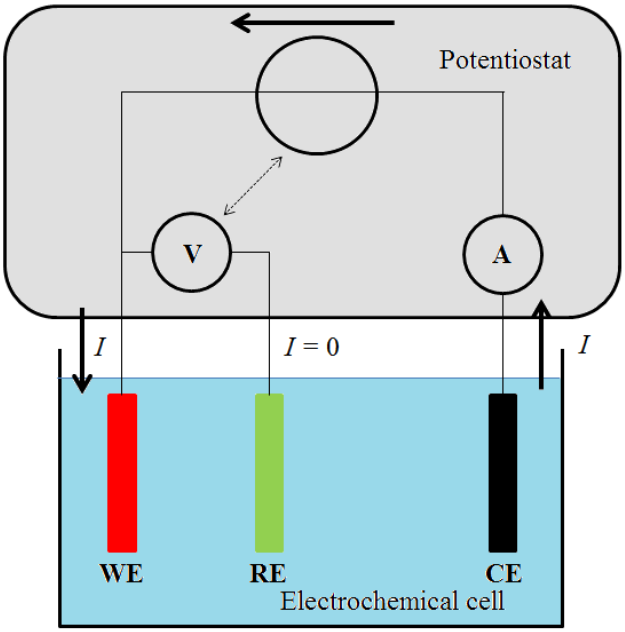

Fig. 3.2.1 Schematic sketch of an electrochemical setup using a potentiostat. The electrochemical cell contains submerged three-electrode system with: working (WE), reference (RE) and counter electrode (CE), respectively. The dotted arrow between voltmeter (V) (controlled voltage between WE and RE) and the voltage delivered by the power supply between WE and CE shows the existing link between them.

A potentiostat is needed for quantitative research studies with a three-electrode system. The three-electrode setup consists of working (WE), reference (RE) and counter (CE) electrodes. The current flows between the CE and WE where the studied reactions take place and the potential is controlled between WE and RE. Usually, the processes at the CE are not interesting for the experimenter. Instead, the role of the CE is providing a path for the current to travel. Therefore its area should be sufficiently large to ensure that the reactions on the CE are not rate limiting. The position of RE electrode should be as close as possible to the WE to minimize the solution resistance. Since there is no current flow through the RE, this electrode can be assumed as ideally nonpolarizable. In situations when a typical reference electrode like silver-sliver chloride electrode (Ag|AgCl|3 M KCl) is difficult to implement, a pseudo-reference electrodes can be used instead. For instance it may be a metal wire (platinum, silver etc.) or e.g. a surface of sputtered metal (gold) on an adhesion layer (titanium or chromium). The important difference is that in contrast to classic reference electrodes, the interface between the pseudo-reference electrode and the electrolyte is not in thermodynamic equilibrium [4,5].

3.2.1.1 Cyclic voltammetry

Cyclic voltammetry (CV) is a very popular tool among the many different electroanalytical techniques. This method gives fast, qualitative information about electrochemical processes. However, cyclic voltammetry can also give quantitative information about the thermodynamics of electrochemical redox reactions or kinetics of the electrochemical electron transfer [6]. The CV technique is commonly used not only for pure electrochemical purposes but is also popular in organic chemistry to follow reaction pathways [7] or to monitor e.g. the effect of ligands on the redox potential of the central metal ion in complexes in multinuclear clusters [8].

In case of mass transfer processes in the simplest electrode reaction the movement of compound from one location in solution to another is driven by a gradient of electrical or chemical potential. Generally the mass transfer to an electrode is described by the Nernst-Planck equation which includes three modes of mass transfer: diffusion, migration and convection. When solution of analyte contains a sufficient concentration of the supporting electrolyte and when the electrochemical measurements are carried out under controlled conditions (constant temperature, avoiding of stirring and vibrations during measurements), the contributions from migration and convection for transport of electroactive species can usually be neglected.

In this particular case the mass transport of redox species is determined by diffusion and only the first part of the Nernst-Planck equation is taken into account:

$$J_{\mathrm{i}}(\mathrm{x}) = -D_{\mathrm{i}} \frac{\partial c_{\mathrm{i}}(\mathrm{x})}{\partial \mathrm{x}} \qquad \text{(Eq. 3.2.1)}$$

Here $J_{\mathrm{i}}(\mathrm{x})$ is the flux of species i at a distance x from the electrode surface, D_{i} is the diffusion coefficient and $\frac{\partial c_{\mathrm{i}}(\mathrm{x})}{\partial \mathrm{x}}$ is the concentration gradient at a distance x.

In case of cyclic voltammetry technique, the applied voltage is changing linearly with time. The schematic of potential changes in cyclic voltammetry measurement are shown in Fig. 3.2.2. The potential applied to the working electrode is scanned from an initial value E_1 towards a predetermined limit E_2 where the scan direction is reversed, resulting in a triangle wave-shape potential curve [4,5].

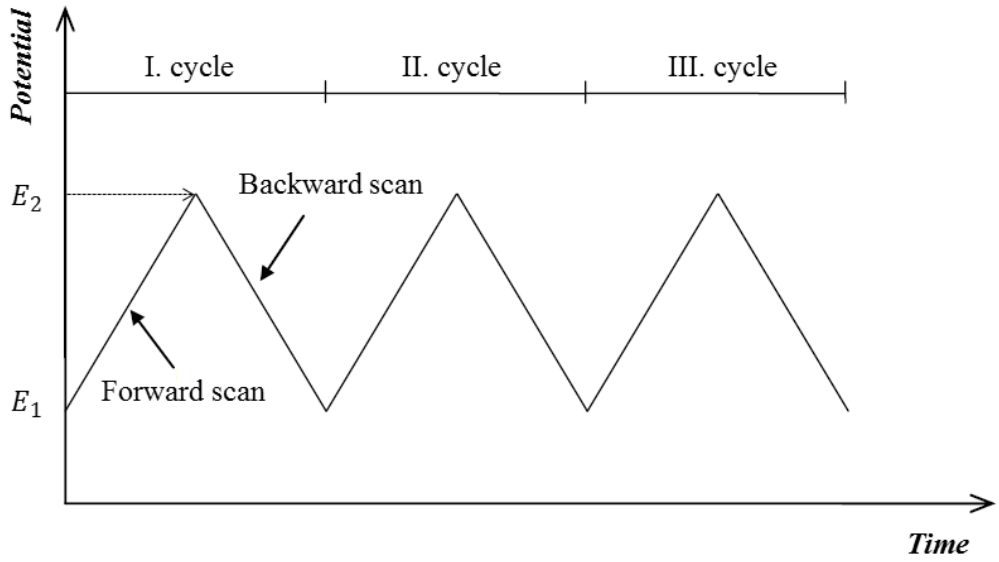

Fig. 3.2.2 The schematic of potential changes versus time in CV.

The plot of current response versus applied voltage in CV is called cyclic voltammogram (Fig.3.2.3). The cyclic voltammetry measurements can be divided into two main stages. The first one is called primary stage where e.g. the potential is scanned in the positive direction and the anodic peak(s) of electrooxidation(s) can be seen. In the reverse stage where the potential is scanned in the negative direction the cathodic peak(s) of electroreduction(s) can be seen. The voltage cycle can be repeated many times, depending on the experiment. Fig. 3.3.2 depicts a cyclic voltammogram where the reduced form

of the electroactive species undergoes electrooxidation and later electroreduction at the working electrode surface.

During scanning, the potentiostat registers the values of the current as a function of applied voltage. To follow the electrooxidation showed in Fig. 3.2.3 when the applied potential reaches the level of formal potential of the electroactive species $E^{o'}$, the electrooxidation reaction begins. In case of an electrooxidation, the concentration of the reduced form decreases since it is converted to the oxidized form. As the applied potential moves past the redox potential the surface concentration of the reduced form drops almost to zero and the mass transfer of the this form reaches the maximum value. In the reverse process application of more negative voltage generates again the reduced form of the electroactive species and a cathodic current starts to flow. Important parameters which can be taken from cyclic voltammogram are anodic $E_{p,a}$ and cathodic $E_{p,c}$ peak potentials, maximum values of anodic $I_{p,a}$ and cathodic $I_{p,c}$ currents and mid-peak potentials of peaks E_{mp} $\left(\frac{E_{pa}+E_{pc}}{2}\right)$. The value of $I_{p,a}$ and $I_{p,c}$ are measured from baseline which is a continuation of the cathodic or the anodic curve [9].

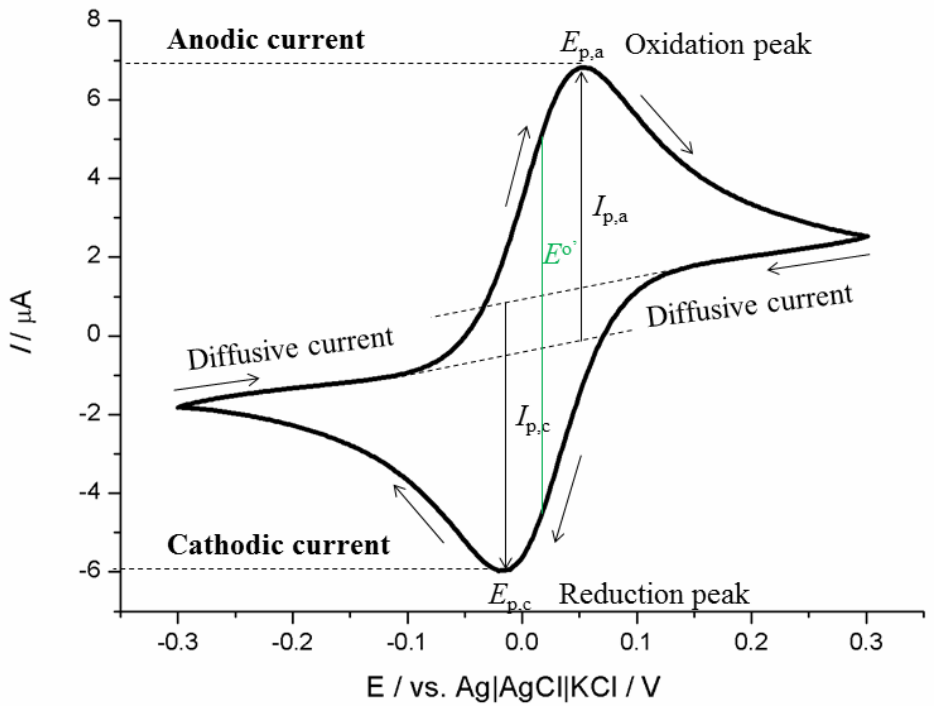

Fig. 3.2.3 Exemplary CV for the reversible electrochemical oxidation of DMFc. I_{pa} and I_{pc} are anodic and cathodic current, respectively. $E_{p,a}$ and $E_{p,c}$ are anodic and cathodic values of potential. Term is $E^{o'}$ is formal potential of the redox couple DMFc/DMFc$^+$.

The reaction can be called electrochemically reversible when it is in agreement with the Nernst equation:

$$E = E^{o'} + \frac{RT}{nF}\ln\frac{c_O}{c_R} \quad \text{(Eq. 3.2.2)}$$

The term of electrochemical reversible reaction is dedicated for reactions where the value of the measured potential equals the potential calculated from the Nernst equation. Other foundations of the reversibility of electrochemical reaction say that the limited step in such reactions is not electron transfer but the transport of the electroactive species to the electrode surface. Other assumptions are that:

- the electrode surface does not react with the reagents;
- the reduced form of the electroactive species is stable in the selected potential window;
- the ratio of the anodic peak current to the cathodic one equals 1 ($I_{p,a}/I_{p,c} = 1$).

In electrochemically reversible system it is possible to determine redox potential of the reaction which in that case is equal to the formal potential of the reaction. The difference between the peak potentials for a reversible reaction at room temperature is described by:

$$\Delta E = E_{p,a} - E_{p,c} = \frac{0.057}{n} \quad \text{(Eq. 3.2.3)}$$

The peak current is described by the Randles-Sevcik equation:

$$I_p = (2.69\text{x}10^5)n^{3/2}AD_o^{1/2}c_o^*v^{1/2} \quad \text{(Eq. 3.2.4)}$$

where D is the diffusion coefficient, n is the number of electrons transferred in the redox reaction, A is the area of the electrode surface, c^* is initial concentration of electroactive species in the solution and υ is the potential scan rate. The current is proportional to concentration of the redox species and the square root of the potential scan rate, but for a reversible reaction it does not depend on the specifics of the reaction itself.

3.2.1.2 Cyclic voltammetry under microfluidic conditions

Analysis of cyclic voltammograms under hydrodynamic conditions differs from classic voltammetric curves. The difference is determined by the type of transport electroactive species to the working electrode. Under hydrodynamic conditions, analyte is delivered to the electrode surface via convective transport controlled by stirring or pumping the solution. Among these techniques, several methods can be distinguished like: rotating disk

electrode (RDE), rotating ring-disk electrode (RRDE) or microfluidic devices. The object of this thesis is the application of microfluidic devices as electrochemical cells.

The dimensions of the microchannel and often used band electrode arrays determine the cyclic voltammetry measurements. The microflow direction is generally perpendicular to the position of the microband electrodes [10]. However, others configurations of electrode pattern in microfluidic channel are also possible like in the paper of Kadilak et al. where gold electrodes are deposited on the sides of microchannel [11]. Other possibility is formation of micropillars as vertical electrodes in the channel [12,13]. The micropillars are made with photo sensitive resin and covered with a thin metal layer to provide conductivity.

The typical cyclic voltammogram for microfluidic conditions is usually called hydrodynamic voltammogram. To understand the characteristic behavior of hydrodynamic voltammetry it is necessary to go into details of diffusion layer thickness controlling the flux of the material to the electrode surface (Fig. 3.2.4b).

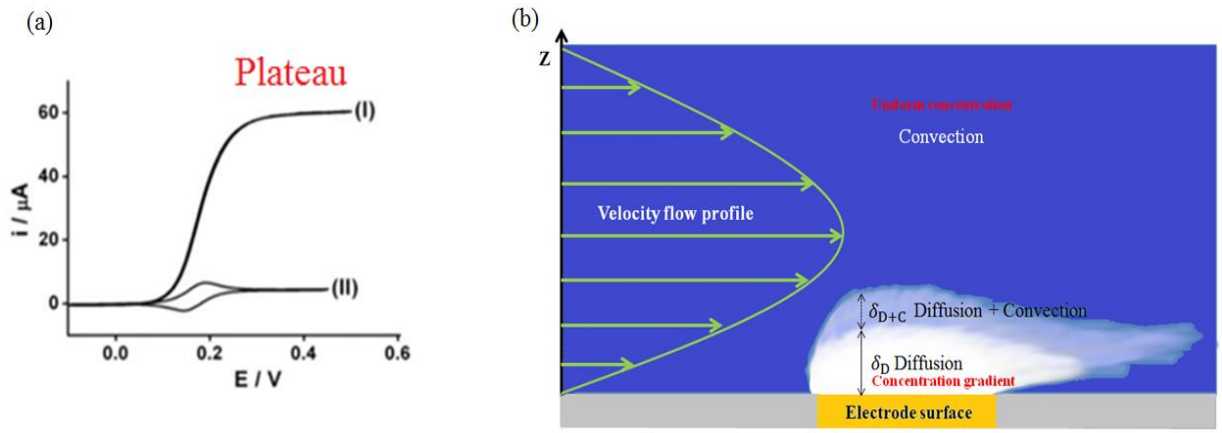

Fig. 3.2.4 (a) Difference in voltammogram shape between stationary (II) and hydrodynamic mode of voltammetry (I) [14]. **(b)** Diffusive/convective phenomena in EMD.

It is necessary also to distinguish major difference between CV measurements performed in classic, unstirred electrochemical cells and EMD (Fig. 3.2.4a). Under static conditions the steady-state current is determined by diffusion of analyte, in contrast to the steady-state current obtained under microfluidic conditions where it is determined by the laminar flow of analyte across the microband electrode. The characteristic shape of the hydrodynamic voltammogram is the consequence of the way of transport of analytic solvent onto band electrode surface. Electroactive species delivered onto electrode surface undergoes electrochemical reaction and afterwards the reaction product is washed out from the electrode surface with flowing solvent. The difference between hydrodynamic and classic voltammogram is visible in Fig. 3.3.3a. Voltammogram performed under the static conditions

(Fig. 3.2.4a II) has standard diffusive shape with visible peaks of oxidation and reduction. As the flow rate is increased the distance that electroactive compound can diffuse from the surface before being removed by convection is decreased. This results in a higher flux of redox species to the surface at higher flow rate values. The mass transport limited current arises from the fact that the system reaches a steady state and the current reaches a plateau once the equilibrium at the surface is driven to the products side. Since the programmed flow rate is critical parameter controlling of delivery the electroactive species onto working band electrode surface and other parameters in Levich equation (Eq. 2.3.1) of EMD so the electrochemical reaction under microfluidic control is mathematically well defined [15].

3.2.1.3 Square-wave voltammetry

Square-wave voltammetry (SWV) is another popular electroanalytical technique. Analytical signal is obtained from waveform curve. Results are facilitated by waveform as consisting staircase scan. Each step in the curve is imposed by a double pulse (one in forward and second one in the reverse direction). One of the visible advantage of this technique in contrast to e.g. CV is elimination of the influence of capacitive current. A large capacitive (background) current makes it difficult to detect the faradaic current from electrochemical reaction and generally is signal of interest. SWV is a pulsed technique and it can discriminate against the charging current and eliminate this obstruction. In general comparison with CV technique, SWV has an advantage over this technique in two main aspects presented below:

a) Speed of the analysis

The possibility of removing the background (nonfaradaic) current allows to program higher scan rates and finally that gives opportunity to analyse fast electrochemical reactions.

b) Dynamic range of detection

The dynamic range of detection defines ability of a detection system to respond to both high and low concentrations of electroactive compound. Since SWV effectively removes nonfaradaic current, that gives the possibility to use concentration of the redox species as an experimental variable.

SWV was mainly developed by the Osteryoungs and coworkers where they showed experimental capabilities of SWV [16]. In this technique the potential changes are presented in the form of staircase shape. The characteristic feature of square-wave voltammetry is fact mentioned above that the potential wave form contains constant amplitude of square wave which is superimposed on a staircase wave form (Fig. 3.2.5).

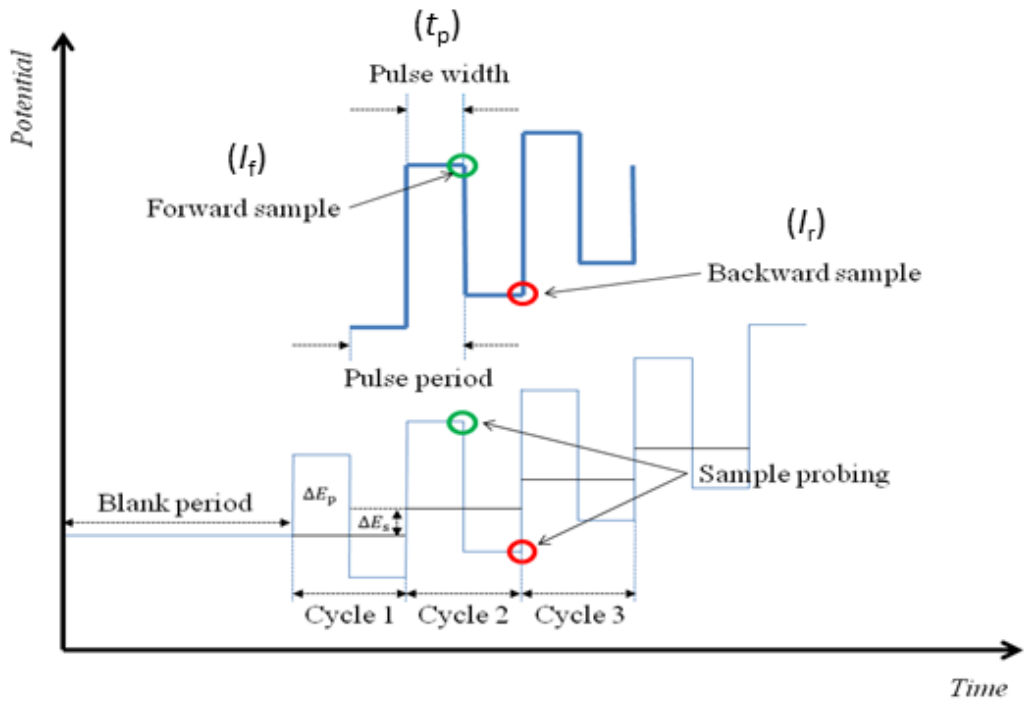

Fig. 3.2.5 The principles of the SWV.

The potential range is scanned through the defined range and this technique is similar to classic voltammetry but an additional square wave is applied. The current is sampled two times during each square wave cycle (green and red circles in Fig. 3.2.5), first time at the end of the forward pulse, called the forward sample and again in the reverse sampling event at the end of the second pulse. From analytical point of view the essential thing is the difference between the values of the forward current sample (I_f) and reverse current sample (I_r) and it gives finally three voltammograms with forward, reverse and differential current. The differential current between the average currents in the forward and the reverse pulse is plotted vs. the potential staircase. Square wave voltammograms show a peak for faradaic processes where the height of the peak is proportional to the concentration of the electroactive compound in the solution. The square wave is characterized by such parameters like: pulse height (ΔE_p) measured according to programmed staircase potential; width of pulse (t_p), the staircase shift (ΔE_s) or frequency of the square wave $\left(f = \frac{1}{2t_p}\right)$.

The possibility to rapid scan of wide potential range gives opportunity using SWV in many experimental purposes. SWV has been used in the study the kinetics and formation constants of complexes [17]. Webber and coworkers showed application of SWV in determination of biological compounds like: investigation of electrochemical reduction of cimetidine which is an antagonist of histamine used in the treatment of gastric ulcers [18];

monitoring of the electrochemical reduction of NADH (nicotinamide adenine dinucleotide) at a static mercury electrode [19]; examination of others adenine and nicotinamide-containing compounds to determine the cathodic stripping voltammetry [20].

3.2.2 Chronoamperometry

Another technique commonly used in many electrochemical purposes is chronoamperometry. The idea of this technique is based on applying a potential step (or a series of steps) to the working electrode and monitoring the resultant current as a function of time. In the situation presented in Fig. 3.2.6 the working electrode is submerged in a solution initially containing only the reduced from of electroactive compound (Red) in an electrolyte solution. At the beginning the potential (E_1) is kept at a more negative value than formal potential $(E^{o'})$. At a time (t_o), the potential is stepped to a much more positive potential than $E^{o'}$.

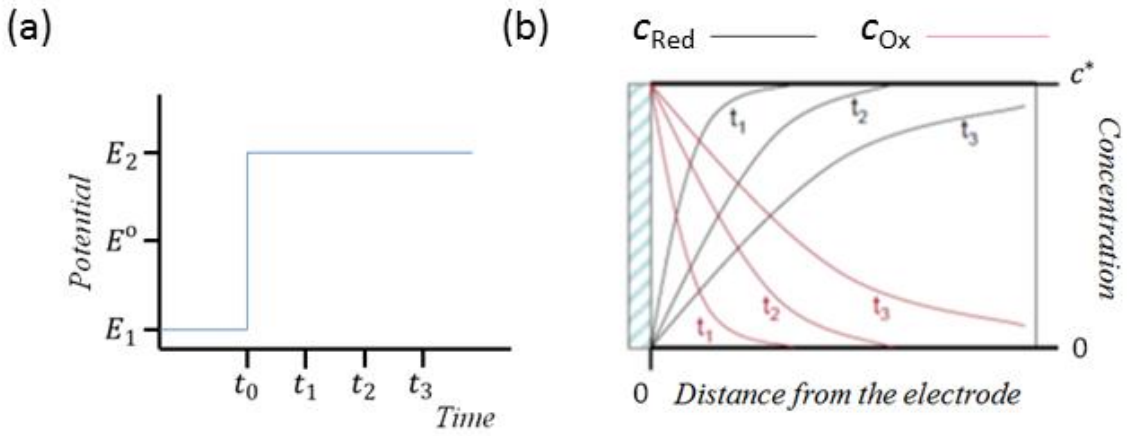

Fig. 3.2.6 The principles of the CA measurements.

In the result of electrochemical reaction at the working electrode boundary the initial concentration (c^*) of electroactive compound Red is immediately oxidized to zero value. The electrochemical reaction leads to the creation of a diffusion zone. The concentration gradient between zone in bulk solution and working electrode surface provokes diffusion of the Red form to the electrode surface. The longer time the oxidizing potential is kept, the further the range of the diffusion zone extends.

Chronoamperometry measurements can usually be performed into two main ways: single potential step or double potential step. In the first case the faradaic current is resulting from the forward step described in above description. In case of double potential step application, the applied potential is returned to his initial value following the time period where potential

is kept in the region of redox process. The opposite case is when the solution contains initially Ox form of electroactive compound.

The important equation in chronoamperometry technique is the Cottrell equation (Eq. 3.2.5) which describes the registered electric current as a function of $t^{-1/2}$ in controlled potential experiment:

$$i = \frac{nFAc^* D_O^{1/2}}{\pi^{1/2} t^{1/2}} \qquad \text{(Eq. 3.2.5)}$$

where n is the number of electrons involved in the reaction, A is the working electrode area, c^* is the initial concentration of electroactive compound and other parameters have their standard meanings. The current measured depends on the rate which analyte diffuses to the working electrode surface and thus the current is under diffusion control. The Cottrell equation described is valid for planar electrodes but is possible to modify this equation with the Cottrell equation then is in agreement with other shapes of electrode surfaces (spherical, cylindrical etc.) [9].

Chronoamperometry technique can be used as a useful tool in many analytic applications like: controlling the concentration of electroactive compound in the function of time [4], the shape of the current curve versus time can be analyze in order to determine coupled chemical reaction or rate the electrochemical process. Silber and coworkers showed application of chronoamperometry to study the kinetic parameters of electron-acceptor complex between *N,N,N′,N′*-tetramethyl-*p*-phenylenediamine (TMPD) and *m*-dinitrobenzene in acetonitrile with $NaClO_4$ as a supporting electrolyte [21]. They calculated rate constants k_f of formation TMPD and reverse reaction rate constant k_b and this information are extracted from chronamperometric curves.

3.2.3 Laser scanning confocal microscopy (LSCM)

Laser scanning confocal microscopy is a type of microscopy technique for making high resolution and to reconstruct three dimensional structures of analyzing micrographs. This kind of microscopy was invented by M. Minsky, a Harvard postdoctoral fellow who was studying interconnections between neuronal cells [22,23]. The characteristic feature distinguishing confocal scanning laser microscopy from classical optical microscopy is the presence of a pinhole aperture that limits out-of-focus light from entering the detector. The principles of the technique have a number of events:

- laser beam which is introduced from light source is reflected and scattered on a dichroic mirror,
- the laser beam goes through the scanning mirrors where the beam direction can be adjusted,
- the objective focuses the laser beam in one spot and the laser beam has ability to excite the specimen which often contains fluorescent dye that gives emission of a longer wavelength,
- the light emitted from points on the specimen pass back through the scanning and dichroic mirrors and reaches the pinhole aperture,
- installed detectors transform the signal from the laser to a digital signal.

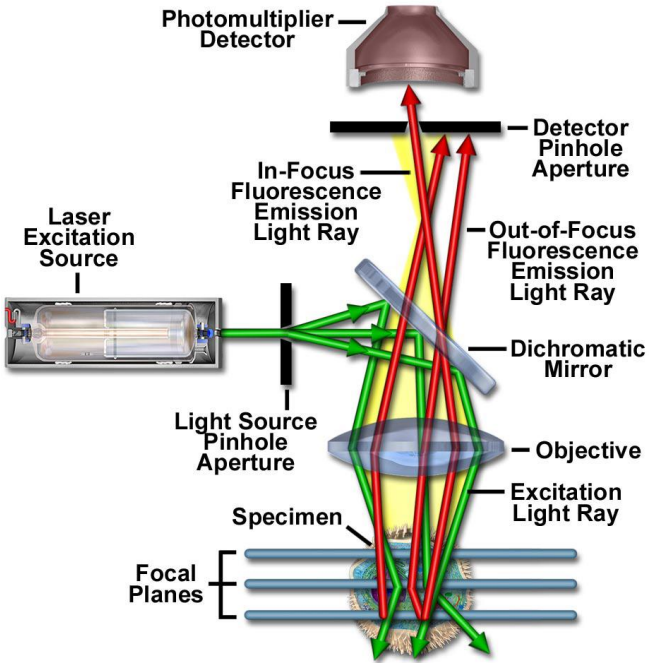

Fig. 3.2.7 Schematic diagram of the optical pathway in a laser scanning confocal microscopy [24].

The light intensity is detected with a photodetection device (often photomultiplier or photodiodes).

From structural point of view the most important part of confocal microscope is the scan head. It has responsibility for rasterizing the excitation scans and also collecting the photon signals from the sample which finally gives the assembled micrograph. The essential feature of confocal microscopy is presence of pinhole aperture which acts as a filter which focuses the image plane in front of detector. The aperture system eliminates additional fluorescence signals from out-of-focus planes. It gives fine resolution and contrast in comparison to standard wide field fluorescence microscopy. The biggest advantage of confocal microscopy

over classical optical microscopy is possibility to collecting the 3D topography structure of specimen and reduction of unnecessary light from other part from not in the focal plane.

Apart from utilization of LSCM in imaging biological samples, this technique is also useful in combination with electrochemistry e.g. in monitoring the evolution of copper surface topography [25]. Herein, LSCM was able to reconstruct surface topography in vertical range from submicrometers to tens of micrometers. In another publication, Fahidy and coworkers showed utilization of LSCM to measure the roughness of the metal sample (copper) deposit on the cathode surface in a copper electrorefining cell [26].

3.3 BIBLIOGRAPHY

[1] S. M. MacDonald, J. D. Watkins, Y. Gu, K. Yunus, A. C. Fisher, G. Shul, M. Opallo, F. Marken, *Electrochem. Commun.* **2007**, *9*, 2105−2110.

[2] A.E. Kamholz, B.H. Weigl, B.A. Finlayson, P. Yager, *Anal. Chem.* **1999**, *71*, 5340.

[3] P.J. Stiles, D.F. Fletcher, Lab Chip **2004**, *4*, 121.

[4] A. J. Bard, L. R. Faulkner, *Electrochemical Methods: Fundamentals and Applications* **2001**, John Wiley & Sons, New York.

[5] C. M. A. Brett, A. M. O. Brett, *Electrochemistry: Principles, Methods, and Applications* **1993** Oxford University Press: New York.

[6] H. Yang, A. J. Bard, *J. Electroanal. Chem.* **1991**, *306*, 87.

[7] E. Gileadi, *Electrode Kinetics for Chemists, Chemical Engineers and Material Scientists* **1993**, VCH, Weinheim.

[8] F. Wang, Y. H. Lai, M. Y. Han, *Org. Lett.* **2003**, 5, 4791.

[9] C. G. Zoski, *Handbook of Electrochemistry* **2007**, Elsevier.

[10] K. Yunus, C. B. Marks, A. C. Fisher, D. W. E. Allsopp, T. J. Ryan, R. A. W. Dryfe, S. S. Hill, Roberts E. P. L., C. M. Brennan, *Electrochem. Commun.* **2002**, *4*, 579−583.

[11] A. L. Kadilak, Y. Liu, S. Shrestha, J. R. Bernard, W. E. Mustain, *J. Electroanal. Chem. 727*, 141.

[12] S. C. Kilchenmann, E. Rollo, E. Bianchi, C. Guiducci, *Sens. and Act. B* **2013**, *185*, 713.

[13] S. Numthuam, T. Ginoza, M. Zhu, H. Suzuki, J. Fukuda, *Analyst* **2011**, *136*, 456.

[14] R. A. B. da Silva, E. G. N. de Almeida, A. C. Rabelo, A. T. C. da Silva, L. F. Ferreira, E. M. Richter, *J. Braz. Chem. Soc.* **2009**, *20*, 1235.

[15] R. G. Compton, A. C. Fisher, R. G. Wellington, *J. Phys. Chem.* **1993**, *97*, 10410.

[16] J. O'Cea, J. Osteryoung, R. A. Osteryoung, *Anal. Chem.* **1981**, *53*, 695.

[17] E. J. Zachowski, M. Wojciechowski, J. Osteryoung, *Anal. Chim. Acta* **1986**, *183*, 47.

[18] A. Webber, M. Shah, J. Osteryoung, *Anal. Chim. Acta* **1983**, *154*, 105.

[19] A. Webber, M. Shah, J. Osteryoung, *Anal. Chim. Acta* **1984**, *157*, 1.

[20] A. Webber, J. Osteryoung, *Anal. Chim. Acta* **1984**, *157*, 17.

[21] M. A. Zon, H. Fernandez, L. Sereno, J. J. Silber, *Can. J. Chem.* **1990**, *68*, 278.

[22] M. Minsky, *Microscopy Apparatus*, US Pat. 3,013,467, **1961**.

[23] M. Minsky, *Scanning* **1988**, *10*: 128.

[24] N. S. Claxton, T. J. Fellers, M. W. Davidson, *Laser Scanning Confocal Microscopy* Department of Optical Microscopy and Digital Imaging, National High Magnetic Field Laboratory, The Florida State University, Tallahassee, Florida 32310.

[25] M. A. Alodan, W. H. Smyrl, *J. Electrochem. Soc.***1998**, *145*, 957.

[26] X. Ling, Z. H. Gu, T. Z. Fahidy, *Electrochem. Acta.* **1995**, *40*, 1789.

Chapter 4

RESULTS AND DISCUSSION

The main inspiration for this work was the application of electrochemical microfluidic device (EMD) as microreactor in electrochemistry of liquid|liquid interface. Electrochemical processes at the liquid|liquid interface are interesting from fundamental point of view in many biological systems and in chemical technologies like in: extraction, separation, organic synthesis or in electrocatalysis [1,2]. EMD offers electrochemistry an increased rate of mass transport in comparison to typical conditions occurring in classic electrochemical cells.

The first subchapter is oriented towards examination of the durability of PDMS made microchannel to different organic solvents like: trifluorotoulene, 1,2-dichlorobenzene, etc. This first part of the work gave information about the stability of the PDMS microchannel during long lasting electrochemical measurements with particular solvents and was a solid base that the EMD used in this thesis was suitable for the further studies.

The second subchapter examins the effect of the flow rate on the electrochemical oxidation of ferrocene (Fc) at a liquid|liquid interface over a wide range of flow rates. Organic NOP|aqueous electrolyte|gold electrode three-phase boundary is examined using cyclic voltammetry (CV) and laser scanning confocal microscopy (LSCM). The curious behavior of the three-phase boundary was described using a simple mathematic model postulating a smallest effective width of the three-phase boundary and that model is in agreement with experimental data.

Subchapter 4.3 is further utilization of EMD in investigations of electrochemically driven ion transfer processes. The effect of ion transfer potential and ion concentration effect on the voltammetric peak potential was compared between droplet and microfluidic three-phase electrodes (TPE). As electrochemical reaction, the oxidation of decamethylferrocene (DMFc) connected with the transfer of anions from aqueous electrolyte solution to organic NOP was studied.

The last subchapter contains experiments performed under static conditions where directly immobilized diphenylcarbinol (DPC) undergoes chemical oxidation to benzophenone (BP)

and this reaction is electrochemically mediated using 2,2,6,6-tetramethyl-1-piperidinyloxy radical (TEMPO). The kinetics of conversion of DPC to BP was studied with 5 different TEMPO derivatives. These experiments were supposed to be an initial study for experiments in an EMD where rate of conversion can be improved by the higher rate of mass transport of TEMPO mediator. However, charge transfer across the liquid|liquid interface could not be achieved in this case.

4.1 IMPACT OF DIFFERENT SOLVENTS ON THE ELECTROCHEMISTRY IN PDMS BASED EMD

In the first section, tests of different organic solvents commonly used in electroanalysis and their impact on the registered electrochemical measurements in PDMS microchannels are presented. Among different materials which are suitable for building microfluidic channels like e.g. glass or polycarbonate [3,4], PDMS is still popular and useful. More specifically, this polymer has a number of advantages like high thermal and oxidative stability, dynamic flexibility, very low surface free energy and, what is important, general inertness. PDMS is well known as a very absorbing material and a consequence of this property is application of PDMS as a matrix e.g. in sampling of substances [5]. However, the swelling of PDMS is considered as negative and undesired characteristic for many applications. In case of electrochemistry under microfluidic control, absorption of solvent by the PDMS result in changing the microchannel geometry and that can have a negative impact on electrochemical measurement since the microchannel width equals to the electrode width.

Knowing these PDMS properties, this part of the thesis showed if solvents, commonly used in electrochemical experiments, are compatible with PDMS microfluidic channels. Among these solvents *N*-octyl-2-pyrrolidone (NOP), a solvent which has been previously been used in electrochemical studies, was tested [6,7]. In this thesis NOP acts as organic flowing phase in studies with ion transfer processes in EMD. The experiments with solvents extend and establish the compatibility between PDMS and solvents which can be used for many electrochemical purposes.

4.1.1 Swelling of PDMS microchannel in solvents

Swelling of PDMS based EMD was tested with four different solvents: trifluorotoluene (TFT), *N*-octyl-2-pyrrolidone (NOP), 4-(3-phenylpropylpyridine) (PPP), and 1.2-dichlorobenzene (DCB). PDMS polymer as a microfluidic microchannel for organic

solvents was tested by Whitesides and coworkers [8]. They determined the compatibility of a range of nasty solvents with operation in PDMS microchannel. Three main parameters of PDMS compatibility were determined: swelling of PDMS in the solvent, the partitioning of solute between PDMS and solvent and the dissolution of PDMS oligomers in the solvent. The parameter which was determined to be the most important in determining solvent compatibility with PDMS was the swelling of the PDMS. Whitesides and co-workers showed that the swelling is closely correlated with the Hildebrand (or solubility) parameter [9-11]:

$$\delta_{\mathrm{H}} = \left(-\frac{U}{V}\right)^{1/2} \qquad \text{(Eq. 4.1.1)}$$

where U is the molar internal energy (cal/mol) and V is the molar volume (cm^3/mol). For two materials to be soluble, the value of their Hildebrand parameters should be similar because it allows to separate the molecules of the solute and insert the molecules of solvent.
In our experiments we introduced four organic solvents: DCB, PPP, NOP and TFT - not investigated by Whitesides et al. [8]. We determined the swelling parameters of the solvents and in case of TFT we demonstrated, using laser scanning confocal microscopy, how this particular organic solvent penetrates the PDMS microchannel.

The way of analysis of the PDMS swelling was through measurements of the dimensions of PDMS pieces submerged in organic solvents. A photo of cubes cut from PDMS was taken after the pieces where immersed in the various solvents for 1, 2 5, and 24 hours, and the size of the pieces was analyzed in the program ImageJ. In Fig. 4.1.1 the measurements of length of edges of PDMS slices submerged in TFT are presented.

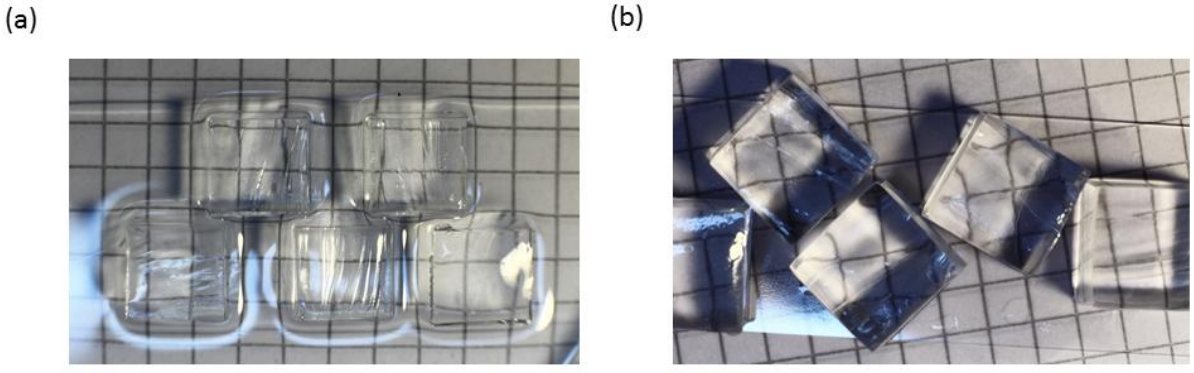

Fig. 4.1.1 Swelling effect recorded on PDMS slices submerged in TFT solvent. **(a)** Fresh PDMS slices submerged in TFT solvent. **(b)** Dry PDMS slices removed from TFT after 24 h.

The degree of swelling is expressed by the swelling ratio:

$$S = \frac{D}{D_o} \qquad \text{(Eq. 4.1.2)}$$

where D is the length of the solid PDMS piece in the solvent and D_o is the initial length of the dry, solid PDMS piece.

In Whitesides's publication the compatibility of organic solvents with PDMS was studied by looking at the swelling of a PDMS block after immersion in the solvent for 24 hours. To be able to compare the results of our "electrochemical compatibility" with the swelling results published by the Whitesides group swelling experiments were conducted with the four liquids in this thesis not included in the original list of solvents [8], i.e. TFT, DCB, NOP and PPP in addition to acetonitrile (ACN) and water, already included in the earlier study. In Fig. 4.1.2 the bars show the swelling of PDMS in the various solvents after 1, 2, 5 and 24 hours.

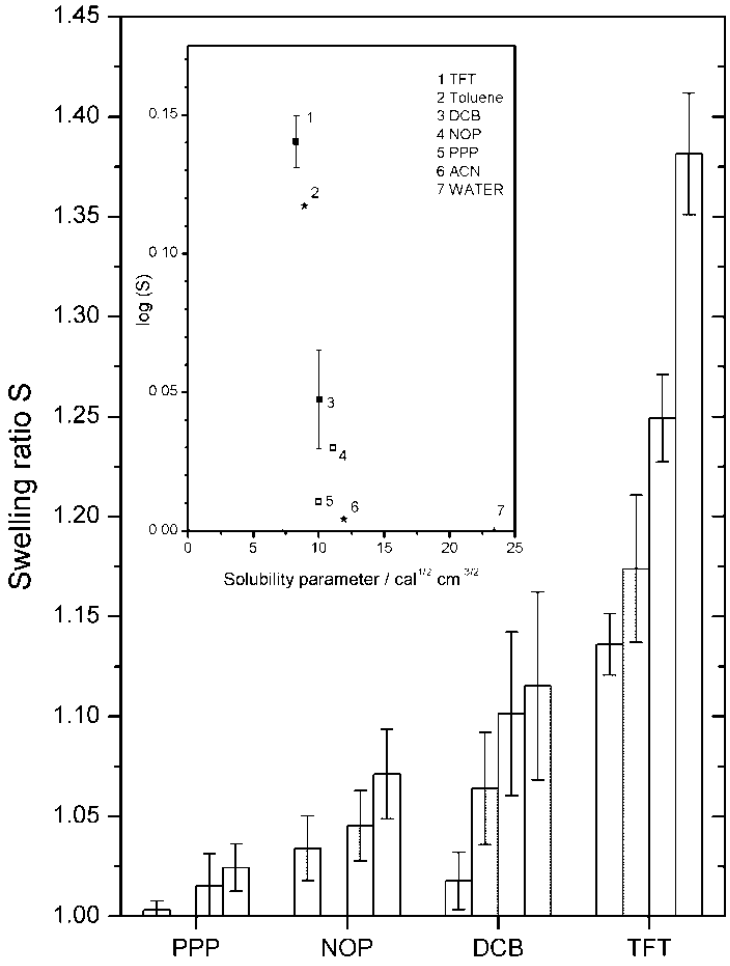

Fig. 4.1.2 Swelling ratio of PDMS blocks in various solvents measured after 1, 2, 5 and 24 hours. Error bars represent standard deviation from 10 measurement + experimental precision. Inset: Swelling ratio (S) as a function of the solubility parameter (δ_H).

It can be seen that significant swelling occurs only with TFT (close to 40 %) and to a smaller extent in DCB (about 10 %). In the inset of Fig. 4.1.1 the swelling ratio is plotted as a function of the solubility parameter, δ_H. This confirms the relationship established by Lee et al. that solvents with a solubility parameter close to that of PDMS (7.3 $cal^{1/2}$ $cm^{-3/2}$) will swell PDMS intensively. The values of the solubility parameters for the solvents used in this study can be found in Tab. 4.1.1:

Tab. 4.1.1 Values of solubility parameter, δ_H. and dipole moments, μ of the tested solvents.

Solvent	**δ_H [$cal^{1/2}$ $cm^{-3/2}$]**	**μ [D]**
trifluorotoluene (TFT)	8.26	2.9
1,2-dichlorobenzene (DCB)	10.02	2.16
4-(3-phenylpropyl)-pyridine (PPP)	~10	2.9
N-octyl-2-pyrrolidone (NOP)	~11	
acetonitrile (ACN)	11.9	4.0
water	23.4	1.9

Values for the first four solvents were taken from ref. [8] and values for other solvents were taken from ref. [13]. The values for PPP and for NOP were estimated.

For PPP and NOP the values of the solubility parameter were estimated from similar compounds found in the literature. The family of pyridines compounds has δ_H. close to 10 $cal^{1/2}$ $cm^{-3/2}$ and according to this data the value for PPP was estimated as well. For NOP the value δ_H was also estimated according tothe value of δ_H for the similar compound *N*-methyl-2-pyrrolidone which is 11.1 $cal^{1/2}$ $cm^{-3/2}$.

4.1.2 Electrochemical test of PDMS microchannel in organic solvents

Electrochemical measurements described in this subchapter were performed with cyclic voltammetry (CV), square-wave voltammetry (SWV) and chronoamperometry (CA) of Fc supported with tetrabutylammonium perchlorate (TBAP) as an electrolyte in each organic solvent with one hour intervals for a total of four hours. The electrochemical oxidation of Fc follows with equation below:

$$Fc - e^- \rightarrow Fc^+ \qquad \text{(Eq. 4.1.3)}$$

Experiments with water were performed with $K_4[Fe(CN)_6]$ as an electroactive compound supported with KCl electrolyte solution. The equation of redox species in water has a form:

$$Fe(CN)_6^{4-} - e^- \rightarrow Fe(CN)_6^{3-} \qquad \text{(Eq. 4.1.4)}$$

As a measure of the compatibility of the solvent with the PDMS channel for electrochemical measurement the stability of the current and redox potential over the series of the experiments were used. The flow rate through the microchannel was set 40 µl min^{-1} during measurements and kept at 1 µl min^{-1} between the measurements, so as to not waste too much of the solvents. Fig. 4.1.2 presents the series of the electrochemical measurements performed with selected organic solvents.

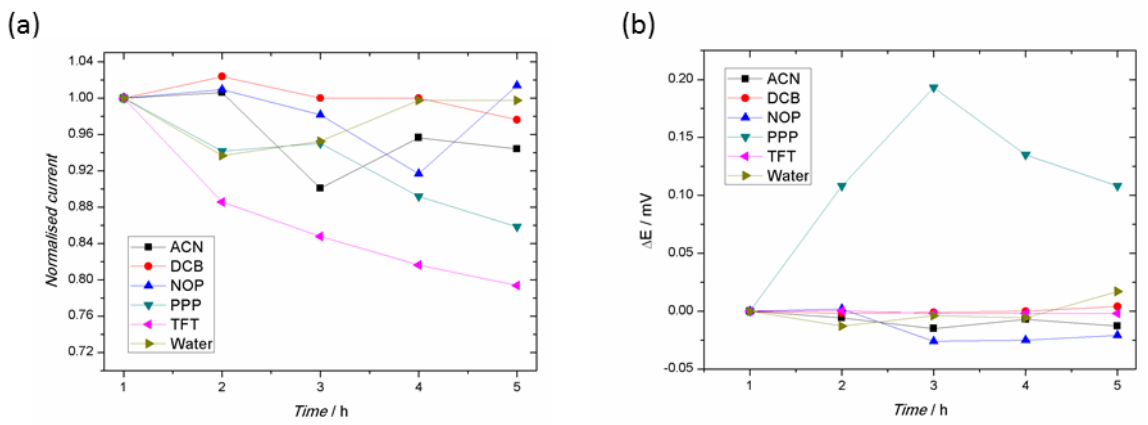

Fig. 4.1.2 Electrochemical measurements performed in EMD with different solvents. **(a)** The plot of the current stability recorded with cyclic voltammetry during course of 1 hour intervals. Scan rate: 20 mV s^{-1}. **(b)** The plot of the potential stability extracted from SWV measurements performed during of hour interwals.

The obtained data allows monitoring if a solvent has an impact on shape of PDMS microchannel. The values of the registered anodic transfer limited current are stable with the following series of measurements. The position of the oxidation peak in square wave voltammograms was also stable. Obtained electrochemical data show that intensive flowing of organic solvents through the PDMS structure does not disturb the electrochemical signal. The obtained electrochemical signal is very stable also for solvents like TFT which penetrates the PDMS structure very quickly and deeply, however the anodic current decreases about 20 % from its onset value (Fig. 4.1.3).

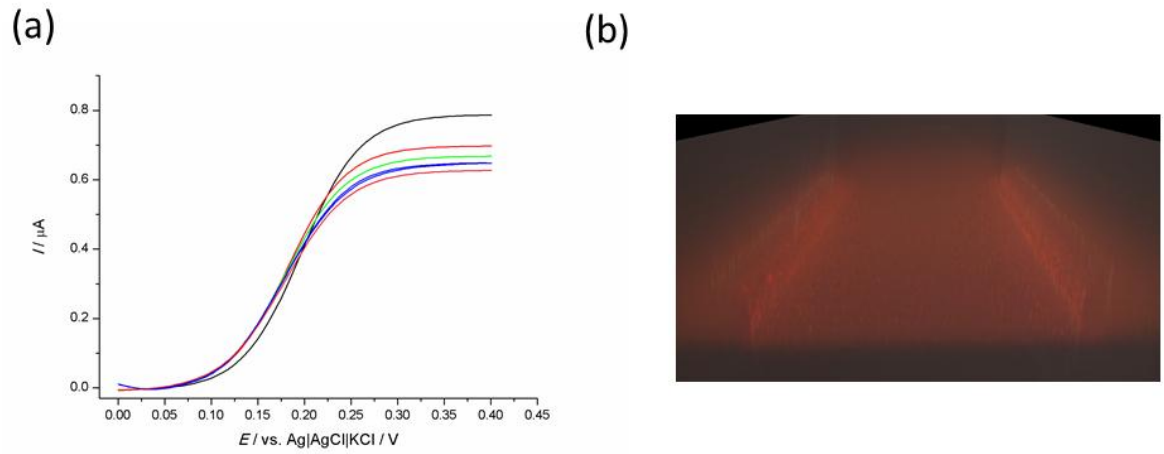

Fig. 4.1.3 (a) Cyclic voltammograms (scan rate 20 mV s^{-1}, $V_{f,org}$ = 40 µL min^{-1}) in microfluidic chip for the oxidation of 1 mM Fc (organic electrolyte: 0.1 M tetrabutylammonium perchlorate) dissolved in flowing organic TFT. **(b)** Confocal image of the cross section of PDMS microfluidic channel where penetration effect of TFT dyed with rhodamine 101 inner salt (Rh 101) is observed.

This could possibly be because part of the redox probe is lost into the PDMS instead of being oxidized at the electrode. The value of the anodic current for PPP is relatively stable, however the shape of the voltammograms makes accurate determination of the peak potential impossible. The curves are very resistive. (Fig. 4.1.2b). PPP is a popular medium for water insoluble transition metal complexes of porphyrins or phthalocyanines [12]. However, electrochemistry in PPP in the literature is restricted to measurements at three-phase boundaries where the low conductivity of the solvent is not an issue [12,13].

4.1.3 Conclusions

The results obtained from test of compatibility solvents on electrochemistry in PDMS microchannel show that is possible perform electrochemical reactions under microfluidic conditions also in many organic compounds. The influence of particular solvents on the PDMS microchannel was checked by the way of series of electrochemical measurements (CV, SWV). Additionally, the dimensions of the pieces of PDMS were measured before and after treated with solvent. Generally, the characteristic of solvents showed a range of from weakly swelling (low soluble) of PDMS like water, PPP and ACN through intermediate level of swelling like DCB and NOP to intensely swelling solvent (high soluble) like TFT. However the electrochemical measurements with selected solvents show that in these cases the swelling effect does not influence the course of the experiments. For four of these solvents (DCB, PPP, NOP, TFT), that were not included in Whitesides' study, the swelling parameter was determined. Our conclusion, contrary to that of Lee et al. [8], is that the solubility parameter is *not* a good indicator of PDMS compatibility, at least for

electrochemistry. In the case of TFT, confocal fluorescence microscopy was used to visualize the real-time penetration of the solvent through the PDMS walls. This part of this thesis expands the use of PDMS microfluidics in non-aqueous solvents in general, and the use of electrochemical instrumentation in these environments in particular.

4.1.4 Bibliography

[1] A. G. Volkov, *Liquid Interfaces in Chemical, Biological, and Pharmaceutical Applications* **2001**, Marcel Dekker, New York.

[2] M. A. Méndez, R. Partovi-Nia, I. Hatay, B. Su, P. Ge, A. Olaya, N. Younan, M. Hojeij, H. H. Girault, *Phys. Chem. Chem. Phys.* **2010,** *12*, 15163.

[3] K. Yunus, C. B. Marks, A. C. Fisher, D. W.E. Allsopp, T. J. Ryan, R. A. W. Dryfe, S. S. Hill, E. P. L. Roberts, C. M. Brennan, *Electrochem. Commun.* **2002**, *4*, 579.

[4] A. Fragoso, D. Latta, N. Laboria, F. von Germar, T. E. Hansen-Hagge, W. Kemmner, C. Gärtner, R. Klemm, K. S. Drese, C. K. O'Sullivan, *Lab Chip* **2011**, *11*, 625.

[5] S. Seethapathy and T. Górecki, *Anal. Chim. Acta*, **2012**, *750*, 48.

[6] S. M. MacDonald, J. D. Watkins, Y. Gu, K. Yunus, A. C. Fisher, G. Shul, M. Opallo, F. Marken, *Electrochem. Commun.* **2007**, *9*, 2105.

[7] S. M. MacDonald, J. D. Watkins, S. D. Bull, I. R. Davies, Y. Gu, K. Yunus, A. C. Fisher, P. C. Bulman Page, Y. Chan, C. Elliott, F. Marken, *J. Phys. Org. Chem.* **2009**, *22*, 52.

[8] J. N. Lee, C. Park, G. M. Whitesides, *Anal. Chem.* **2003**, *75*, 6544.

[9] Y. Du, Y. Xue, H. L. Frisch, *Physical Properties of Polymers Handbook* **1996**, AIP Press: Woodbury, NY.

[10] J. E. Mark, A. Eisenberg, W. W. Graessley, L. Mandelkern, J. L. Koenig, *Physical Properties of Plymers* **1984**, American Chemical Society: Washington DC.

[11] J. L. M. Abboud, R. Notario, *Pure Appl. Chem.* **1999**, *71*, 645.

[12] F. Marken, K. J. McKenzie, G. Shul, M. Opallo, *Faraday Discuss.* **2005**, *129*, 219.

[13] S. M. MacDonald, M. Opallo, A. Klamt, F. Eckert, F. Marken, *Phys. Chem. Chem. Phys.* **2008**, *10*, 3925.

4.2 THE ANOMALOUS EFFECT OF FLOW RATE ON ELECTROCHEMISTRY AT THE GOLD ELECTRODE|LIQUID|LIQUID THREE-PHASE BOUNDARY

This chapter presents the investigations of different flow conditions on the behavior of the liquid|liquid interface in a biphasic EMD. The goal of this part of the dissertation was to examine if the flow rate has an impact on the mass transfer limited current of ferrocene (Fc) as the redox species at a three-phase electrode. Here, we present a general explanation of the flow rate effect as a to competition between diffusion and convection processes and using laser scanning confocal microscopy we showed also that the electrode|liquid|liquid three-phase boundary is stable at a wide range of flow rates. As organic phase the polar solvent *N*-octyl-2-pyrrolidone (NOP) was chosen.

4.2.1 The effect of flow rate on the three-phase boundary in EMD

This part of work describes the electrochemical behavior of the gold electrodeliquid|liquid three-phase boundary interface under microfluidic conditions. The inspiration to study this problem was the work of Marken and coworkers [2] where they made fundamental investigations of ion transfer process in biphasic EMD driven by electrochemical oxidation of *N*-butyloferrocene (nBuFc) dissolved in an organic liquid phase. The second liquid phase was water with dissolved salts. Electrochemical oxidation was accompanied with transfer of ions (ClO_4^-) from the aqueous to the organic phase to maintain electroneutrality as $nBuFc^+$ cations are generated in the organic phase [2]. The paper focused on the unusual behavior of the registered transport limited current which was inconsistent with Levich characteristics. The transfer limited current decreased as the flow rate increased and this observation was explained by reduction of the diffusion zone of ions since this zone decrease with the increased flow rate of the parallel colaminar flow of organic and aqueous phase (see Fig. 4.2.2b).

Under multiphase flow conditions, simultaneous reduction of hexaaminеruthenium(III) chloride in the aqueous stream and oxidation of *N*,*N*,*N′*,*N′*-tetramethyl-1,4-phenylenediamine in 1,2-dichloroethane stream was also studied by Fisher and coworkers [3]. The main conclusion comes from Fisher's work is that the reduction and oxidation currents were proportional to the cube root of the flow rate as expected from the Levich equation. This disagreement between the works of Marken and Fisher was the main motivation of the studies of the three-phase boundary electrochemistry presented in this thesis.

In Fig. 4.2.1, cyclic voltammograms of the oxidation of Fc at the three-phase boundary are presented.

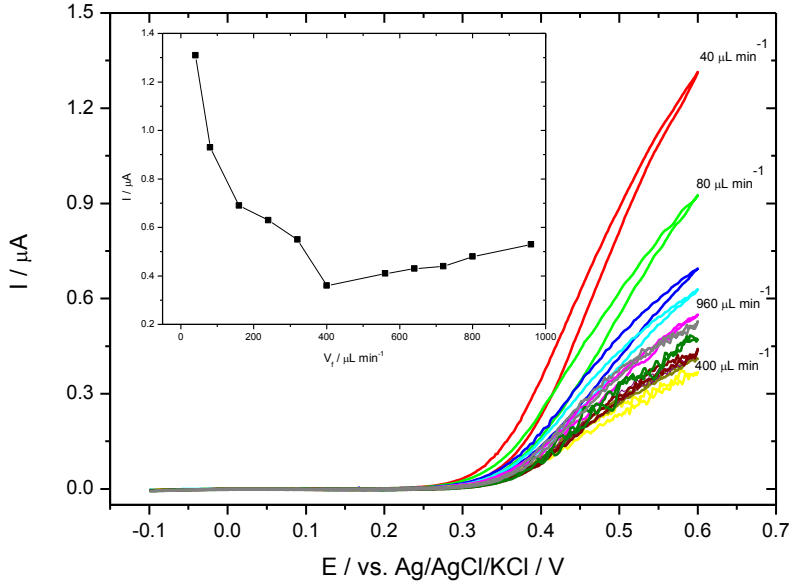

Fig. 4.2.1 Cyclic voltammograms of the oxidation of 10 mM Fc in *N*-octyl-2-pyrrolidone at the NOP|0.1 M $NaClO_4$ in water|gold electrode boundary. Aqueous flow rates 40, 80, 160, 240, 320, 400, 560, 640, 720, 800, and 960 μL min^{-1}. The potential scan rate was set on 0.02 V s^{-1}. The inset on the left upper corner shows the current at 0.6 V as a function of flow rate.

The whole idea of this reaction based on ion transfer theory. The overall reaction showed in Fig. 4.2.1 can be described as follows:

$$Fc_{(org)} + ClO_{4\,(aq)}^{-} \rightleftarrows Fc_{(org)}^{+} + ClO_{4\,(org)}^{-} + e^{-} \qquad \text{(Eq. 4.2.1)}$$

Electrochemical oxidation of Fc is accompanied by transfer of ClO_4^- anions from the aqueous to the organic phase. The organic phase (NOP) does not contain supporting electrolyte and the conductivity of the organic phase increases with the run of the electrochemical oxidation as more ions are created and transferred. The whole process is based on electrochemical extraction, intensively studied under stationary conditions [4]. The observation coming from experiment above is in agreement with studies of Marken and coworkers at low flow rates. The transport limited current decreased with the flow rate to some value of flow rate and then the current surprisingly increases with the flow rate. Marken's explanation for the decreasing current was that diffusion of ions into the organic phase forms an extended reaction zone depicted in Fig. 4.2.2b. As the flow is increased, the width of the reaction zone decreases, leading to a lower current.

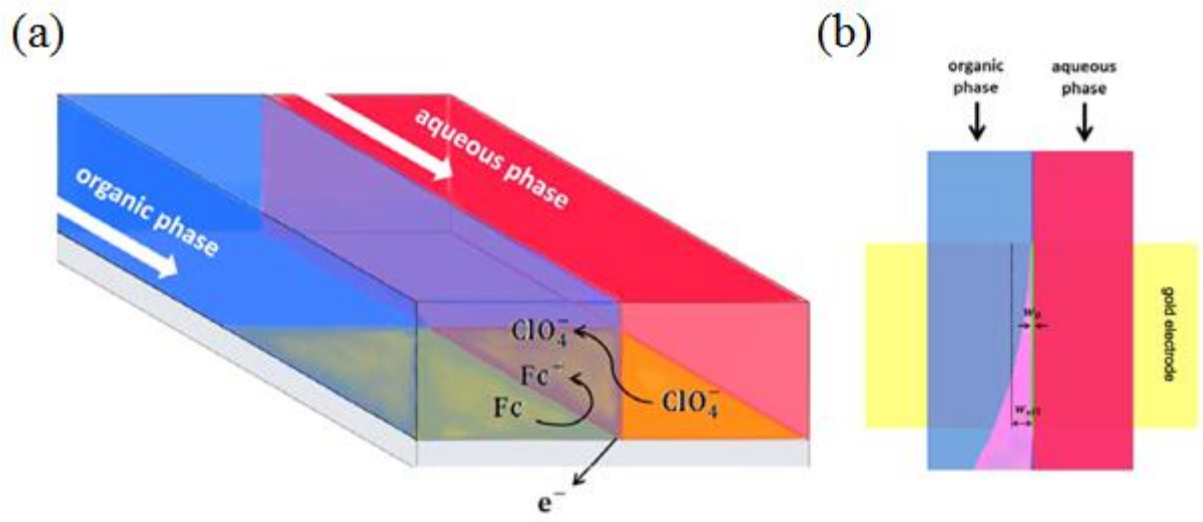

Fig. 4.2.2 (a) Sketch of the flow system where the ion transfer is driven by the electrochemical oxidation of Fc and the process takes place at the three-pahse boundary. **(b)** Schematic sketch of the proposed model of extended reaction zone. The width of the microchannel is 500 μm and its height is 200 μm. The flow rate ratio was kept 1:8 of organic and aqueous phase, respectively to provide the same conditions in each series of measurements.

To describe this idea we constructed a model which is basically a modification of the Levich equation (Eq. 2.3.2). Our suggestion says that the decrease of the current can be attributed to the narrowing of the reaction zone while the eventual increase is an effect of the typical Levich type behavior. To construct the mathematical model we have assumed that the width of the diffusion zone is proportional the square root of diffusion coefficient multiplied by the time needed to diffuse a molecule to traverse the gold band electrode [5]:

$$w_{\text{diff}} \propto \sqrt{Dt} \qquad \text{(Eq.4.2.2)}$$

In our model the electrode width, w, is replaced by an effective reaction zone width, w_{eff}. This is the part of the band electrode where the electron transfer process takes place because of the conductivity conferred by the ions. We assumed that effective reaction zone consisted of a minimal width of the three-phase boundary w_{o} and the width of the diffusion zone w_{diff}:

$$w_{\text{eff}} = w_{\text{o}} + w_{\text{diff}} \qquad \text{(Eq. 4.2.3)}$$

The range of diffusion of ions into the organic phase is determined by the speed of the liquid phases and also by the flow rate. Since the width of the diffusion zone decreases with the flow rate we assumed that w_{diff} increases as $V_{\text{f}}^{-\alpha}$, where the letter α symbolizes a positive number. Since diffusion distance is proportional to the square root of the diffusion time, we simplified

that $\alpha = 1/2$. This gives, after insertion to w_{eff}, a dependence where $w_{\text{eff}} = w_{\text{o}} + \frac{w'_{\text{diff}}}{V_{\text{f}}^{1/2}}$. As we know the parameters of reaction and also geometry of the microchannel have constant values, we denoted this parameter as a constant Z.

$$I_{\text{lim}} = Zw_{\text{eff}}V_{\text{f}}^{1/3} = Zw_{\text{o}}V_{\text{f}}^{1/3} + Zw'_{\text{diff}}V_{\text{f}}^{-1/6} + K \qquad \text{(Eq. 4.2.4)}$$

where the parameter Z is $0.925nFcD^{2/3}(h^2d)^{-1/3}x^{2/3}$ and K is the offset of the current in the model. The model derived from Levich equation, gave us a fitted value of the minimal width of the three-phase boundary and this value is 21±7 μm and is reasonable in comparison with the literature data [6,7]. The shape of the theoretical model presented in Fig. 4.2.3 is in agreement with our experimental data (Fig. 4.2.1).

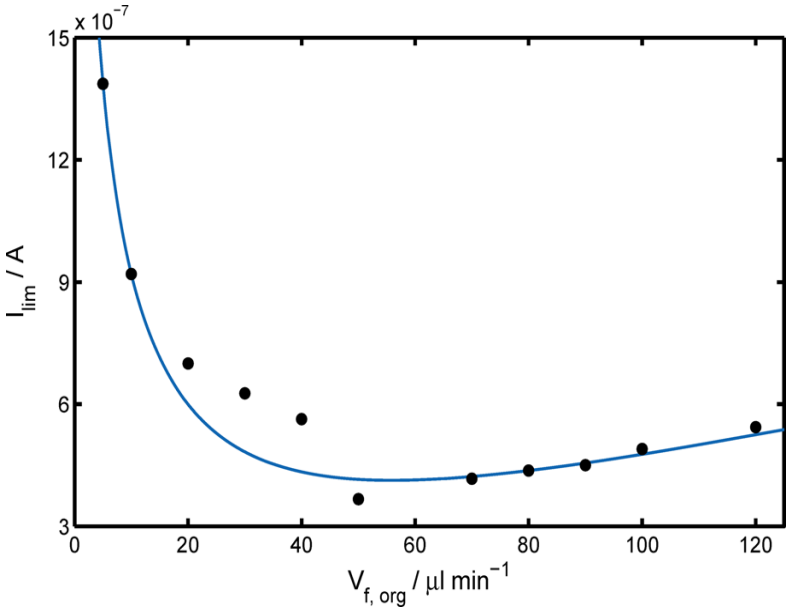

Fig. 4.2.3 Oxidation current as a function of flow rate taken from Fig. 4.2.1. The line is a fit to the data using the formula $I_{\text{lim}} = AV_{\text{f}}^{1/3} + BV_{\text{f}}^{-1/6} + \text{K}$.

4.2.2 Confocal microscopy monitoring of the liquid|liquid interface in EMD

Fig. 4.2.4 shows the cross section of the biphasic microchannel where the aqueous phase is fluorescently dyed in red color and adjacent organic phase does not contain a fluorescent dye. The pictures were taken during electrochemical measurements. The working electrode surface is visible on the picture as green reflection of the excitation laser.

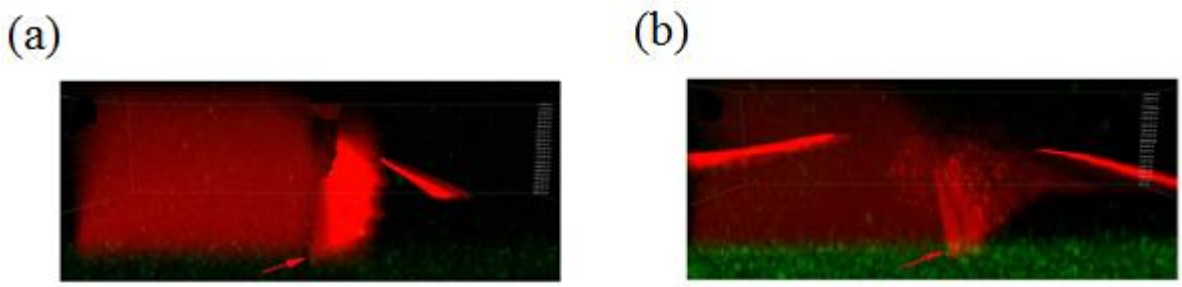

Fig. 4.2.4 Laser scanning confocal microscopy images of the liquid|liquid interface under microfluidic conditions. The red colour of the aqueous phase is visible thanks to fluorescence dye (rhodamine 101), the gold working electrode is green and the organic phase is invisible. Images show the area microchannel before the working microband electrode at **(a)** low ($V_{f,\ aq}$ = 160 μL min^{-1}) and **(b)** high ($V_{f,\ aq}$ = 640 μL min^{-1}) flow rates, respectively. The potential applied to the microband working electrode was set 0.6 V. The red arrows show the position of the three-phase boundary.

The liquid|liquid interface is marked by strong fluorescence because the dye partly adsorbs on the interface. In the images at low flow rate (Fig. 4.2.4a) and high flow rate (Fig. 4.2.4b) it is visible as a sharp edge and the organic phase undercuts the aqueous phase, as described in the Marken publications, is clearly visible. In contrast to the sharp at edge at low flow rates the liquid|liquid interface at higher flow rates looks blurring with irregular fluorescence. The most important information is that at the lower and higher flow rates the electrode|liquid|liquid junction is very stable. Another thing is the shape of liquid|liquid interface at the working microband electrode surface. In the beginning of microband electrode there is not significant conversion in a shape of liquid|liquid interface. The stable shape of liquid|liquid interface indicates that the ion transfer process exists not from mixing of the liquid phases.

4.2.3 Conclusions

We have shown that the ion transfer processes driven by electrochemical oxidation is a tool to monitor the behavior the liquid|liquid interface under microfluidic conditions. Studies of the anomalous effect of oxidation transfer limited current was presented in case of higher flow rate application and reversal trend of transfer limited current was recorded in opposite to the previous reported work [2]. At low flow rates the transfer limited current decreases with increasing value of V_f and this observation is in contrast to Levich characteristic. On the contrary, the transfer limited current comes back to expected Levich equation (Eq. 2.3.2) after some value of the flow rate. We explained this fact by introduction of a simple model based on Levich equation and the model assuming that a minimum width of the three-phase boundary exists and a diffusion-controlled width inversely proportional to the square root of V_f.

We have also shown the topography of the liquid|liquid interface under microfluidic conditions monitored by laser scanning confocal microscopy. The confocal microscopy images show that the electrode|liquid|liquid interface is stable under a wide range of flow rates and the fluorescent images clearly show the organic undercutting the aqueous phase. In the cross section of the microchannel the difference between the top and the bottom of the microchannel is visible. The observation of the liquid|liquid interface blurring is visible as in confocal images when the standard light inverted microscopy is employed (Fig. 4.2.5). This is probably due to the different wetting properties of the glass at the bottom of the channel and the PDMS.

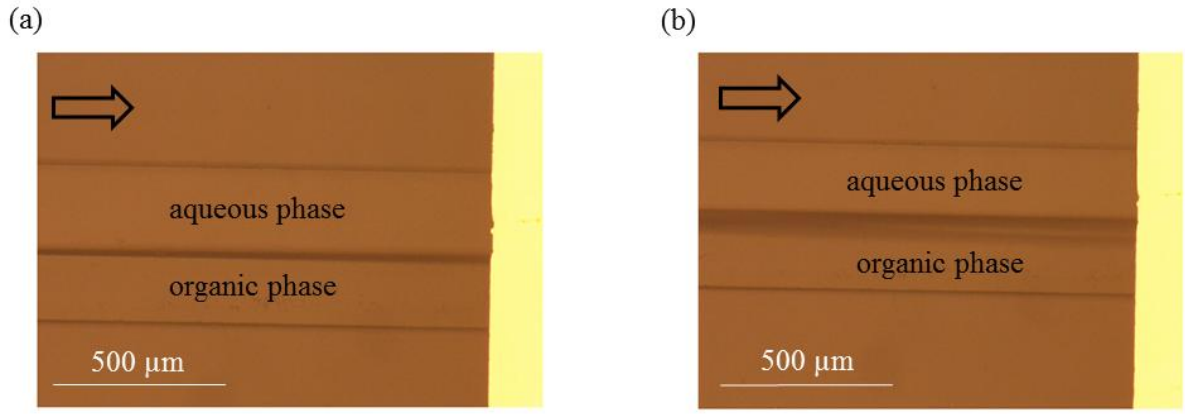

Fig. 4.2.5 Flow rate regimes under a normal light microscope in case of application of low and high flow rate. The focus is on the upper part of the channel, and the blurring of the liquid|liquid interface is clearly seen. The aqueous phase is in the upper half of the microchannel and the organic phase is in the lower half, respectively. The scale bar is 500 µm. The black arrows show the direction of the flow.

The obtained results and the observation that the three-phase boundary is stable over wide range of flow rates gave us the starting point to perform ion transfer studies under microfluidic conditions with different anions dissolved in the aqueous phase.

4.2.4 Bibliography

[1] J. N. Lee, C. Park, G. M. Whitesides, *Anal. Chem.* **2003,** *75*, 6544.

[2] S. M. MacDonald, J. D. Watkins, Y. Gu, K. Yunus, A. C. Fisher, G. Shul, M. Opallo, F. Marken, *Electrochem. Commun.* **2007**, *9*, 2105.

[3] K. Yunus; C. B. Marks; A. C. Fisher; D. W.E. Allsopp; T. J. Ryan, R. A. W. Dryfe, S. S. Hill; E. P. L. Roberts; C. M. Brennan, *Electrochem. Commun.* **2002**, *4*, 579.

[4] J. M. Reyna-González, A. A. J. Torriero, A. I. Siriwardana, I. M. Burgar, A. M. Bond, *Anal. Chem.* **2010**, *82*, 7691.

[5] A. J. Bard, L. R. Faulkner, *Electrochemical Methods: Fundamentals and Applications* **2001**, John Wiley & Sons, New York.

[6] T. J. Davies, S. J. Wilkins, R. G. Compton, *J. Electroanal. Chem.* **2006**, *586*, 260.

[7] J. Niedziolka, M. Opallo, *Electrochem. Commun.* **2008**, *10*, 1445.

4.3 COMPARISON OF ION TRANSFER UNDER STATIC AND MICROFLUIDIC CONDITIONS

In this part of the thesis a comparison of ion transfer thermodynamics at microfluidic and droplet-based three-phase electrode is presented. We have studied if the theory of ion transfer developed for static systems can be applied to the EMD. The ion transfer was analyzed by the effect of ion transfer potential and ion concentration on the voltammetric peak potential recorded both at droplet modified electrodes and in EMD. The transfer of ions from the aqueous phase (W) is driven by the electrochemical oxidation of DMFc dissolved in the organic solvent. The results were analyzed in terms of the model for droplet systems derived from the Nernst equation. We also determined the unknown values of Gibbs energies for transfer of ions in the organic solvent used (NOP).

4.3.1 Determination of transfer potentials in biphasic system with TFE

Thermodynamic data (Gibbs transfer energy, standard potential of the transfer of ion) for the ion transfer driven by electrochemical reactions in NOP does not appear in the literature and it was necessary to determine it. The determination of the thermodynamic data for NOP is based on a method where both the organic and aqueous phases contain electrolytes with an ion in common to control the potential difference at the liquid|liquid interface [1]. The transfer of the common ion is accompanied with electrochemical reaction of an electroactive compound. The both processes like electron and ion transfer are simultaneous so the voltammetric signal from the experimental system represents the overall electron-ion transfer reaction. The concentration of the common ion is keept in excess compared to the redox species and thanks to that fact, the Galvani potential difference between the two immiscible liquids is kept constant.

Fig. 4.3.1 presents series of cyclic voltammograms (CV) recorded under static conditions where a GC working electrode is modified by a thin film of NOP. The method gives direct information in which potential the transfer of analyzed anions occurs during generation of $DMFc^+$ cation in the organic phase:

$$DMFc - e^- \rightleftarrows DMFc^+ \qquad \text{(Eq. 4.3.1)}$$

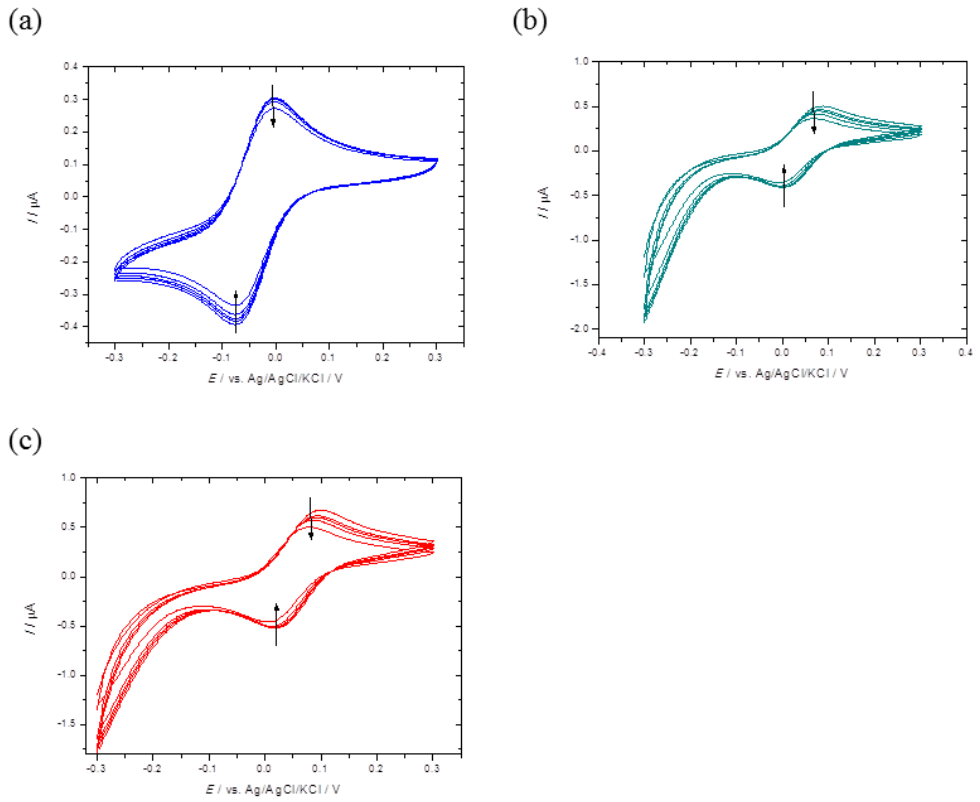

Fig. 4.3.1 CV curves recorded on thin film electrode immersed in different 0.1 M aqueous electrolytes. The GC working electrode was modified with 2 μL droplet of NOP solution containing 1 mM DMFc and 10 mM organic electrolyte. The potential scan rate was set on 0.05 V s^{-1}. The experimental system are visible for **(a)** (ClO_4) anion dissolved in the aqueous phase and $THxClO_4$ electrolyte in the organic phase; **(b)** NO_3^- anion and $TOANO_3$ electrolyte in the organic phase; **(c)** Br^- anion and TOABr electrolyte in the organic phase.

The registered anodic and cathodic peaks from electrochemical oxidation of DMFc in thin organic film when $TPAs^+$ and TPB^- are transferring ions are relatively stable during the scan, however it is visible that the current decreases slightly with each cycle. The position of the $DMFc/DMFc^+$ peaks is related to the ability of the anion present in the aqueous phase to move to the organic phase.

The formal potential of the determined anions was precisely measured from square wave voltammograms (SWV) net peak potentials. Normalized SWV curves recorded for different transferring anions whose transfer potentials were to be determined are shown in Fig. 4.3.2. First, transfer potentials across the NOP|W interface, $\Delta\phi_i^{o,\ W\rightarrow NOP}$, were determined.

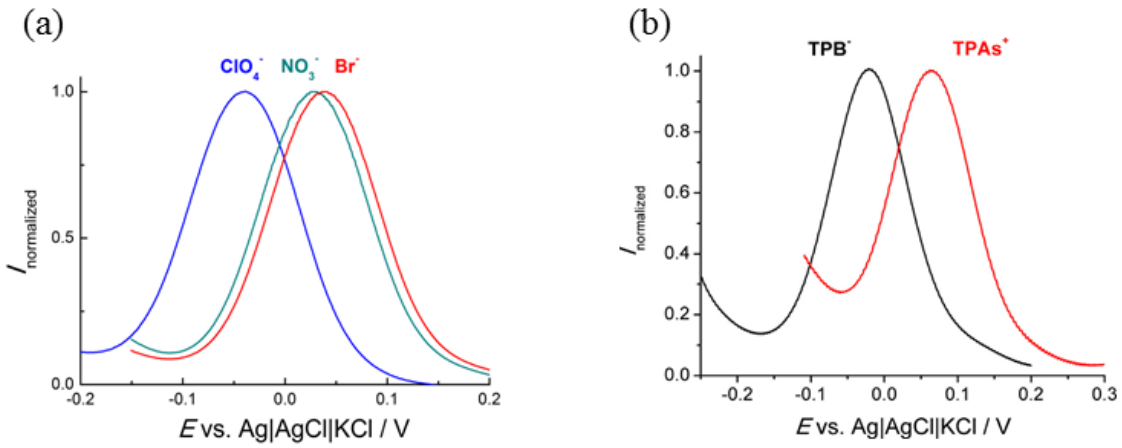

Fig. 4.3.2 (a) SWV curves recorded on thin film electrode submerged in 0.1 M different aqueous electrolytes (ClO_4^-, NO_3^-, Br^-). The GC working electrode was modified with 2 µL droplet of NOP solution containing 1 mM DMFc and 10 mM organic electrolyte. (b) SWV recorded at GC working electrode modified with 1 mM DMFc|NOP solution and immersed in 10 mM Na^+TPB^- (black curve) or 0.1 M $TPAs^+TPBCl^-$ (red curve) aqueous solutions. The NOP phase contained 10 mM $THepA^+TPB^-$ (for black curve) or 10 mM $TPAs^+TPBCl^-$ (for red curve).

Both liquid phases contained an electrolyte with an ion in common, i.e. the ion whose transfer potential was to be determined (Tab. 4.3.1). The concentration of the common ion was adjusted to be bigger than the electroactive compound to stabilize the potential difference between the phases. Depending if the common ion (anion or cation) is present in both phases, the overall electrochemical oxidation of DMFc in NOP can be represented by the reactions presented below (Eq. 4.3.2 and 4.3.3). In the first one, electrochemical oxidation can induce the transfer of anions (An^-) from the aqueous to the organic phase in order to preserve charge neutrality of the organic phase.

$$DMFc_{(NOP)} + An^-_{(W)} \rightleftarrows DMFc^+_{(NOP)} + An^-_{(NOP)} + e^- \qquad \text{(Eq. 4.3.2)}$$

Alternatively, if the ion is sufficiently hydrophilic the electrochemical oxidation of DMFc can instead provoke the transfer the DMFc cation from the NOP to the water phase:

$$DMFc_{(NOP)} + Cat^+_{(NOP)} \rightleftarrows DMFc^+_{(NOP)} + Cat^+_{(W)} + e^- \qquad \text{(Eq. 4.3.3)}$$

In order to determine the values of the transfer potential of anions, $\Delta\phi_i^{o,\ W\rightarrow NOP}$, the values of the net peak potentials E_p of the DMFc/$DMFc^+$ couple in the presence of the anions ClO_4^- (-0.039 V), NO_3^- (0.029 V), Br^- (0.038 V), TPB^- (0.016 V) and the cation $TPAs^+$ (0.068 V) were taken from the SWV data presented in Fig. 4.3.2a. It can be seen that the peak potential for hydrophilic anions like Br^- is more positive than for hydrophobic ones

like ClO_4^-. This reflects the difference in transfer potentials between these two anions, i.e. the more hydrophobic the anion is, the more facilitated is the electrochemical process and a lower applied potential is needed to run the process.

The transfer potential of the transferring ion was calculated using the equation [1]:

$$\Delta\phi_{\mathrm{i}}^{\mathrm{o},\ \mathrm{W}\rightarrow\mathrm{NOP}} = E_{\mathrm{p}} - E^{\mathrm{o}}_{\mathrm{DMFc/DMFc^+}} + \frac{RT}{z_{\mathrm{i}}F}\ln\frac{c_{\mathrm{i}}(\mathrm{NOP})}{c_{\mathrm{i}}(\mathrm{W})} \qquad \text{(Eq. 4.3.4)}$$

where E_{p} is the net peak potential determined from SWV, $E^{\mathrm{o}}_{\mathrm{DMFc/DMFc^+}}$ is the standard redox potential of DMFc/$DMFc^+$ couple, z_{i} is the charge number of the transferring ion, $c_{\mathrm{i}}(\mathrm{NOP})$, $c_{\mathrm{i}}(\mathrm{W})$ are bulk concentrations of the transferring ion in NOP and W phase, respectively. Other symbols have their usual meanings. The value of $E^{\mathrm{o}}_{\mathrm{DMFc/DMFc^+}}$ can be determined by considering the extra-thermodynamic assumption that $\Delta\phi_{\mathrm{TPAs^+}}^{\mathrm{o},\ \mathrm{W}\rightarrow\mathrm{NOP}} = -\Delta\phi_{\mathrm{TPB^-}}^{\mathrm{o},\ \mathrm{W}\rightarrow\mathrm{NOP}}$ and comparing the formal potentials measured in separate experiments where either of these ions are transferred. Under this assumption one can rewrite Eq. 4.3.4 to obtain:

$$E^{\mathrm{o}}_{\mathrm{DMFc/DMFc^+}} = \frac{1}{2}\left[E_{\mathrm{p}}(\mathrm{TPAs^+}) + E_{\mathrm{p}}(\mathrm{TPB^-}) + \frac{RT}{F}\ln\frac{c_{\mathrm{TPAs^+}}(\mathrm{NOP})\ c_{\mathrm{TPB^-}}(\mathrm{W})}{c_{\mathrm{TPAs^+}}(\mathrm{W})\ c_{\mathrm{TPB^-}}(\mathrm{NOP})}\right] \qquad \text{(Eq. 4.3.5)}$$

where E_{p} ($TPAs^+$) and E_{p} (TPB^-) are the SWV peak potentials recorded when $TPAs^+$ or TPB^- are the transferring ions. Concentrations of analyzed ions were $c_{\mathrm{TPAs^+}}(\mathrm{NOP})$=0.01 M, $c_{\mathrm{TPAs^+}}(\mathrm{W})$ = 0.1 M, $c_{\mathrm{TPB^-}}(\mathrm{NOP})$ = 0.01 M, and $c_{\mathrm{TPB^-}}(\mathrm{W})$ = 0.01 M. Finally, we calculated the value of the standard potential $E^{\mathrm{o}}_{\mathrm{DMFc/DMFc^+}}$ to 0.001 V versus Ag|AgCl|3 M KCl reference electrode.

The formal potential of the redox couple DMFc/$DMFc^+$ $E^{\mathrm{o}'}$ is defined by:

$$E^{\mathrm{o}'} = E^{\mathrm{o}}_{\mathrm{DMFc/DMFc^+}} + \Delta_{\mathrm{W}}^{\mathrm{NOP}}\phi^{\mathrm{o}}_{\mathrm{An^-\ or\ Cat^+}} + \frac{RT}{zF}\ln\frac{c_{\mathrm{An^-\ or\ Cat^+(W)}}}{c_{\mathrm{An^-\ or\ Cat^+(NOP)}}} \qquad \text{(Eq. 4.3.6)}$$

To transform Eq. 4.3.6 is possible to calculate the standard potential for the transfer of the ion:

$$\Delta\phi_{\mathrm{An^-\ or\ Cat^+}}^{\mathrm{o},\ \mathrm{W}\rightarrow\mathrm{NOP}} = E^{\mathrm{o}'} - E^{\mathrm{o}}_{\mathrm{DMFc/DMFc^+}} + \frac{RT}{zF}\ln\frac{c_{\mathrm{An^-\ or\ Cat^+(W)}}}{c_{\mathrm{An^-\ or\ Cat^+(NOP)}}} \qquad \text{(Eq. 4.3.7)}$$

Since in SWV the peak potential is equal to the formal potential this is the same as Eq. 4.3.4. The last step was calculating Gibbs transfer energies of ions:

$$\Delta G^{o,\ W\rightarrow NOP}_{An^- \text{or } Cat^+(W)} = -\Delta\phi^{o,\ W\rightarrow NOP}_{An^- \text{ or } Cat^+}\, z_i\, F \qquad \text{(Eq. 4.3.8)}$$

where z_i is the charge number of transferring ion, and other symbols have their usual meanings.

Tab. 4.3.1 The results of calculations of transfer potentials and transfer energies for different anions in NOP.

Transferring ion	**Organic electrolyte**	**Aqueous electrolyte**	$\Delta\phi^{o,\ W\rightarrow NOP}_{An^-}$ **[V]**	$\Delta G^{o,\ W\rightarrow NOP}_{An^-}$ **[kJ mol^{-1}]**
ClO_4^-	$THxA^+ClO_4^-$	$Na^+ClO_4^-$	0.019	1.8
NO_3^-	$TOA^+NO_3^-$	$K^+NO_3^-$	0.087	8.4
Br^-	TOA^+Br^-	K^+Br^-	0.097	9.3

Concentration of organic electrolyte was 10 mM and concentration of aqueous electrolyte was 0.1 M and the concentration of redox species DMFc was 1 mM.

Additionally, we also have estimated the values of Gibbs transfer energy for anions which have used in our experiments but could not be determined directly through experiments. According to the Born equation (Eq. 2.1.1, chapter 1.) the ion is assumed as sphere shaped individual and solvents are a homogenous dielectric. It is expected that the larger ionic radius the more hydrophobic it becomes and finally the radius has an impact on Gibbs transfer energy value. In case of more hydrophobic anions, Gibbs transfer energy has a low value in comparison to more hydrophilic anions. Fig. 4.3.3 shows the dependence of the Gibbs transfer energy of ions as a function of the reciprocal of ionic radius of the transferring ions.

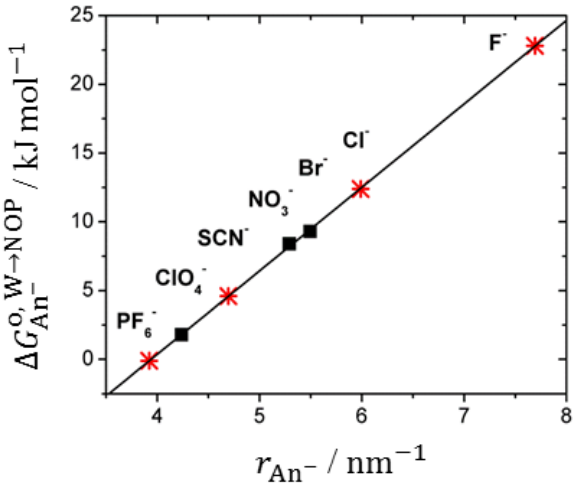

Fig. 4.3.3 The dependence of Gibbs energy transfer across NOP|W interface on reciprocal of ion radius. The regression line is calculated for ClO_4^-, NO_3^- and Br^- datapoints (squares). Datapoints (red stars) for PF_6^-, SCN^-, Cl^- and F^- were calculated from Eq. 4.3.9. The ion radius of PF_6^- was taken from ref. [2] and for other anions from ref. [3].

$$\Delta G^{o,\,W\to NOP}_{An^-} = 6.1\, r^{-1} - 23.9 \qquad \text{(Eq. 4.3.9)}$$

According to equation above, we have estimated the Gibbs transfer energies and transfer potentials for ions whose ionic radii are known but whose transfer energies have not been measured. The values of the Gibbs transfer energies and ionic radii are listed in Tab. 4.3.2.

Tab. 4.3.2 Estimated parameters of $\Delta\phi^{o,\,W\to NOP}_{An^-}$ and $\Delta G^{o,\,W\to NOP}_{An^-}$.

Anion	**Radius [nm]**	**Estimated $\Delta\phi^{o,\,W\to NOP}_{An^-}$ [V]**	**Estimated $\Delta G^{o,\,W\to NOP}_{An^-}$ [kJ mol^{-1}]**
PF_6^-	0.255	-0.001	-0.1
SCN^-	0.213	0.048	4.6
Cl^-	0.167	0.129	9.4
F^-	0.133	0.225	22.8

The radius for PF_6^- was taken from ref. [2] and for SCN^-, Cl^-, F^- from ref. [3].

4.3.2 Ion transfer at droplet and microfluidic TPEs

4.3.2.1 Voltammetry of DMFc dissolved in NOP droplet in contact with aqueous electrolyte

Fig. 4.3.4 shows cyclic voltammograms (CV) recorded at the three phase electrode modified with a droplet of DMFc solution in NOP to examine the reproducibility and current stability by repetitive cycling of the potential. The CV data for the system indicates stable ratio of anodic and cathodic peak without decreasing of the registered current. This indicates electrochemical reversibility of the process, under the experimental conditions, and that the $DMFc^+$ cation expulsion to the aqueous phase does not occur. The peak potential separation of 65 mV is constant with the scan rate up to at least 100 mV s^{-1}.

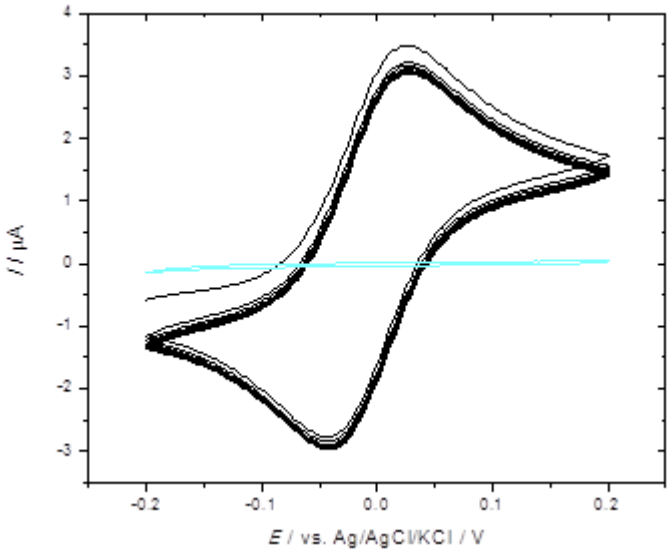

Fig. 4.3.4 CV (10 subsequent cycles overlayed) recorded on GC electrode modified with a droplet of 10 mM DMFc solution in NOP. The electrode was immersed in aqueous solution of 0.1 M $NaClO_4$. The scan rate was set on 0.05 V s^{-1}. The light blue curve indicates the blank current response from bare GC electrode immersed in aqueous electrolyte solution.

a) Verification the effect of the flow rate on the position of SWV peak potential

In order to check the validity of the equilibrium hypothesis it is important that the measured peak potentials are not affected by the flow rate. Fig. 4.3.5a shows a typical steady state voltammogram (red curve) recorded in the EMD. The half-wave potential of 0.04 V corresponds accurately to the peak potential determined from hydrodynamic square wave voltammetry (black). The peak potential is basically unaffected by a change of the flow rate

of aqueous phase from 40 μL min^{-1} to 960 μL min^{-1} (Fig. 4.3.5b). This indicates that the flow rate does not influence of the peak potential. This is important information for further studies, because it allows for reliable comparison of peak potential-containing dependencies between microfluidic systems and droplet modified electrodes.

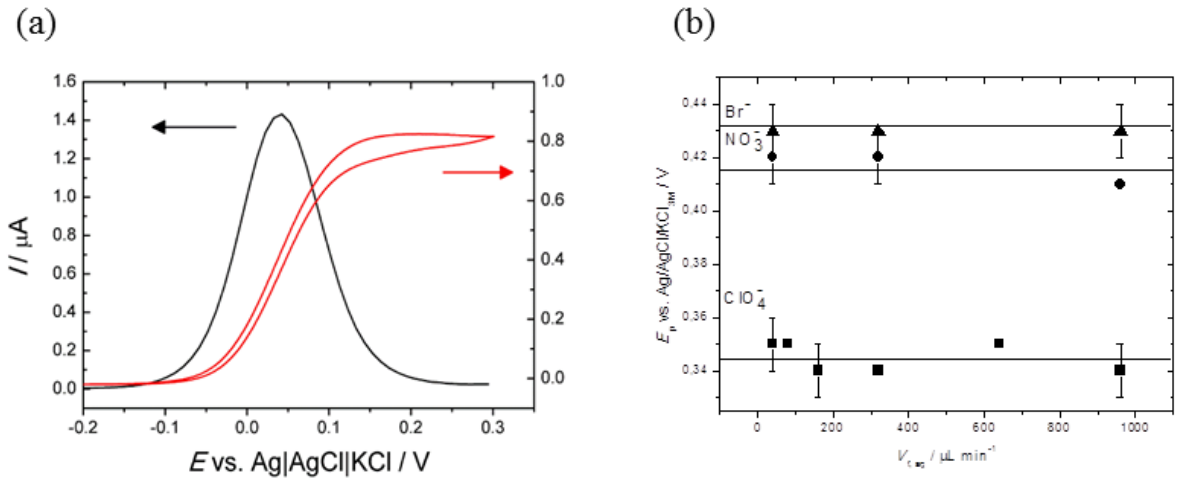

Fig. 4.3.5 (a) CV (red) and square wave voltammogram (black) recorded in the microfluidic system. The organic phase contains 10 mM DMFc solution in NOP and the aqueous phase contains 0.1 M $NaClO_4$. The flow rate of the organic and the aqueous phase was 5 μL min^{-1} and 40 μL min^{-1}, respectively. **(b)** The effect of the flow rate of the aqueous phase contains different electrolyte solutions (ClO_4^-, NO_3^-, Br^-) on the SWV peak potential. The organic phase contains 10 mM DMFc solution. The presented range of flow rate of the organic was set from 5÷120 μL min^{-1} and the flow rate of the aqueous phase was kept 8 times higher to maintain the same width of both phases in the microchannel [4].

4.3.2.2 Ion transfer and anion effect

Typically, electrochemical oxidation of a redox probe on a three-phase electrode is accompanied by the transfer of anions from the aqueous to the organic phase. The whole process mechanism can have the form:

$$DMFc_{(org)} + An^-_{(aq)} \rightleftarrows DMFc^+_{(org)} + An^-_{(org)} + e^- \qquad \text{(Eq. 4.3.10)}$$

The reaction above occurs in case of presence of relatively hydrophobic anions in the aqueous phase. The nature of the anion dissolved in the aqueous phase has an impact on the formal potentials of the redox species reaction on the recorded voltammograms. This causes peak potential to be more negative due to fact that process is more thermodynamically favoured (DMFc is easier oxidized). In the opposite case, in the presence of very hydrophilic anions, anion transfer is unfavourable and in consequence inducing of the transfer of the generated $DMFc_{(org)}^+$ cations to the aqueous phase which can be seen with the peak potential shift towards more positive potentials. In that case the Nernst equation has a form of:

$$E = E^{o}_{DMFc/DMFc^{+}} - \Delta\phi^{o,\ NOP\rightarrow W}_{DMFc^{+}} + \frac{RT}{F}\ln\frac{c_{DMFc^{+}(W)}}{c_{DMFc\,(NOP)}} \qquad \text{(Eq. 4.3.11)}$$

Where $\Delta\phi^{o,\ NOP\rightarrow W}_{DMFc^{+}}$ is the standard transfer potential of $DMFc^{+}$ transfer from the NOP to the aqueous phase.

Figure 4.3.6 shows SWV recorded on droplet TPEs and in microfluidic systems in the presence of different anions in the aqueous phase. It can be seen that in both cases the peak potentials are lower for more hydrophobic anions and follow the order of hydrophilicity: PF_6^- < ClO_4^- < SCN^-< NO_3^- < Br^- < Cl^- ≈ F^-.

The comparison of the anion effect in both systems can be presented as the dependence of E_p on $\Delta\phi^{o,\ W\rightarrow NOP}_{An^-}$ (Fig. 4.3.7) using the values of the transfer potential determined in the previous subchapter. The dependence is described by the equation derived for electrochemically driven anion transfer at a droplet TPE [6]:

$$E_p = E^{o}_{DMFc/DMFc^{+}} + \Delta\phi^{o,\ W\rightarrow NOP}_{An^-} - \frac{RT}{F}\ln c_{An^-}(W) + \frac{RT}{F}\ln\frac{c_{DMFc}}{2} \qquad \text{(Eq. 4.3.13)}$$

where c_{DMFc} is the concentration of DMFc in the organic phase. According to Eq. 4.3.13, E_p is a linear function of $\Delta\phi^{o,\ W\rightarrow NOP}_{An^-}$ with a unity slope. Analyzing the slopes (1.07 ± 0.07) of obtained at droplet TPE and in the microfluidic system where linear regression gives a slope of 0.85 can indicate the escape of cation to the aqueous phase. The obtained results under microfluidic conditions are still in the range of unity if 95 % confidence bands are considered. This is evidence of that the anion effect at the droplet modified electrode is in agreement with the results obtained in microfluidic chip (Fig. 4.3.6).

It should also be noted that in both systems E_p does not depend on the ion transfer potential when Cl^- or F^- are present in the aqueous phase. This is likely to be due to expulsion of $DMFc^{+}$ cations from NOP to W in the presence of hydrophilic anions.

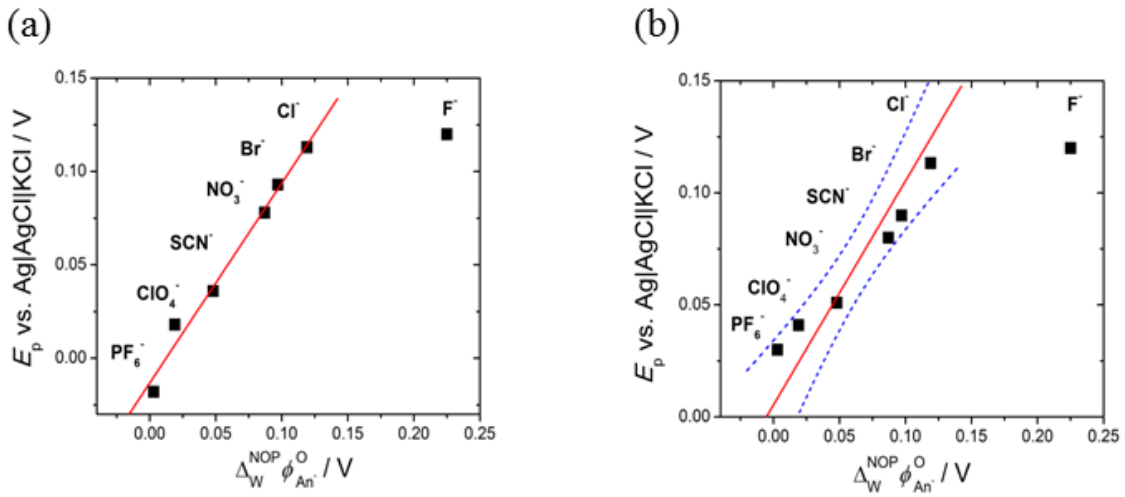

Fig. 4.3.6 Dependence of the peak potential on the standard transfer potential of the transferring ion. The peak potentials were taken from SWV curves recorded **(a)** at the droplet TPE and **(b)** in the microfluidic system. The slope of the solid line in **(a)** is equal to 1.07. The solid line in **(b)** is the regression line with a slope of 1. The dashed lines are confidence bands of 95 %. The flow rate conditions as in Fig. 4.3.6.

4.3.3 Studies of ion transfer and anion concentration effect

The useful method to investigate the ion transfer pathway is electrochemical measurement with different concentrations of the electrolyte in the aqueous phase. Analyzing Eq. 4.3.13, the peak potential recorded at a TPE depends on the logarithm of aqueous anion concentration. The formal potential should shift by ca. 59 mV per decade in the case of presence more transferable anion in the aqueous phase. In the Fig. 4.3.8 the concentration dependences for droplet-modified electrode and for microfluidic system in the presence of hydrophobic anion, here ClO_4^- and hydrophilic anions, Cl^- in the aqueous phase.

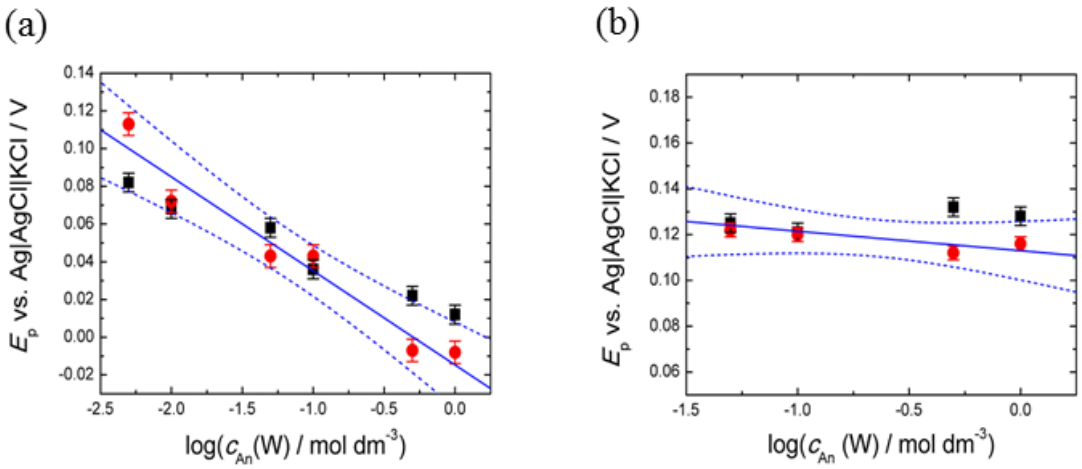

Fig. 4.3.8 Dependence of the peak potential on the logarithm of concentration of the aqueous solution containing **(a)** $NaClO_4$, **(b)** NaCl. The peak potentials were determined from SWV curves recorded at droplet modified electrodes (squares) and in microfluidic systems (circles). The solid lines are the regression lines for droplet modified TPE with a slope of -50 ± 8 mV dec^{-1} for $NaClO_4$ and -6 ± 3 mV dec^{-1} for NaCl. The dashed lines represent confidence bands of 95 %. The flow rate conditions as in Fig. 4.3.6.

In both systems there is no dependence in the presence of Cl^- anion in the aqueous phase. This is due to the transfer of $DMFc^+$ cations from NOP to W:

$$DMFc - e^- \rightleftarrows DMFc^+ \qquad \text{(Eq. 4.3.14)}$$

This is a well-known effect for very hydrophilic ions such as Cl^- and F^-, and has been observed in other aqueous-organic solvent systems [7-9]. In these cases the resistance to transfer of anions to the organic phase instead favors the expulsion of the $DMFc^+$ cation to the aqueous phase. The electrode potential is then given by the equation [10]:

$$E = E^{o}_{DMFc/DMFc^+} - \Delta^{W}_{NOP}\phi^{o}_{DMFc^+} + \frac{RT}{F}\ln\frac{c_{DMFc^+}(W)}{c_{DMFc}(NOP)} \qquad \text{(Eq. 4.3.15)}$$

where $\Delta\phi^{o,\ NOP\rightarrow W}_{DMFc^+}$ is $DMFc^+$ transfer potential from NOP to W. Since this equation does not contain any term related to aqueous electrolyte anions, it explains lack of concentration dependence for Cl^-. In the presence of ClO_4^- the dependence is linear with a negative slope of -50 mV per decade. This is in agreement with Eq. 4.3.4 and confirms the anion transfer mechanism.

4.3.4 Conclusions

We have shown that the theory of thermodynamic of electrochemically driven ion transfer processes at droplet TPE can be applied to EMD. We have focused on two phenomena which are typically observed in droplet TPE and which are normally seen as indicative of the anion transfer model, i.e. the effect of ion hydrophobicity and the effect of ion concentration on the voltammetric peak potentials.

We also showed that two processes like effect of type of anion presented in the aqueous phase and concentration effect are the same in the EMD as on droplet TPE. Both dependences were in agreement with the Nernst-like equation derived previously for the anion transfer mechanism at droplet TPE. Importantly, it was also found that the peak potential measured in the microfluidic system was independent of the flow rate. The comparison of the ion effect in both systems was possible thanks to determination of Gibbs energies of transfer across NOP interface using the thin-film electrode approach. These experiments give a solid foundation to further attempts of investigations using EMD as useful microdevice in direct analysis of the solution of different ions dissolved in aqueous phase. These studies can be completed with e.g. ionophores (Fig. 4.3.9), ie. chemical compounds which reversibly bind ions [11].

In the case of EMD, ionophores can be introduced into one flowing liquid phase.

The work presented in this subchapter complements previous attempts of studies of the electrochemically driven ion transfer under static and microfluidic conditions [4,7,9,12,13].

4.3.5 Bibliography

[1] F. Quentel, V. Mirceski, C. Elleouet, M. L'Her, *J. Phys. Chem. C* **2008**, *112*, 15553.

[2] G. Feng, R. Qiao, J. Huang, S. Dai, B.G. Sumpter, V. Meunier, *Phys. Chem. Chem. Phys.* **2011**, *13*, 1152.

[3] A.G. Volkov, *Liquid Interfaces in Chemical, Biological, and Pharmaceutical Applications*, Marcel Dekker, **2001**.

[4] S. M. MacDonald, J. D. Watkins, Y. Gu, K. Yunus, A. C. Fisher, G. Shul, M. Opallo, F. Marken, *Electrochem. Commun.* **2007**, *9*, 2105.

[5] V. Mirceski, F. Quentel, M. L'Her, A. Pondaven, *Electrochem. Commun.* **2005**, *7*, 1122.

[6] F. Scholz, S. Komorsky-Lovric, M. Lovric, *Electrochem.Commun.* **2000**, *2*, 122.

[7] W. Adamiak, M. Opallo, *J. Electroanal. Chem.* **2008**, *82*, 642.

[8] S. Komorsky-Lovric, K. Riedl, R. Gulaboski, V. Mirceski, F. Scholz, *Langmuir* **2002**, *18*, 8000.

[9] G. Shul, M. Opallo, *Electrochem. Commun.* **2005**, *7*, 194.

[10] F. Scholz, U. Schroeder, R. Gulaboski, *Electrochemistry of Immobilized Particles and Droplets*, Springer, **2005**.

[11] https://quizlet.com

[12] J. D. Watkins, S. M. MacDonald, P. S. Fordred, S. D. Bull, Y. Gu, K. Yunus, A. C. Fisher, P. C. Bulman-Page, F. Marken, *Electrochim. Acta* **2009**, *54*, 6908.

[13] W. Adamiak, G. Shul, M. Opallo, *Electrochem. Commun.* **2009**, *11*, 149.

4.4 ELECTROCATALYTIC MEDIATED CONVERSION AT THE SOLID-SOLID INTERFACE

In this subchapter the two-phase chemical conversion of an antioxidant substance, diphenyl carbinol (DPC) to benzophenone (BP) electrochemically mediated by 2,2,6,6-tetramethyl-1-piperidinyloxy radical (TEMPO) and TEMPO derivatives is studied. Both initial substrate and product are solids and are located on the working electrode surface. The initial idea was to perform the experiment where a high area working electrode is modified by an oil solution of methyllaurate contained DPC substrate and the electrode is in contact with aqueous solution of TEMPO and the electrochemical monitoring of DPC converted to BP possibly takes place at the oil|water interface. We demonstrated an example of such an electrode based on carbon microparticles bonded together with polystyrene for oil analysis. This reaction would then be performed in a biphasic microfluidic system with a moving liquid|liquid interface to improve the mass transport of reactants. Unfortunately test experiments showed that there are technical problems with mechanical stability of carbon nanoparticles modified with polystyrene is not sufficient to give the electrochemical signal Instead of that, we showed the impact of different TEMPO mediators in direct chemical conversion of DPC to BP at the interface between GE and DPC solid|solid interface.

4.4.1 Voltammetry with TEMPO-mediated solid|solid oxidation of DPC to BP

Initially, we have performed the electrochemistry of 1 mM TEMPO alone in 0.1 M aqueous solution of carbonate buffer NaOH and $NaHCO_3$ keeping alkaline conditions (pH 11). Fig. 4.4.1a shows CVs recorded at a GE working electrode using a potential scan rate of 50 mV s^{-1} with 1 mM TEMPO solution in carbonate 11 pH buffer without DPC on the working electrode surface. The CV data for the TEMPO system indicated a stable ratio of anodic and cathodic current indicating the electrochemical reversibility of the reaction in case of absence of DPC in aqueous solution. Peak currents are proportional to the square root of the potential scan rate consistent with a diffusion controlled one-electron transfer. From previous investigations it is well known that electrochemical oxidation of $TEMPO^+$ (oxoammonium cation) is a very pH sensitive reaction [1,2]. In case of basic conditions it has been suggested that obtained $TEMPO^+$ in the way of reaction with hydroxide anion provides the conversion of $TEMPO^+$ to hydroxylamine and finally that is responsible for reformation of the TEMPO reagent [3,4]. In the opposite situation, under acidic pH, the rate of recovery

of the TEMPO radical is slower. The value of pH kept in range ca. 11 provides a good balance between conversion and decomposition of the mediator by a detrimental side-reaction of the oxoammonium cation with hydroxide anions [2].

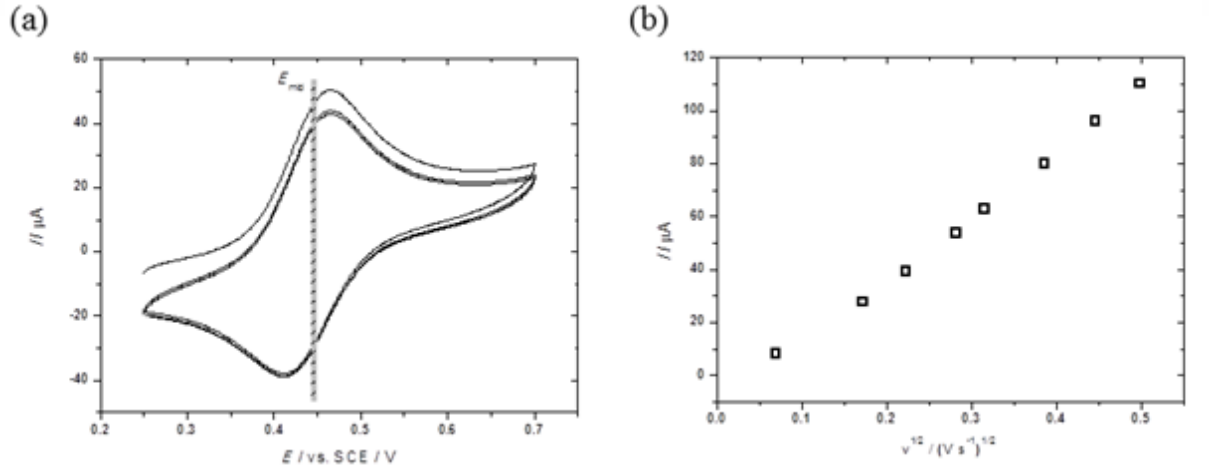

Fig. 4.4.1 (a) Cyclic voltammograms (scan rate 0.05 V s^{-1}) recorded at a 4.9 mm diameter graphite electrode for the oxidation of 1 mM TEMPO in carbonate buffer, pH 11 (3 potential cycles over-layed). **(b)** The plot of anodic peak current versus square root of potential scan rate.

The midpoint potential for TEMPO oxidation is E_{mid}= ½ $E_{p,\ ox}$+ ½ $E_{p,\ red}$= 0.44 V vs. SCE with a peak-to-peak separation of 0.07 V for a scan rate ranging from 5 to 250 mV s^{-1}. The plot in Fig. 4.4.1b shows that scan-rate dependence has slight non-linear behavior. This might possibly be due to some adsorption of TEMPO onto the electrode surface.

In order to ensure that the chemical conversion of DPC to BP is dependent on the presence of the TEMPO mediator, the voltammetric response (Fig. 4.4.2a) for DPC deposited onto GE in the absence of TEMPO was measured. The voltammogram shows no Faradaic peaks without TEMPO and this is evidence that electrochemical conversion without the redox mediator cannot be conducted. Fig. 4.4.2a also demonstrates voltammograms for three different amounts of DPC (40, 80 and 160 nmol).

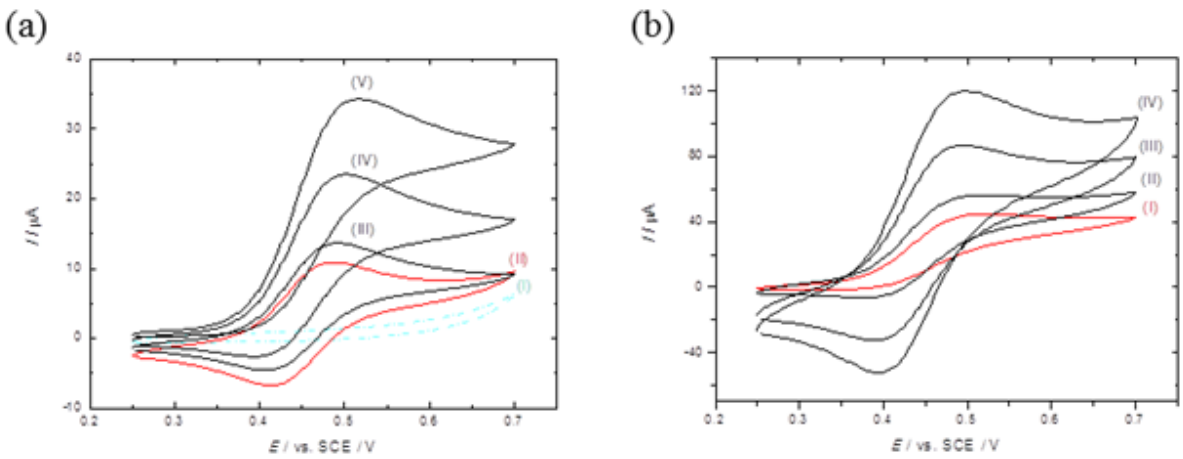

Fig. 4.4.2 (a) Cyclic voltammograms (scan rate 0.005 Vs^{-1}) for (I) DPC added in the absence of TEMPO, (II) 1 mM TEMPO without DPC deposit on the graphite electrode, (III) 40 nmol DPC, (IV) 80 nmol DPC, and (V) 160 nmol DPC. **(b)** Cyclic voltammograms (scan rate (I) 0.005 Vs^{-1}, (II) 0.05 Vs^{-1}, (III) 0.1 Vs^{-1}, and (IV) 0.2 Vs^{-1}) for the oxidation of 1 mM TEMPO. pH conditions of experiments as in Fig. 4.4.1.

The general trend and shape of the resulting voltammograms is in agreement with the catalytic reaction of regeneration of the electroactive species in a homogenous reaction (EC'). This is a special type of EC reaction and the letter E symbolizes the electron transfer and C is a homogenous chemical reaction. In this reaction the non-electroactive compound reacts with the product of the electrochemical reaction, finally gives the regeneration of the starting electroactive compound [6]. An enhancement in the response of the current is recorded as the homogenous reaction between TEMPO and DPC can regenerate the electroactive mediator (TEMPO) which can be afresh oxidized at the electrode surface. In our case the proposed EC' pathway has the form presented below:

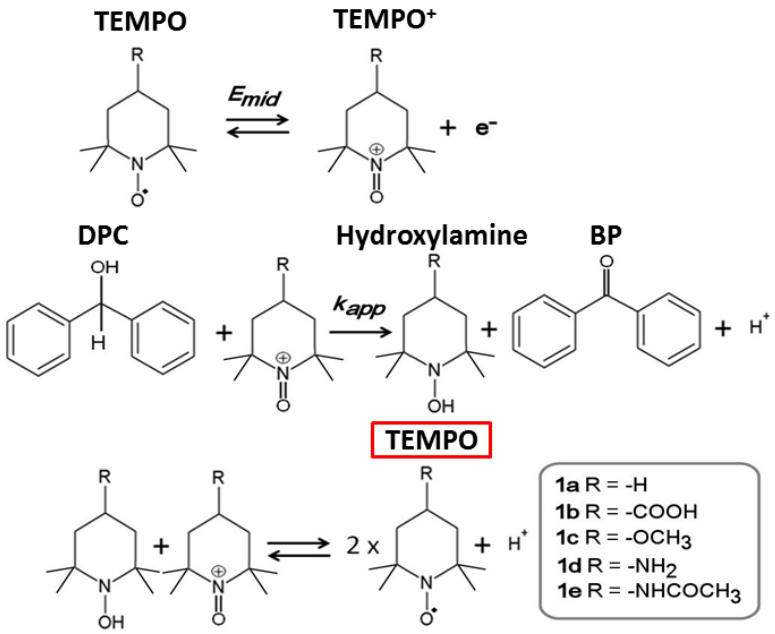

Fig. 4.4.3 Reaction scheme for the TEMPO electrochemical mediated oxidation of diphenyl carbinol (DPC) to benzophenone (BP) under carbonate buffer (pH11).

In the reaction pathway presented in Fig. 4.4.3, the $TEMPO^+$ cation reacts with the DPC solid substrate which gives the appropriate concentration of hydroxylamine and BP product. A final interconversion between formed hydroxylamine and free $TEMPO^+$ cation results in the reformation of the TEMPO radical. According to the reaction mechanism which we proposed, the conversion of DPC to BP consumes overall two equivalents of the $TEMPO^+$ cation. When the amount of deposited DPC is larger than 160 nmol, the enhancement of the catalytic current becomes slower than expected from the reaction pathway. This can be the result of the active surface of the working electrode becoming blocked by the high amount of deposited DPC and availability of contact between TEMPO and the electrode is more difficult.

Another experiment performed in the way to analyze the EC' mechanism proposed in this thesis was CV measurements of for 80 nmol DPC deposited onto electrode as a function of the potential scan rate (Fig. 4.4.2b). With a scan rate of approximately 0.05 V s^{-1}, the electrochemical back-reduction of $TEMPO^+$ can be observed, which suggests how interaction of $TEMPO^+$ with DPC is going on and that on this time scale the chemical reaction of $TEMPO^+$ with DPC is too slow to compete with TEMPO electrochemical conversion. Another word, the more favorable is electrochemical oxidation/reduction of TEMPO mediator than reaction of oxidized form of the mediator ($TEMPO^+$) with DPC.

4.4.2 The kinetic analysis of the solid|solid TEMPO-mediated oxidation of DPC to BP

Fig. 4.4.4 shows CV data for 4 different types of TEMPO mediator. We have shown here that different TEMPO derivatives can react with different rates depending on their midpoint potential position and also can depending on converted substrate structure.

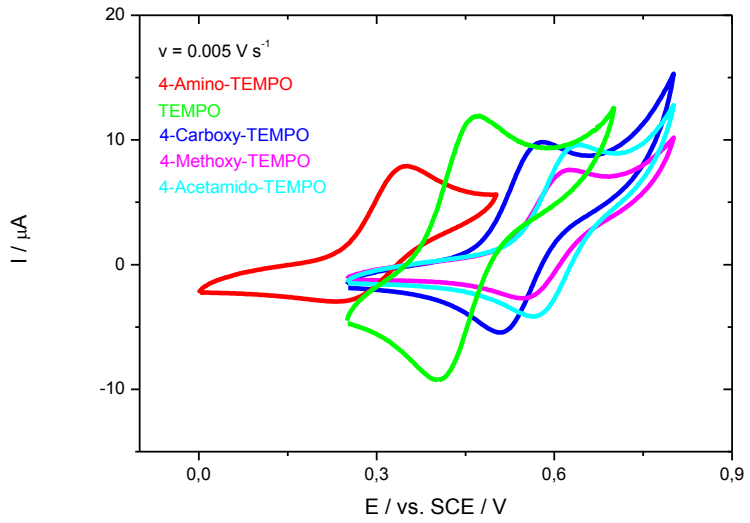

Fig. 4.4.4 CV curves for 4-Amino-TEMPO, TEMPO, 4-Carboxy-TEMPO, 4-Methoxy-TEMPO; 4-Acetamido-TEMPO. pH conditions of experiments as in Fig. 4.4.1. Scan rate was set on 0.005 Vs^{-1}.

The conversion of the solid state DPC substrate to a solid BP product can be directly monitor with chronoamperometry measurements where the Faradaic current can be directly measured as a function of time. This experimental method ensures that at a high enough applied potential a known and stable concentration of $TEMPO^{+}$ mediator is present to react with the solid substrate (Fig. 4.4.5).

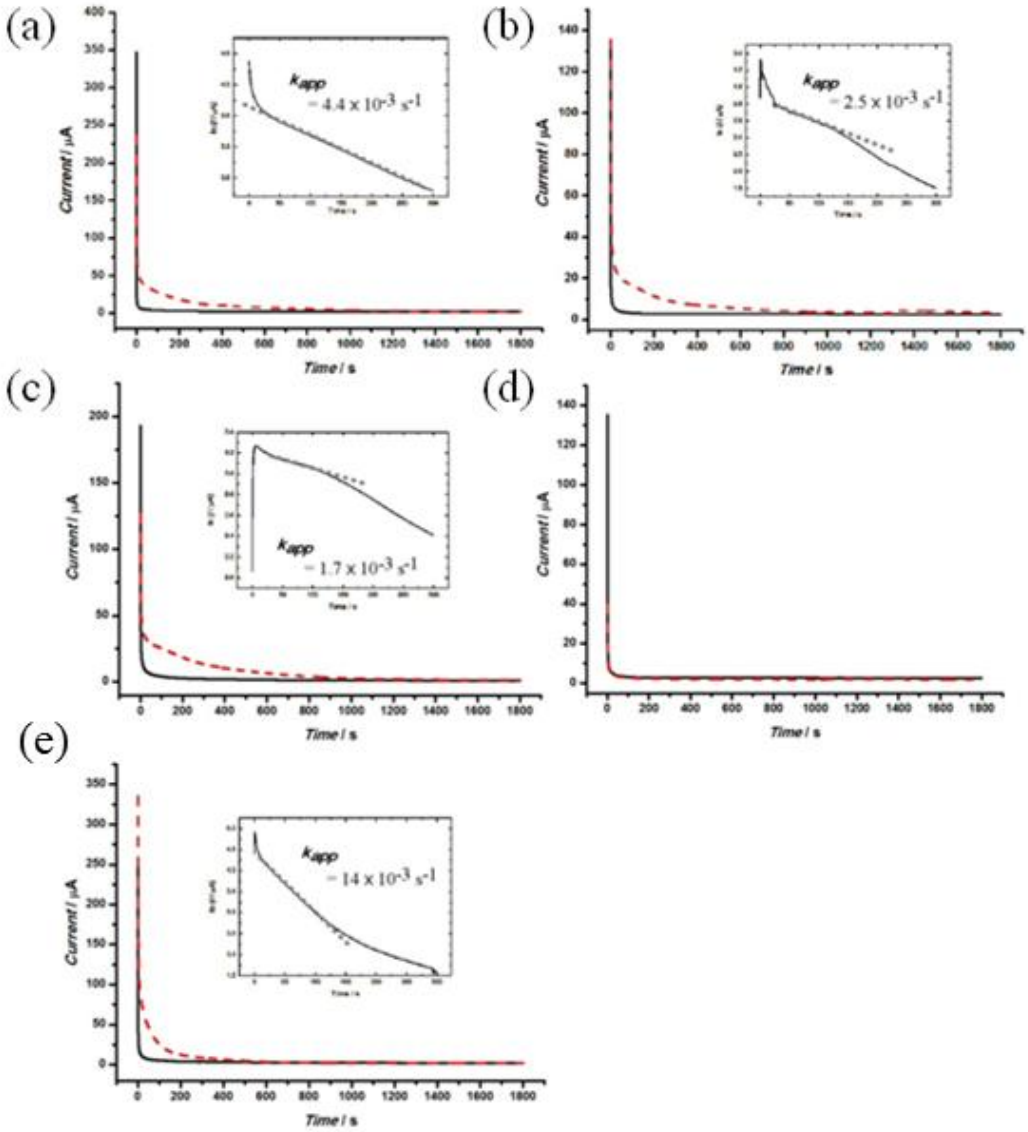

Fig. 4.4.5 Chronoamperometry data for oxidation of 80 nmol of DPC immersed in 0.1 M carbonate buffer pH 11 and 1 mM **(a)** TEMPO, **(b)** 4-carboxy-TEMPO, **(c)** 4-methoxy TEMPO, **(d)** 4-amino-TEMPO, and **(e)** 4-acetamido-TEMPO. Black curve indicates measurement only with appropriate TEMPO derivative and red-dashed curve depicts adding of DPC to the system. Each plot contains inset where linearity region of reaction $TEMPO^+$ with DPC is showed. Each inset has calculated value of apparent rate constant of the reaction (k_{app}).

Fig. 4.4.5 shows CA data for five different TEMPO derivatives which are mediators for the oxidation of 80 nmol DPC deposited on the graphite electrode. It can clearly be observed that the kinetics of the mediated reaction is different for each kind of TEMPO derivative. A visible interaction between the mediator and substance can be seen in case of 4-amino-TEMPO (Fig. 4.5.5d). In the interaction between diphenyl carbinol and 4-amino-$TEMPO^+$ cation, the mediated reaction is not observed at all and the chronoamperometry curves with and without diphenyl carbinol present appear identical. For all other TEMPO derivatives, reaction is observed usually within the first 10 minutes of the experiment.

Detailed analysis of the Faradaic current was possible in the way to integrate the chronoamperometric curves registered during DPC oxidation suggest between 1 and 2 electrons per substrate molecule are consumed (see Table 4.4.1). The number of mol of electrons $n\mathrm{e}^-$ which take part in reaction can be calculated by dividing the value of the total charge q taken from electrochemical TEMPO oxidation by the Faraday constant F:

$$n\mathrm{e}^- = \frac{q}{F} \qquad \text{(Eq. 4.4.1)}$$

Calculated number of mol of electrons can be further use to check the number of electrons were employed in conversion of DPC to BP. Tab. 4.4.1 summarizes the calculated data for different TEMPO derivatives and also shows the mead-peak potential (E_{mid}) values.

Tab. 4.4.1 The summary of voltammetry and the number of electrons taking part in mediated oxidation of DPC solid substrate to BP solid product. pH conditions of experiments as in Fig. 4.4.1.

TEMPO mediator and conditions	**E_{mid} / vs. SCE / V**	**Number of electrons per DPC molecule**
TEMPO	0.44	1.3
4-carboxy-TEMPO	0.55	1.2
4-methoxy-TEMPO	0.59	1.2
4-amino-TEMPO	0.32	-
4-acetamido-TEMPO	0.61	1.1

It is clearly visible that obtained results showed incomplete conversion of DPC substrate and less than 2 electrons take part in reaction. The problem of lack in conversion can be due to the fact of length of the experiment and in consequence possibility of losing some DPC substrate from the electrode surface during progress of the experiment. In order to analyze the reaction kinetics we investigated the progress of the reaction. Fig. 4.4.5 shows that for all TEMPO derivatives there are regions of linearity where rate constant of the reaction can be estimated. We assumed that this 5 minutes linear region can be possibly according to first order apparent rate constant k_{app}. The whole reaction has a form of sequence of equation presented below [7]:

$$\mathrm{TEMPO}^+ + \mathrm{DCP} \rightarrow \mathrm{TEMPO} + \mathrm{BP} \qquad \text{(Eq. 4.4.2)}$$

$$\frac{\mathrm{d[TEMPO]}}{\mathrm{dt}} = k_{\mathrm{app}}[\mathrm{TEMPO^+}][\mathrm{DCP}] \qquad \text{(Eq. 4.4.3)}$$

In this first period of reaction registered in chronoamperometry curve, the reaction is diffusion controlled and depends on the TEMPO concentration gradient. Calculated apparent rates constant for TEMPO and TEMPO derivatives are presented in Tab. 4.4.2.

Tab. 4.4.2 The summary of calculation of apparent first order rate constant (k) reaction of TEMPO and TEMPO derivatives with DPC solid substrate onto electrode. pH conditions of experiments as in Fig. 4.4.1.

TEMPO mediator	**Apparent reaction rate constant** k_{app} **/ s^{-1}**
TEMPO	4.4×10^{-3}
4-carboxy-TEMPO	2.5×10^{-3}
4-methoxy-TEMPO	1.7×10^{-3}
4-amino-TEMPO	-
4-acetamido-TEMPO	14×10^{-3}

Rate constant data range from 1.7×10^{-3} s^{-1} to 14×10^{-3} s^{-1} informs that the most potent mediator in this case is 4-acetamido-TEMPO in contrast to 4-methoxy-TEMPO which shows less affinity of interaction with DPC substrate. When comparing to the midpoint potentials for TEMPO mediators, 4-acetamido-TEMPO clearly appears to be the mediator with the highest driving force for this oxidation. However, this correlation does not give expected result for 4-methoxy-TEMPO which reacts surprisingly slowly.

4.4.3 The determination of the mechanism of the solid|solid TEMPO mediated oxidation of DPC to BP

The CA data in showed in the previous section tell that after some time, the reaction leaves the first order regime. The initial fast reaction rate (in the first seconds of the reaction) is likely to reflect the direct interaction of $TEMPO^+$ derivatives with the diphenylcarbinol crystal surface. However, the apparent rate constant k_{app} associated with the first order mechanism observed during the first 5 minutes must be controlled by another rate limiting step. Fig. 4.4.6 presented possible scenario of the interaction between $TEMPO^+$ cation and DPC solid crystals present on to electrode surface.

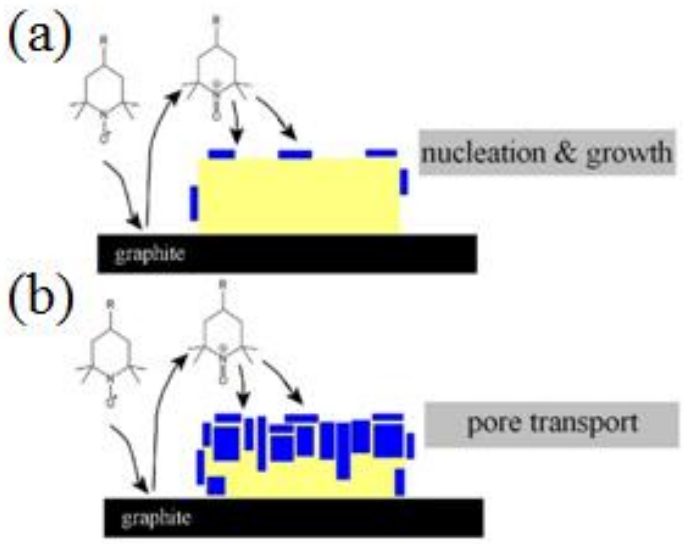

Fig. 4.4.6 Schematic sketch of the initial "nucleation and growth" stage and the "pore transport" stage of the solid-solid reaction (yellow = diphenylcarbinol, blue = benzophenone). pH conditions of experiments as in Fig. 4.4.1.

Initially, $TEMPO^+$ cation reacts with DPC substrate and the reaction goes to obtaining BP crystal product in the vicinity of DPC surface starting material in form of crystals. The surface stage of the reaction is going to the moment when the DPC starting material surface is covered by nucleated BP solid product. This is likely to cause a blocking of the reactive surface and a switch of the rate limiting step from surface reaction controlled to transport controlled in the way of transport DPC molecules through the pores to reach the reaction zone with TEMPO at the solid|aqueous electrolyte interface. This specific mechanism occurs e.g. in case of oxide film growth on alloys. Briefly, the charged species (interstitials or vacancies) is transported in the presence of both concentration and potential gradients on metal surfaces such as titanium [8] and iron [9].

Another investigation which we have tested in order to analyze the reaction mechanism is checking the influence of the electrolyte pH on the speed of the reaction. For every unit of pH increase the reaction rate is increased by a factor of approximately four. It is well known that more alkaline conditions increase the reaction rate for TEMPO systems, which is associated with the loss of protons from the substrate during oxidation [2]. Tab. 4.4.3 contains the data for TEMPO rate constant and number of electrons taking part in DPC conversion in order to increased pH values.

Tab. 4.4.3 Summary of voltammetry and chronoamperometry data for the reactivity of DPC deposited onto a graphite electrode surface towards TEMPO mediated oxidation in the presence of different pH conditions of carbonate buffer.

Effect of solution pH (with 80 nmol DPC)		
TEMPO mediator	**Number of electrons per DPC molecule**	**Reaction rate** k_{app} / s^{-1}
TEMPO (pH 10)	1.1	1×10^{-3}
TEMPO (pH 11)	1.3	4×10^{-3}
TEMPO (pH 12)	1.4	16×10^{-3}
TEMPO (pH 13)	1.2	57×10^{-3}

The fact that characteristic differences in reaction rate are seen as a function of TEMPO derivative and solution pH can be traced back to the initial stages of the solid-solid conversion, which is likely to be associated with nucleation and growth of the BP product. An additional explanation can be based on the idea that rapid nucleation in the early stages of the reaction will yield many smaller nuclei of DPC which leaves more pores towards the surface during the later stages of the reaction transport controlled.

The effect of the TEMPO mediator concentration was investigated (Tab. 4.4.4) and although there is some variability, the trends seem insignificant even when TEMPO concentration is increased four times. This suggests that under the conditions employed here, the concentration of $TEMPO^{+}$ does not affect the reaction rate and it can be further evidence that transport of DPC molecules though the pores is the limiting step of the whole process.

Tab. 4.4.4 Summary of voltammetry and chronoamperometry data for the reactivity of diphenylcarbinol microcrystals deposited onto a graphite electrode surface towards TEMPO mediated oxidation. pH conditions of experiments as in Fig. 4.4.1.

Effect of TEMPO concentration (with 80 nmol DPC deposited on to electrode surface)		
TEMPO mediator	**Number of electrons per DPC molecule**	**Reaction rate k_{app} / s^{-1}**
TEMPO (1 mM)	1.3	4×10^{-3}
TEMPO (2 mM)	1.0	5×10^{-3}
TEMPO (3 mM)	1.7	8×10^{-3}
TEMPO (4 mM)	1.4	4×10^{-3}

4.4.4 Conclusions

It has been shown that the reaction of water-insoluble crystalline solids DPC substrate with redox TEMPO mediator dissolved in aqueous buffer solution can be studied directly. Immobilisation of the substrate DPC has been demonstrated to affect the voltammetric and chronoamperometric behaviour of TEMPO derivatives consistent with the theory of a solid-solid EC' reaction mechanism, where DPC is converted into BP. The chronoamperometry measurement performed without electrode blocking effect by initial amount of DPC, provides direct information about two events occurred during run of experiment: (I) an onset period with higher currents associated with initial nucleation and growth and (II) a first order rate process associated with a transport-controlled reaction, presumably the transport of DPC into the reaction zone.

This methodology could be of wider use and beneficial in particular for the screening of anti-oxidants [10]. Insights into the reaction mechanism are of use also for the development of water-based electro-organic synthesis approaches [11] where starting material and product are solids and they will be able to be separated from the electrolytic buffer solution.

4.4.5 Bibliography

[1] R. Barhdadi, C. Comminges, A. P. Doherty, J. Y. Nedelec, S. O'Toole, M. Troupel, *J. Appl. Electrochem.* **2007**, *37*, 723.

[2] E. M. Belgsir, H. J. Schafer, *Electrochem. Commun.* **2001**, *3*, 32.

[3] M. Zhao, J. Li, E. Mano, Z. Song, D. M. Tschaen, E. J. J. Grabowski, P. J. Reider *J. Org. Chem.* **1999**, *64*, 2564.

[4] A. De Mico, R. Margarita, L. Parlanti, A. Vescovi, G. Piancatelli, *J. Org. Chem.* **1997**, *62*, 6974.

[6] R. A. Green, J. T. Hill-Cousins, R. C. D. Brown, D. Pletcher, S. G. Leach, *Electrochim. Acta*, 2013, 113, 550.

[7] F. Scholz, *Electroanalytical methods.* **2005**, Springer.

[8] J. F. Vanhumbeeck, J. Proost, *Corr. Rev.* **2009**, *27*, 117.

[9] H. Brookes, F. Graham, *J. Chem. Soc-Faraday Trans.* **1993**, *89*, 547.

[10] G. A. Ayoola, H. A. B. Coker, S. A. Adesegun, A. A. Adepoju-Bello, K. Obaweya, E. C. Ezennia, T. O. Atangbayila, *Trop. J. Pharm. Res.* **2008**, *7*, 1019.

[11] D. Nematollahi, S. S. Hosseiny Davarani, P. Mirahmadpour, *ACS Sustainable Chem. Eng.* **2014**, *2*, 579.

Chapter 5

SUMMARY AND CONCLUSIONS

The electrochemical microfluidic device (EMD) can be a very useful tool in studying electrochemical processes and this thesis focuses on this fact. The EMDs have a lot of advantages like: laminar flow which is well established at the electrode surface and the rate of mass transfer to and from the microband electrode is easily controlled. Another valuable aspect is that measurements in these systems can be performed under steady-state conditions. Bigger part of this thesis shows results of ion transfer process driven by electrochemical reaction of electroactive compound dissolved in immiscible, organic phase. The main aim of this dissertation was to understand the foundation of thermodynamic the ion transfer processes performed under microfluidic conditions and to examine the behavior of the EMD on application different flow regimes. The major problems and questions which are related with the content of this thesis are:

1) Whether PDMS material to fabricate the EMD is fine compatible to nasty organic solvents used in electrochemical measurements. The word compatible means the interaction of PDMS with the solvent like: adsorption the solvent through the PDMS structure or deformation of PDMS microchannel during flowing time and the influence of this effect on electrochemical measurements.

2) Whether the reaction zone formed during experiments with electrochemically driven ion transfer processes under microfluidic conditions increases with the value of the flow rate both organic and aqueous phases.

3) Whether the thermodynamic model for ion transfer, developed for static conditions, can be used in microfluidics.

4) Whether different types of TEMPO mediator can have different impact on the chemical oxidation of the direct immobilized crystalline compound.

To solve the problems mentioned above the electrochemical oxidation of electroactive compounds like: Fc, DMFc or TEMPO mediator was involved. In the way to perform the hydrodynamic electrochemistry experiments, the PDMS based EMD was employed with the gold microband electrode system, perpendicularly located to the flow direction and with stable silver-silver chloride reference electrode. DPC crystals were immobilized on the electrode surface using micropipette procedures. Electroanalytical methods used to perform the studies above were: cyclic voltammetry (CV), square wave voltammetry (SWV) and chronoamperometry (CA). The position of the three-phase boundary was controlled by laser scanning confocal microscopy. Fabrication of PDMS EMD was possible thanks to soft photolithography procedures.

In the **subchapter 4.1**, the first step was the verification of PDMS microchannel compatibility on the different solvent is presented. The test depicted functionality of PDMS microchannel and gave the answer that this material is suitable in performing of long lasting electrochemical experiments with flowing selected solvents.

The **subchapter 4.2** contains the ion transfer process assisted electrochemical oxidation of Fc at a flowing organic solvent|aqueous electrolyte|electrode three-phase boundary.

- It was shown that transfer limited current registered during ion transfer reaction in some value of the flow rate increases in the unexpected way.
- The transfer limited current behavior can be explained by a mathematical model assuming the minimum width of the three-phase boundary and the width of the diffusion reaction zone, inversely proportional to the flow rate value.
- The fluorescence images clearly show the presence of the sharp line of the three-phase boundary at the bottom of the microchannel in different microfluidic conditions, however there is a difference between the layout the organic and the aqueous phase in the bottom of the microchannel and the top. The reason is the difference in wetting angle for the PDMS|organic solvent and PDMS|aqueous electrolyte interfaces.

Subchapter 4.3 presents an extended the former studies performed in subchapter 4.2 of simultaneous electron-ion transfer processes under microfluidic conditions to wider range

of studied anions dissolved in the aqueous phase. Additionally the values of Gibbs transfer energies of anions for the organic solvent which this data does not appear in the literature.
The most important conclusions are as follows:

- The effect of anion hydrophilicity is the same under the static TPE and under microfluidic conditions.
- The ion concentration effect under the static and microfluidic conditions and concentration of DMFc electroactive compound can be analyzed using Nernst-like equation.
- Microfluidic TPE can be used to determine the concentration of the transferring anion.

Subchapter 4.4 is the effort to perform TEMPO mediated electrocatalytic conversion of DPC to BP product. Five different TEMPO mediators were tested according to their different impact on the rate of conversion. It was the intial point to transfer the experiments under static conditions to microfluidic device.

- The chronoamperometry and voltammetry behavior of TEMPO and TEMPO derivatives mediated conversion of DPC to BP is consistent with the occurrence of a solid-solid EC' mechanism.
- The solid-solid EC' mechanism pathway of DPC to BP is controlled by mass transport of the nuclei of DPC substrate towards the reaction zone.
- Different types of TEMPO mediator exhibit different impact on rate of conversion of DPC to BP.

The performed studies in this thesis showed that EMD can be a valuable tool in the investigations of simultaneous electron-ion transfer processes. These studies complement the previous studies on ion transfer in microfluidic systems and extend our knowledge about liquid|liquid electrochemistry under multiphase flow conditions.
The experiments with ion transfer under microfluidic conditions can be further improved towards more oriented applications research like analysis of anions in solution. Analysis of solution can be conducted in the way of using ionophores or other substances which selectively recognize appropriate anion. The experiments with electro-mediated oxidation of antioxidant are good starting point to transfer these experiments to EMD where delivering of mediator can be utilized with pumped liquid.